Theses and Dissertations--Civil Engineering | Civil Engineering

2017

SEDIMENT TRANSPORT MODELLING USING DYNAMIC (DIS)CONNECTIVITY PREDICTION FOR A BEDROCK CONTROLLED CATCHMENT

David Tyler Mahoney
University of Kentucky, tyler.mahoney@uky.edu
Author ORCID Identifier:
https://orcid.org/0000-0003-0523-508X
Digital Object Identifier: https://doi.org/10.13023/ETD.2017.307

STUDENT AGREEMENT:

I represent that my thesis or dissertation and abstract are my original work. Proper attribution has been given to all outside sources. I understand that I am solely responsible for obtaining any needed copyright permissions. I have obtained needed written permission statement(s) from the owner(s) of each third-party copyrighted matter to be included in my work, allowing electronic distribution (if such use is not permitted by the fair use doctrine) which will be submitted to UKnowledge as Additional File.

I hereby grant to The University of Kentucky and its agents the irrevocable, non-exclusive, and royalty-free license to archive and make accessible my work in whole or in part in all forms of media, now or hereafter known. I agree that the document mentioned above may be made available immediately for worldwide access unless an embargo applies.

I retain all other ownership rights to the copyright of my work. I also retain the right to use in future works (such as articles or books) all or part of my work. I understand that I am free to register the copyright to my work.

REVIEW, APPROVAL AND ACCEPTANCE

The document mentioned above has been reviewed and accepted by the student's advisor, on behalf of the advisory committee, and by the Director of Graduate Studies (DGS), on behalf of the program; we verify that this is the final, approved version of the student's thesis including all changes required by the advisory committee. The undersigned agree to abide by the statements above.

<div align="right">

David Tyler Mahoney, Student

Dr. James Fox, Major Professor

Dr. Y. T. Wang, Director of Graduate Studies

</div>

SEDIMENT TRANSPORT MODELLING USING DYNAMIC (DIS)CONNECTIVITY PREDICTION FOR A BEDROCK CONTROLLED CATCHMENT

_____

THESIS

_____

A thesis submitted in partial fulfillment of the
requirements for the degree of Master of Science
in Civil Engineering in the College of Engineering
at the University of Kentucky

By

David Tyler Mahoney

Lexington, Kentucky

Director: Dr. James Fox, Professor of Civil Engineering

Lexington, Kentucky

2017

ABSTRACT OF THESIS

SEDIMENT TRANSPORT MODELLING USING DYNAMIC (DIS)CONNECTIVITY
PREDICTION FOR A BEDROCK CONTROLLED CATCHMENT

The (dis)connectivity of sediment, defined as the detachment and transport of sediment from source to sink between geomorphic zones, is a major control on sediment transport rates but has seldom taken precedence in sediment transport models that focus on assessment of sediment impacts on water supply. A watershed-scale sediment transport model was formulated that incorporates sediment (dis)connectivity knowledge and subroutines and predicts sediment flux through coupling with an excessive shear stress erosion equation. The intersecting probabilities of sediment supply, detachment, transport, and (dis)connectivity produce the probability of sediment connectivity for a watershed or region of a watershed. The integration of the net watershed probability of sediment connectivity yields an estimate of the active watershed area in terms of sediment transport when multiplied times the entire watershed area. The sediment transport model was tested for a bedrock controlled catchment in the Southeastern United States for which extensive historic water and sediment flux data was available. It is expected that the model presented here can be used as a tool to assess the regional impacts of natural and anthropogenic sources of (dis)connectivity on sedimentation rates that lead to problems such as reservoir sedimentation and water quality degradation.

KEYWORDS: connectivity, disconnectivity, erosion, watershed, watershed
                 modelling, sediment transport modelling

  David Tyler Mahoney

  6/14/017

SEDIMENT TRANSPORT MODELLING USING DYNAMIC (DIS)CONNECTIVITY PREDICTION FOR A BEDROCK CONTROLLED CATCHMENT

By

David Tyler Mahoney

James Fox

Director of Thesis

Y. T. Wang

Director of Graduate Studies

6/14/2017

Table of Contents

List of Tables

List of Figures

Chapter 1 Introduction

1.1 Watershed Sedimentation Concerns

The study of sedimentation in watersheds is particularly important because of the harmful impact sediments can have on aquatic life, algae, civil infrastructure (i.e. reservoirs), and water quality (Wood and Armitage, 1997; FISRWG, 1998; Morris and Fan, 1998; USEPA, 1999; Zappou, 2001 USEPA, 2004). Fine sediments are of concern because of their acknowledged impact on primary producers due to the increase of turbidity in water bodies, thus limiting light penetration necessary for photosynthesis (Wood and Armitage, 1997). The connection of sediments from watershed uplands into stream networks has been studied for quite some time by ecologists (Pringle, 2001) in particular. This is because sediments can reduce the growth rate, reproduction rate, and life span of fish and macroinvertebrates by impairing the ability of aquatic organisms to hunt, reducing their immunity to disease, and clogging their respiratory systems (Wood and Armitage, 1997; Richardson and Jowett, 2002).

Fine sediments are defined as particulate organic and inorganic matter less than 63 µm in diameter and are one of the primary causes of stream impairment in the United States and in the Commonwealth of Kentucky, (Bailey and Waddell, 1979; Rabeni et al., 2004; Kentucky Division of Water, 2012). The cohesive nature of fine sediments promotes chemical bonding of nutrients and contaminates that can adversely affect the water quality of stream networks (Long et al., 1998; Owens et al., 2001). Nutrients can cause eutrophication within water bodies, promoting algal blooms (Castro and Reckindorf, 1995), which further hinder water quality and aquatic ecosystems by decreasing the

dissolved oxygen within water bodies, decreasing food supply for aquatic organisms, and decreasing available habitat for aquatic organisms. Some algae, known as blue-green algae or cyanobacterial algae, can be toxic to humans to consume and touch (Smith et al., 2015; Brooks et al., 2016). Fine sediments that bond with heavy metals also pose health problems to humans and aquatic life (USEPA, 2004).

Sedimentation affects water supply capacity as well as water quality. Reservoir sedimentation reduces reservoir storage capacity, meaning there is less water available for human use (USEPA, 2009). The quantification of watershed sedimentation has proven to be precarious over many years due to what Walling (1983) has defined as the sediment delivery problem. The sediment delivery problem is conceptualized by the idea that only a fraction of detached sediment is yielded at the basin outlet.

1.2 Sedimentation and Water Supply

Abundant water supply is vital to the survival, sustainability, and growth of communities. One common threat to urban water supply systems is reservoir sedimentation, which is defined as the deposition of sediment to the bed of a water supply basin (Murray, 1970; Sumi and Hirose, 2005; Randle and Collins, 2012). Sedimentation threatens water supply in two primary ways: (i) sediments may clog water distribution system intakes, increasing the difficulty for communities to receive water (Randle and Collins, 2012; Morris and Fan, 2009); and (ii) sedimentation may decrease the effective water storage capacity of the reservoir (Haregewyn et al. 2012; Morris and Fan, 2009; Annandale, 1987). The latter threat suggests the need for assessment of current water storage and projected future storage losses due to sedimentation. In order to quantify reservoir sedimentation, it is necessary to estimate transport rates of sediment to reservoirs;

2

and knowledge of sediment source, transport, and fate within a watershed provide the basis for such estimates. Sediment originates from erosion of weathered rock and soils in the uplands of watersheds and bank and legacy sediments in the stream corridor. Sediment detachment occurs when shear stress due to water, wind, and ancillary processes overcomes the critical shear stress binding sediment particles together (Partheniades, 1965). Sediment is transferred to the stream network through various erosional processes such as sheet wash, gulley, and rill erosion in the uplands, and streambank and channel erosion within the stream corridor (Reid and Dunne, 1996; Toy et al, 2002). Flow acceleration during an onset of major storm events is a major catalyst for sediment entering stream networks, although low flow and moderate events have also been found to assist with the long-term propagation of sediment from low order to high order streams (Russo and Fox, 2012).

Figure 1.1 shows how intensifiers, such as urbanization, land use change, population growth, and climate change affect both the processes governing reservoir sedimentation and water supply and demand rates. Sedimentation is exacerbated as long-term watershed scale changes, such as urbanization, and environmental changes enhance sediment transport to reservoirs. Urbanization is typically accepted to decrease the infiltration capacity of soils across a watershed and increase runoff depth, peak streamflow rates, and hence increase the rates of upland and stream erosion processes that lead to reservoir sedimentation (Russo and Fox, 2012; McGriff, 1972; Trimble, 1997). Similarly, climate change causes variations in rainfall amounts and intensities over time (Kundzewicz et al., 2007), which in turn has the potential to increase runoff depths and peak flows, thus exacerbating sedimentation. Recent climate forecasts suggest that the mean annual rainfall

amount (ensemble average) will increase by 10% in the inner Bluegrass physiographic region of Kentucky (NCA, 2014). In addition to the mentioned sediment processes, urbanization increases the demand of water taken from reservoirs while simultaneously decreasing the available supply of water from reservoirs. Climate change could potentially decrease the supply of water available during drought periods (Backlund et al., 2008). Therefore, both supply and demand should be budgeted when considering the future forcings.

Due to the low energy of water movement within water supply reservoirs, sediment particles are prone to deposition. The trapping efficiency of some water supply reservoirs is near 100%, meaning that all sediment that enters the reservoir is trapped there indefinitely (McCully, 1996). Thus, water supply capacity is threatened by the existence of high sediment concentrations of incoming flows. In order to mitigate the effects of sedimentation on water supply, researchers and consultants use a variety of methods to estimate reservoir sedimentation rates. These include bathymetric surveys, turbidity measurements, sediment borings, sediment trapping, and the development of empirical regression curves (Furnans and Austin, 2008; Juracek, 2013; Morris and Fan, 1998; Effler et al., 2006; Singh and Durgunoglu, 1989),

There are several sediment control strategies commonly practiced to mitigate the effects of reservoir sedimentation on water supply including: (1) limiting upstream erosion and sediment transport to reduce sediment inflow, (2) routing sediments around or through the retaining facility, and (3) manually removing or excavating deposited sediments from the reservoir floor (Morris and Fan, 1998; Sumi and Hirose, 2009; Haregeweyn et al., 2012). Reducing sediment inflow involves preventing erosion at the sediment source

4

through common best management practices (BMPs) such as bank stabilization and riparian buffer reestablishment (Brown, 2000; Burt et al., 1999). Spatially explicit erosion models are commonly used to estimate locations within the watershed where erosion and sedimentation are most pronounced. These are locations where BMPs can be implemented to reduce the amount of sediment entering the stream network. Sediment transport can also be limited longitudinally (i.e. within small tributaries and concentrated flow pathways) through the use of check dams designed to catch and deposit sediment prior to entering the stream network (Haregeweyn et al., 2012). Once sediment has been deposited, however, it can be removed through manual excavation (Sumi and Hirose, 2009). Examples of this are dredging, the process of scooping/digging sediments and moving them elsewhere, and dry excavation, the emptying of the reservoir and using excavating equipment to remove sediments.

Sedimentation's detrimental impact on water supply remains a threat to national and international water infrastructure (US Interagency Meeting on Sedimentation, 2012; EOS, 2014). Therefore, researchers are working towards quantifying how human and natural intensifiers govern water supply reduction through sedimentation processes. One of the greatest sources of uncertainty in predicting sedimentation and its impacts on water supply is connecting upland soil erosion processes with downstream sedimentation, which can indicate where sedimentation and erosion are most pronounced in watershed.

1.3 Contents of Thesis

Chapter 1 of this thesis lists the threats posed by fine sediments and the processes of watershed erosion and sedimentation that affect water supply.

Chapter 2 discusses watershed erosion models that have been previously developed how they can be improved with the coupling of the geomorphologic concept of sediment (dis)connectivity. A literature review is provided discussing advancements in watershed erosion modelling and the concept of (dis)connectivity. The motivation and objectives of the research are also presented here.

Chapter 3 describes the model framework and formulation of the (dis)connectivity and erosion model.

Chapter 4 provides information about the study site within the Kentucky River Basin. The physiography, climatology, and dominant sediment transport processes of the study watershed are outlined.

Chapter 5 provides the methodology of the WAVES Protocol, an in-house watershed visual assessment protocol that elucidates watershed erosion and sedimentation processes in the field.

Chapter 6 discusses the model set up, inputs, parameterization, calibration, and validation for the (dis)connectivity and watershed erosion model.

Chapter 7 provides the results of the (dis)connectivity and watershed erosion models.

Chapter 8 discusses the results of the models and compares the results and methods of this thesis to previously developed watershed models.

Chapter 9 provides the conclusions of this thesis.

Figure 1.1: Conceptualization of the effect of intensifiers on reservoir sedimentation processes
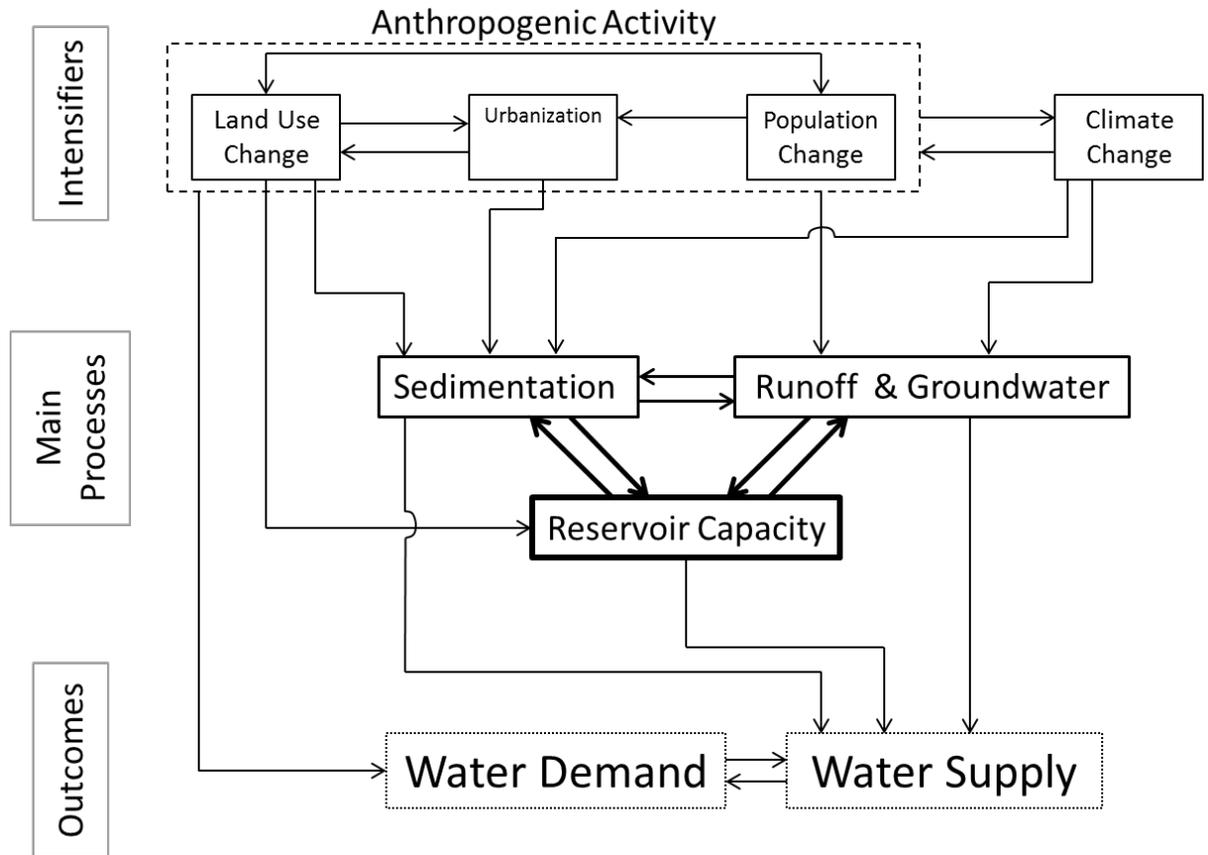
Chapter 2 Literature Review, Research Needs, Motivation and Objectives:

2.1 Watershed Erosion Modelling: Past Advancement and Future Needs

The authors argue that currently there is a need for the advancement of watershed erosion modelling tools within the environmental water resources community. Watershed erosion modelling has seen substantial advancement over the past four decades resulting from the intensive field data collection systems and experimental watersheds of the 1970s and 1980s, the coupled hydrologic formula advancement of the 1980s, and the computational and geospatial data advancements of the 1990s and 2000s that have produced watershed modelling platforms (Walling, 1983; Merritt et al., 2003; Russo, 2009). Nevertheless, watershed erosion modelling is currently hindered by a number of weaknesses that do not allow proper representation of landscape hydrologic and sediment transport processes. As a precursor to detailing the current limitations, the authors review the three classes of watershed erosion models known as empirical, conceptual, and physically based models (Merritt et al., 2003; Russo, 2009).

2.2 Classification of Watershed Erosion Models

Empirical models are data driven, meaning that many years of data collection are necessary to predict future conditions (Merritt et al., 2003). Empirical models are invalidated if used outside of the study area for which data was collected or if significant alterations to the study area occur because the conditions under which data collection occurred have likely changed (Merritt et al., 2003). In order to predict dependent variables (i.e. sediment yield), empirical models relate independent variables (such as flow rate) to the dependent variable. Thus, empirical models do not directly model the individual processes of watershed sedimentation and erosion (Zoppou, 2001).

Conceptual models typically lump watershed areas with similar characteristics together and apply process-based equations across the lumped unit. Typically conceptual models are not spatially explicit, thus do not detail specific processes at their actual location within the watershed (Zoppou, 2001; Merritt et al., 2003; Aksoy and Kavvas, 2005). Unlike empirical models, conceptual models can be applied to many different study sites or watersheds given that they are calibrated correctly. Because of the lumped-nature of conceptual models, data input requirements are generally not extensive (Merritt et al., 2003).

Physically based watershed erosion and sedimentation models use the laws of physics to predict sediment flux. Physically based models most accurately model specific processes, however typically the parameters used to model and calibrate processes are only applicable at small scales (i.e. hillslopes) and cannot be up-scaled (Letcher et al., 2002; Merritt et al., 2003). Physical models use conservation laws such as the law of conservation of mass and the law of conservation of momentum to predict sediment transport. Often, data input requirements are large for physically based models (Adams and Elliot, 2006).

It should be noted that some lumped parameter models are physically based in regards to their attempt to simulate physical processes, but use global calibration approaches to parameterize the model. Hence, not all lumped parameter models are conceptual models and not all physically based models are spatially explicit.

2.3 Limitations of Current Watershed Erosion Models

The authors point out that the readily used classification of watershed erosion models as empirical, conceptual or physically based is in some ways incorrect, or at best has fuzzy boundaries. That is, even the most empirical models typically incorporate

conservation principles to some degree while the most physically based models incorporate empiricism. For example, the Universal Soil Loss Equation (USLE) (Wischmeier and Smith, 1978) is a widely used empirical model in the United States that incorporates the energy of rainfall during hydrologic events within its model structure. And, the Watershed Erosion Prediction Project (WEPP) model (Laflen et al., 1991) is a widely used, continuity based physical model that relies on many empirical coefficients within its model structure that can be adjusted during the model evaluation stage.

The point the authors strive to put forth is that all watershed erosion models attempt to incorporate conservation principles, require some empiricism, and exhibit some scale dependence. These characteristics of watershed erosion models can be used to highlight a number of weaknesses of watershed erosion models that do not allow proper representation of landscape hydrologic and sediment transport processes.

First, the conservation of mass, momentum, and energy applied within watershed erosion models is typically incomplete or highly simplified. For example, even the process-based WEPP model relies on the assumption of one dimensional flow on the hillslope and considers transport phenomena as steady state equilibrium. It is not yet computationally practical to simulate three dimensional unsteady flow across the landscape that comprises a watershed. Further, even if it were computationally feasible, scientists still lack a comprehensive understanding of transitional flow and turbulent flow interactions with sediment grains and aggregates over the fairly thin flow layers that make up overland flows.

Second, the heterogeneity of sediment properties across the landscape as well as the previously mentioned lack of understanding of fluid-sediment coupled currently require

empiricism within watershed erosion modelling. For example, the process-based WEPP uses the excessive stress function to simulate fluvial erosion within rills; and it is well recognized that over thirty different soil properties can impart some influence upon the empirical critical shear stress of cohesive sediment used within the excessive stress function. Fine sediment, by its nature, is highly heterogeneous with four aggregation levels of different shear strength considered just for features smaller than a few millimeters. Scientists currently lack an understanding of sediment strength, and therefore empiricism will continue to be incorporated into our models.

Third, watershed erosion models are by their nature scale limited. Scale limitations of watershed erosion models show an interdependency with the assumed simplified state of the conservation principles applied within a particular model as well as the sediment parameter spatial scales assumed to control sediment resistance. However, perhaps more so, scale limitations arrive from the lack of watershed erosion models to explicitly consider the configuration of the landscape. The catchment configuration in terms of its morphologic features and their connectivity, or lack thereof, is now well recognized to impart non-linearity upon the sediment transport phenomena within watersheds (Phillips, 2003). Yet, watershed erosion models have tended to stay focused on modelling sediment transport phenomena specific to a given watershed feature, e.g., floodplains, rills, or sheet flow.

Overcoming the three watershed erosion modelling limitations will likely require on-going and future research initiatives the next few decades. Such endeavors will be focused most likely on computational fluids research to better incorporate conservation principles at higher dimensions, improved basic science of the bio-physio-chemical matrix

that makes up sediment to overcome empiricism of sediment properties, and greater spatiotemporal investigation of landscape morphology and connectivity to overcome scale dependence.

2.4 Current Motivation of this Thesis Research

In the current research, the authors aim to advance watershed erosion modelling by coupling erosion formula with a greater spatiotemporal investigation of landscape morphology and connectivity to overcome scale dependence, i.e., the third limitation mentioned above. The authors argue that the time is ripe to advance watershed erosion modelling by improving its spatiotemporal context for several reasons. Highly resolved topographic and landscape featured datasets are now available, often freely available, that makes incorporation of such data into watershed platforms feasible. Also, geomorphologic field-based and geospatial-based investigation has been highly advanced in recent years to focus on the topic of sediment connectivity. Sediment connectivity is now recognized to be a major control on sediment budgets (Fryirs et al., 2007), but has seldom taken precedence in quantitative sediment transport models (Ambroise, 2004; De Vente et al., 2005; Heckmann and Schwanghart, 2013).

Therefore, the present work aims to represent the watershed configuration and its connectivity within watershed erosion modelling. The motivation of this thesis is to couple the conceptual idea of dynamic sediment connectivity and (dis)connectivity within watershed erosion modelling, and thus advance modelling platforms, in order to predict how sedimentation will affect water supply. In this manner, sediment disconnectivity can be used as a precursor to simulation of watershed erosion modelling in order to focus on the active morphologic features that might produce sediment.

2.5 Features of Sediment Connectivity and (Dis)Connectivity

The concept of sediment connectivity and (dis)connectivity has been advanced over the past few decades and requires some review of its features prior to incorporation within a watershed erosion model framework. The overarching aim of sediment connectivity and (dis)connectivity is to understand the configuration of the watershed and its role within the sediment continuum. This aim is achieved through interrelated field investigation and geospatial assessment of the watershed.

Geomorphologists have now introduced us to the concept of sediment connectivity and disconnectivity. In the geomorphic body of literature, three types of connectivity are assessed: (1) landscape connectivity, (2) hydrologic connectivity, and (3) sediment connectivity, and in this thesis the third type of connectivity is focused upon. Sediment connectivity refers to the transfer of sediment through detachment and transport from source to sink between various geomorphic zones at the catchment scale (Jain and Tandon, 2010; Bracken et al., 2015). The conceptual development of landscape (i.e., morphologic) and hydrologic connectivity has progressed the knowledge of sediment connectivity; however, hydrologic connectivity does not necessarily imply sediment connectivity. (Bracken et al., 2015). Hydrologic connectivity specifically refers to the connected transfer of water between sources and sinks amongst geomorphic zones, and the governing processes relegating runoff production and sediment production are well known to differ. The concept of catchment connectivity has existed in the ecological community for quite some time, but has only recently been applied to hydrologic and sedimentologic processes in catchments (Ward, 1989; Pringle, 2003). Connectivity is used to help remedy what Walling (1983) named the sediment delivery problem; i.e. that only a fraction of eroded

sediment is yielded at the catchment outlet. Analysis of this concept includes: (1) the identification of sediment sources, (2) the mechanics of sediment detachment via excessive shearing forces, (3) the entrainment and transport of sediment to downstream locations, and (4) the deposition of sediment in stores and sinks (Walling, 1983).

Sediment disconnectivity measures the distribution of sediment stores and sinks, their routes and distances of sediment transport, and assesses the inability of source to sink transport during hydrologic events (Fryirs et al., 2007); and sediment disconnectivity specifically emphasizes the impedance of sediment transport from morphologic features such as buffers, barriers, blankets (Fryirs, 2013). Buffers refer to lateral disconnecting features that limit the movement of sediment from the uplands into the stream network, such as long floodplains, which cause sediment deposition. Barriers refer to longitudinal disconnecting features that limit the movement of sediment within the stream network. Examples of barriers include manmade dams and sand bars, which accumulate sediment. Blankets refer to vertically disconnecting features that limit the surface-subsurface movement of sediment. Armoring materials found within streambeds act as blankets by preventing buried streambed sediments from erosive fluvial shear forces (Fryirs, 2007; Fryirs, 2013). Land that actively contributes to the sediment cascade at any particular time step is referred to as the active contributing area of watershed (Ambroise, 2004). Thus, sections of the catchment that do not contribute sediment to the watershed outlet (i.e. are disconnected) are not considered as a part of the active contributing area. The period when a particular landscape contributes sediment to the watershed outlet is known as the active contributing period of sediment erosion (Harvey, 2002; Fryirs, 2013). Because of disconnectivities, much of the sediment initially displaced by upland erosion is deposited

14

and seldom quickly makes it downstream to the catchment outlet at the event timescale—a phenomena referred to as the "Jerky Conveyor Belts" of sediment transport (Ferguson, 1981; Fryirs, 2013).

In general, sediment connectivity research has focused on theoretical development; and therefore most sediment connectivity models thus far are conceptual in nature or represent connectivity as an index. Previous developed sediment connectivity and (dis)connectivity models in the literature include the following. Fryirs et al., (2007) mapped disconnectivity via the active contributing area using a slope threshold method. Borselli et al., (2008) developed the index of connectivity (IC) Model, which relates the probability of upstream transport and the probability of downstream transport to an overall probability of sediment connectivity. Souza et al. (2016), Lopez-Vincent et al. (2013), Cavalli et al. (2013), Vigiak et al. (2012), and Messenzehl et al. (2014) all have used iterations of the IC model. D'Haen et al. (2013) mapped connectivity using sediment fingerprinting techniques coupled with Borselli's index of connectivity to assess sediment connectivity in Eastern Europe. Heckmann and Schwanghart (2013) used graph theory to assess the network of sediment pathways. Michaelides and Wainwright (2002) developed a basic model of connectivity that is applicable to the hillslopes. Medeiros et al (2009), modeled connectivity using re-infiltration and lateral distribution parameters to account for distributed (dis)connectivity.

2.6 Dynamic Connectivity

Connectivity is dynamic by its nature, meaning that it varies temporally based on long-term geomorphologic change and constantly changing hydrologic conditions within the catchment (Bracken et al., 2015). Long-term geomorphologic change refers to the

evolution of landscapes over time due to fluvial, eolian, or ancillary forces. Short-term hydrologic conditions refer to antecedent moisture conditions of the soil, precipitation, and runoff depth and volume. Typically, sediment connectivity models do not conceptually account for the dynamic nature of connectivity. Rather, popular connectivity models tend to assess only the static connections (i.e. physical connections) within catchments, e.g., Borselli et al., (2008). Few models capture the dynamic processes that commence sediment detachment and transport (Fryirs, 2013).

2.7 Sediment Connectivity Modeling Needs

Based on review of the sediment connectivity concepts, the authors find that few models exist that quantify sediment connectivity based on processes and rather rely on empirical indices and proxies of sediment connectivity (Medeiros et al., 2009; Bracken et al., 2015). A theoretical basis is needed that allows prediction of sediment connectivity based on the many controlling factors and processes. Therefore, herein a probabilistic framework will be proposed to meet this research need.

In addition, the authors find that dynamic sediment (dis)connectivity that incorporates temporarily varying hydrology has not been widely included in connectivity estimates (Ambroise, 2004; Lexartza-Artza and Wainwright, 2009). Therefore, herein the authors develop a theoretical basis that allows coupling of sediment connectivity formula with hydrologic modeling such as via an off-the-shelf watershed scale model.

2.8 Considerations for Coupling the Sediment Connectivity within Watershed Erosion Modelling

As mentioned, the current motivation of this research is to couple the conceptual idea of dynamic sediment connectivity and (dis)connectivity within watershed erosion

modelling, and thus advance the watershed erosion modelling platform for sedimentation and water supply needs. In this light, reservoirs serve as a major source of longitudinal sediment disconnectivity; and thus should be considered in reservoir sedimentation models. The authors suggest that several features of sediment transport phenomena should be considered in such a coupling to improve models. These features are suggested to provide a checklist to consider model effectiveness and include: consideration of conservation criteria; consideration of site specific processes within the watershed configuration; and consideration of spatiotemporal complexity. Even empirical models should at the least consider these concepts to some degree.

Conservation criteria refers to the conservation laws controlling sediment transport in a watershed and includes the conservation of mass, momentum and energy. Conventional methodologies now typically represent conservation ideas within sediment transport models through the ideas of supply, shear, and transport limitations. That is, the supply limitation refers to the conservation of mass idea, or lack thereof, in that sediment supply must be available for erosion and transport to occur. Similarly, the shear limitation refers to fluid momentum, or lack thereof, needed to initiate detachment of sediment and cause erosion; and therefore takes on a force, or momentum, derivation. Finally, the transport limitation suggests that the fluid must have sufficient power, i.e., conservation of energy, to keep sediment in transport through a watershed system.

The consideration of site specific processes within the watershed configuration suggests that a watershed erosion model that is applied to a given site should be able to represent the prominent site specific processes within the watershed. For example, if fluvial processes dominate the system then excessive shear should be explicitly considered.

17

This consideration can be addressed in watershed modelling through a mixture of conversations with watershed managers and field visits to inspect the site specific processes occurring.

The consideration of spatiotemporal complexity is perhaps somewhat specific to the advancement sought after in this research, but nevertheless the authors highlight its importance. The spatial resolution of the watershed configuration should be explicitly considered, if possible, in order that the spatial variability of processes be ascertained. Further, temporal complexity associated with hydrologic events and the runoff it produces should be considered.

2.9 Thesis Objectives

The overall goal of this research was to improve watershed erosion modelling through coupling the dynamic sediment connectivity and (dis)connectivity concepts within numerical modeling to predict how sedimentation will impact water supply. Specific objectives were:

1. Develop a watershed erosion modelling framework that explicitly incorporates sediment connectivity and disconnectivity concepts.

2. Develop a theoretical probability of sediment connectivity model that can incorporate the multiple processes impacting connectivity and (dis)connectivity.

3. Develop a theoretical method to predict dynamic connectivity and couple it with a hydrologic model.

4. Apply the watershed erosion model within a geospatially explicit computational framework that includes sediment (dis)connectivity to the water supply problem in Kentucky USA.

Chapter 3 Probability of (Dis)Connectivity Model Framework and Formulation

3.1 Probability-based Model for Sediment (Dis)Connectivity

The probability of sediment (dis)connectivity is defined as the probability that a watershed or region of a watershed is connected with respect to its ability to produce and transport sediment laterally and longitudinally within the fluvial network (Borselli et al., 2008). Using a probability-based model, the probability of connectivity is theorized to reflect the intersecting probabilities (i.e., multiplicative probabilities) of numerous sub-components of sediment transport. In this manner, the probability of sediment (dis)connectivity model reflects the co-occurrence, or lack thereof, of sediment supply, detachment, transport, and disconnectivity via features or human interaction, as these processes are well known to potentially control transport (Renard et al., 1996; Fryirs et al., 2007; Russo and Fox, 2012; Bracken et al., 2015). The probability-based model presented in this thesis for sediment connectivity aims to incorporate the hydrologic conditions for which transport may occur and therefore the energy of individual hydrologic events to initiate transport of sediment is explicitly included in the model. Such explicit representation of hydrologic events allows for representation of the temporal variability (i.e. dynamic nature) of sediment connectivity within a probabilistic framework and allows for inclusion of hydrologic connectivity within a watershed, which is expected to partially control some aspects of sediment connectivity (Jensco et al., 2009). Non-hydrologic connectivity, i.e. connectivity caused by non-fluvial processes, is also included within the model framework given the recent realization of its prevalence in some systems at some time scales (Bracken et al., 2015). Further, it is intended that the probability-based model of connectivity could be discretized spatially across a watershed such that as within a

spatially explicit sediment transport model for a watershed. Finally, the concept of disconnectivity (Fryirs et al., 2007, Fryirs, 2013) via morphologic features and anthropogenic obstacles and revetments is explicitly included into the probability-based modeling framework given the recent realization that buffers, barriers, and blankets can create sediment disconnectivity within a watershed system.

With the aforementioned processes in mind, Figure 3.1 shows the authors' concept of a probability-based model for sediment connectivity. The intersecting probabilities of sediment supply, detachment, transport, and a lack of disconnectivity produce the probability of sediment connectivity for the watershed or region of a watershed. In Figure 3.1, the union of both hydrologic and non-hydrologic processes are included within sediment detachment as well as sediment transport. Mathematically, the probability of sediment connectivity, $P(C)$, can be expressed as

$$P(C) = P(S) \cap P(D_H \cup D_{NH}) \cap P(T_H \cup T_{NH}) \cap \{1 - P(D_C)\} \qquad \text{(Eq. 3.1)}$$

where S denotes supply, D_H is hydrologic detachment, D_{NH} is non-hydrologic detachment, T_H is hydrologic transport, T_{NH} is non-hydrologic transport, and D_C is disconnectivity. The intersections and unions of probabilities is further expressed via their multiplicative and summation definitions as

$$P(C) = \{P(S)\} \times \{P(D_H) + P(D_{NH}) - P(D_H)P(D_{NH})\} \times \{P(T_H) + P(T_{NH}) -$$

$$P(T_H)P(T_{NH})\} \times \{1 - P(D_C)\} \qquad \text{(Eq. 3.2)}$$

In this manner, the probability of sediment connectivity can be calculated when each individual process-associated probability is known or can be estimated.

The general probability-based model shown by Equation (3.2) can be applied to a given region of a watershed (i.e., plot, hillslope, or low order catchment) or calculated for an entire watershed by using spatially explicit information across the landscape. The former reflects a lumped parameter estimation of the probability of sediment connectivity while the latter reflects a distributed watershed modeling framework. The latter has specific utility in sediment transport modeling because the probability of sediment connectivity associated with a hydrologic event for a set of distributed differential watershed areas could be integrated. Integration of the net watershed probability of sediment connectivity has the potential efficacy of providing an estimate of the active watershed area in terms of sediment transport when multiplied by the watershed area.

It is intended that the multiplicative probabilities in Figure 3.1 and Equation (3.2) provide a general conceptual framework for the probability of sediment connectivity. Parameterization of the individual probability distributions will vary depending on the timescale of intent, the spatial scale reflecting a plot, hillslope, catchment, or entire watershed, the dominant sediment transport processes distributed across the upland landscape (e.g., mass wasting, fluvial erosion, eolian transport), and the geomorphologic template of the watershed coupled with anthropogenic landscape features. In the present thesis and for the example illustrated in this work, the authors parameterize the probability of sediment connectivity by specifically considering fluvial dominated systems with the potential for mixed landscape features by varying a spectrum of anthropogenic disturbance, as detailed in Chapter 6. At the same time, the authors keep in mind a prevalence of agricultural practices that might promote an unconsolidated and low cover soil surface, at least at some times of the annum in some portions of the watershed. In this manner, the

authors' intent for the present probability model specification is to illustrate how the individual probability-based components of the probability of sediment connectivity can be mathematically coupled within Equation (3.2) by incorporating both process-based formula and the physical conditions of the landscape geomorphology and anthropogenic disturbances.

It is intended for hydrologic modelling to be coupled with geospatial data and field disconnectivity reconnaissance to dynamically predict the probability of connectivity at the watershed scale at a specified time step. The probability of connectivity result indicates the percent of the catchment that has the potential to contribute sediment to the watershed outlet at a particular time step, which identifies the active contributing area and period as described by Ambriose (2004).

The probability of connectivity can then be coupled with an erosion or sediment transport model to predict sediment flux at the watershed outlet. Figure 3.2 summarizes this methodology.

Figure 3.1: Graphical representation of the probability of connectivity model to predict sediment connectivity in the uplands of watersheds

SUPPLY

DETACHMENT

TRANSPORT

DISCONNECTIVITY

CONNECTIVITY

Probability of Sediment Supply, $P(S)$

Probability of Hydrologic Detachment, $P(D_H)$

Probability of Nonhydrologic Detachment, $P(D_{NH})$

Probability of Hydrologic Transport, $P(T_H)$

Probability of Nonhydrologic Transport, $P(T_{NH})$

Probability of Sediment No Disconnectivity, 1-$P(D)$

Probability of Sediment Connectivity, $P(C)$

SUPPLY

DETACHMENT

TRANSPORT

DISCONNECTIVITY

CONNECTIVITY

$P(S)$

$\cap$

$P(D_H \cup D_{NH})$

$\cap$

$P(T_H \cup T_{NH})$

$\cap$

$[1 - P(D_C)]$

$P(C)$

Figure 3.2: Sediment flux prediction methodology

```
┌──────────────┐    ┌──────────────────┐    ┌──────────────────┐
│              │    │ Field Disconnect.│    │                  │
│ Geospatial   │    │ Reconnaissance   │    │ Hydrologic       │
│ Data         │    │                  │    │ Modeling         │
└──────┬───────┘    └────────┬─────────┘    └────────┬─────────┘
       │                     │                       │
       │            ┌────────▼─────────┐             │
       └───────────►│  Probability of  │◄────────────┘
                    │  Sediment        │
                    └────────┬─────────┘
                             │
┌──────────────┐    ┌────────▼─────────┐
│ Erosion      │───►│ Active           │
│ Modelling    │    │ Contributing Area│
└──────────────┘    └────────┬─────────┘
                             │
                    ┌────────▼─────────┐
                    │ Sediment flux    │
                    │ prediction       │
                    └──────────────────┘
```
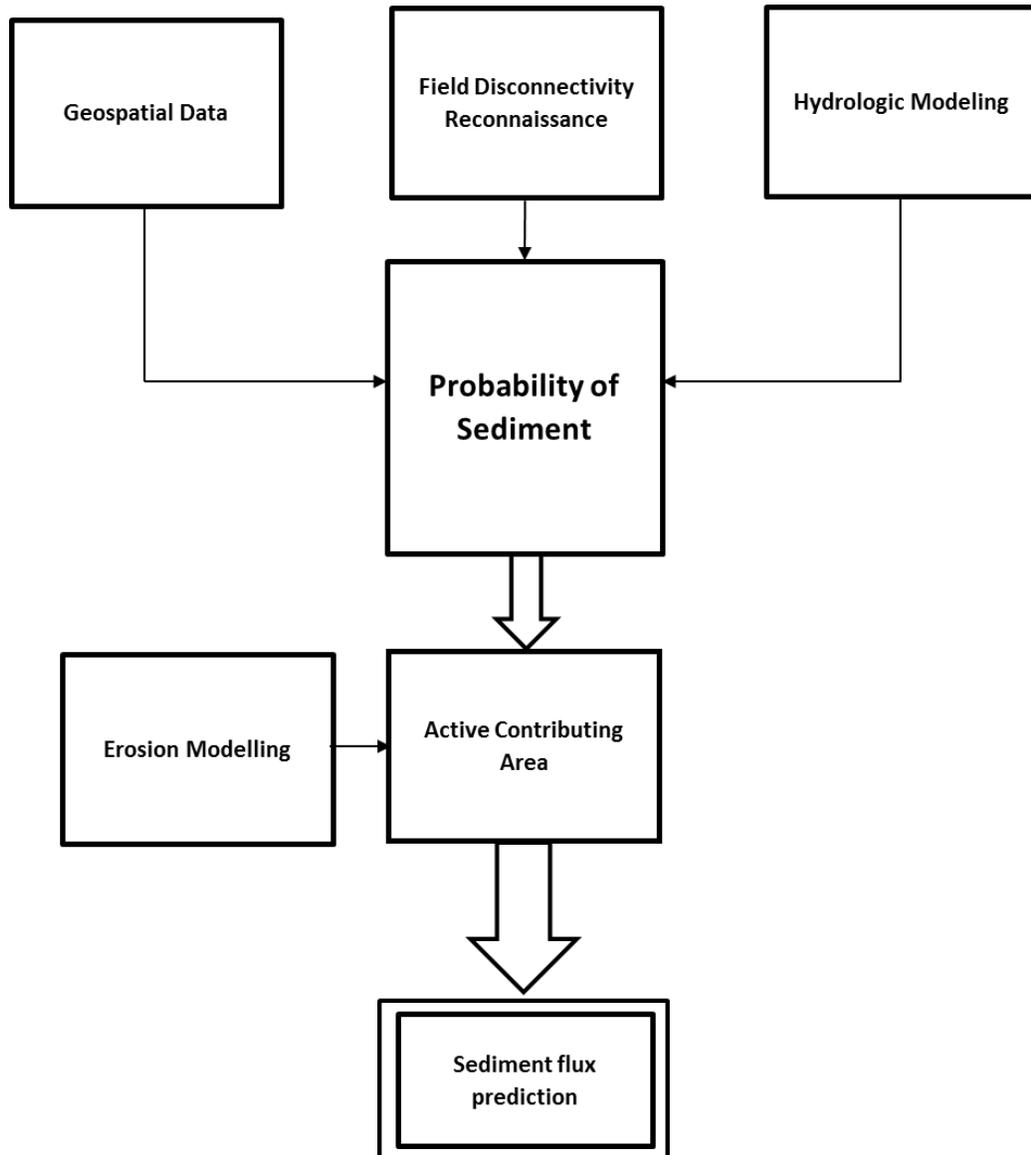
Chapter 4 Physiogeographic Characterization of the Study Watershed

4.1 Kentucky River Basin Characteristics

The Kentucky River Basin is a HUC 6 watershed (ID 051002) that drains 18,038.8 km^2 over four physiographic regions in central and southeastern Kentucky, as shown in Figure 4.1 (Kentucky Division of Water, 1998). The Kentucky River flows 255 miles northwest from the convergence of the North, Middle, and South forks of the Kentucky River in eastern Kentucky to the Ohio River as shown in Figure 4.2 (U.S. Geologic Survey, 2004; USGS Kentucky Water Science Center, 2014). It serves as the main source of water supply for nearly 710,000 people in the state, servicing water to several major cities such as Lexington, Frankfort, and Versailles and 42 of the 121 counties within the state (Johnson and Parrish, 1999; Banks, 2014; KRA, 2016).

4.1.1 Kentucky River Physiography, Geology, Soils, and History

The Kentucky River Basin encompasses four of Kentucky's nine physiographic regions: the Inner Bluegrass, Outer Bluegrass, Knobs, and Eastern Coal Fields. Within the Kentucky River Basin, topography widely ranges from approximately 3,290 feet in the uplands of the watershed in eastern Kentucky to approximately 420 feet at the watershed outlet to the Ohio River as shown in Figure 4.3 (KYAPED, 2014). Unique topography, geology, and pedology control the static connectivity of the Kentucky River Basin and characterize each physiographic region in Kentucky, as shown in Figure 4.4, 4.5, and 4.6, respectively (KYAPED, 2014). The geologic, geomorphologic, and anthropogenic history of the Kentucky River Basin has also been chronologized to understand historic sediment source pathways and disconnectivities, as well as catalysts of watershed erosion and sedimentation.

4.1.1.1 Inner Bluegrass Region

The Inner Bluegrass region is located in central Kentucky and houses several of the State's major cities. Together, the Inner Bluegrass, Outer Bluegrass, and Knobs region make up the Bluegrass Plateau that is generally flat with rugged edges. The topography of the Inner Bluegrass is characterized by gently rolling hills and relatively mild slopes (Kentucky Department of Fish and Wildlife Resources, 2013). Steep slopes on the banks of the Kentucky River indicate that bank erosion may contribute to the Kentucky River's sediment yield in this region. The highest elevation within the region is approximately 1000 feet above mean sea level (MSL) while the lowest is approximately 700 feet above MSL according to DEMs created by Kentucky Aerial Photography and Elevation Data (KYAPED, 2014). The region makes up approximately 19% of the entire Kentucky River Basin.

The central portion of the Inner Bluegrass consists primarily of McAfee-Maury silt loam, which tends to drain well with moderately slow permeability. The soil's depth to bedrock tends to be from 20 to 40 inches. Other soils within the Inner Bluegrass region are classified as Lowell, Nicholson, Faywood, and Fairmont series that are well-drained and formed from limestone residuum in watershed uplands. The depths of these soils range from shallow to deep depending on the series (USDA, 2006).

The Inner Bluegrass is intensely prone to karst due to the high amount limestone found within the region. (Campbell, 1996; Currens et al., 2012; KGS, 2012; Newell, 2001). Karst can serve as a vertical and longitudinal source of disconnectivitiy within stream networks. Nearly 55% of Kentucky has the potential for karstic geography (Currens and Paylor, 2009). Within the Kentucky River Basin, 30% of the basin has at least moderate

27

potential for karst. Large amounts of underlying limestone that heavily compromise the bedrock in the Bluegrass Physiographic region attribute to the karstic geography. The dissolution of limestone particles from acidic runoff and groundwater leads to the formation of fissures, aquifers, sinkholes, and swallets, which can convey and store water and sediment (Smart and Hobbs, 1986). Figure 4.6 shows potential karstic landscapes and sinkhole locations in the Kentucky River Basin (Currens et al., 2012; KGS, 1998; Currens and Paylor, 2009).

Stratigraphic units in the Kentucky River Basin range in age from the Late Ordovician period (approximately 450 million years ago) to the Middle Pennsylvanian period (approximately 350 million years ago). The Kentucky River Basin comprises of five stratigraphic units: the Ordovician System, the Silurian System, the Devonian System, the Mississippian System, and the Pennsylvanian System (McDowell et al. 1986). The Inner Bluegrass region is primarily underlain by Lexington-Limestone and shale from the Ordovician period. Alluvium, which is made up of clays, silts, gravels, and some fine sands, surrounds the Kentucky River in the northern part of the Inner Bluegrass region. Small amounts of Ordovician-aged siltstone can also be found in the northern- and southern-most parts of the region (McGrain, 1983; McDowell et al. 1986; Andrews, 2004; Kentucky Department of Fish and Wildlife Resources, 2013). Ordovician rocks formed from sediment deposition from shallow tropical seas, lagoons, and tidal flats. Calcite and microspar cemented sediments to form the fossiliferous limestones. These rocks were buried and have since been outcropped through erosive processes (McDowell et al., 1986).

Land use in the Inner Bluegrass region consists of primarily agricultural and urban areas, as shown in Figure 4.8. Approximately 37% of the region consists of agricultural

land and 45% of the region consists of urban land, with the remaining 18% forested areas (NLCD, 2006). The Inner Bluegrass houses several of Kentucky's major cities, including Lexington and Frankfort. Tributaries in the Kentucky River Basin often experience moderate to severe bank erosion due to increased peak flow rates from urbanization. Within the stream corridors of the Inner Bluegrass, sediment sources include stream bank erosion, streambed erosion, and erosion of the surficial fine-grained laminae. In the uplands of the Inner Bluegrass, sediment sources include construction sites, agricultural lands, and concentrated flow paths from roadways. The lock and dam system on the Kentucky River, as shown in Figure 4.9, is a major source of longitudinal disconnectivitiy in the Kentucky River Basin. The lock and dam system on the Kentucky River was implemented in the mid- to late-1800s and originally served as year-round transportation for local commerce by fixing the minimum stage of each pool (Johnson and Parrish, 1999). By the mid-1900s, no commercial navigation of the Kentucky River existed, but the lock and dam system remained intact for water supply purposes. Only several of the locks on the Kentucky River are presently functional. Dredging occurs upstream and downstream of functional locks due to occasional sediment build up (KRA, 2015). Six of the fourteen lock and dams on the Kentucky River are located in the Inner Bluegrass.

Many researchers (Leverett, 1902; Tight, 1903; Andrews, 2004) have debated the historic geomorphologic configuration of the Kentucky River Basin. It is hypothesized that the headwaters of the Kentucky River originated in the Blue Ridge Mountains, and due to tectonic activity have shifted to their current location (Jillson, 1963). Geographic Information Systems and the mapping of fluvial deposits has led to the identification of paleochannels and abandoned meanders within the Basin, several of which are located

between kilometers 22 and 87 of the Kentucky River. Andrews (2004) mapped many of the abandoned meanders and paleochannels in his doctoral dissertation. Generally, the Kentucky River flows to the northwest at a slope of approximately 0.15 m/km. In the lower (downstream) zones of the Kentucky River, alluvium deposits have been mapped as wide as 1,500 m. In the upper (upstream) zones, alluvium deposits are only approximately 200 m at times (Andrews, 2004).

4.1.1.2 Outer Bluegrass Region

The Outer Bluegrass region surrounds the Inner Bluegrass region and is characterized by rugged and deep valleys as compared to the Inner Bluegrass (Kentucky Department of Fish and Wildlife Resources, 2013). The slope of the land is slightly steeper in the northern portion of the region than the Inner Bluegrass. The highest portions of the watershed are approximately 1,100 feet above MSL in the southeastern portion of the region and the lowest elevations near the basin outlet are approximately 600 feet above MSL (KYAPED, 2014). This region makes up approximately 24% of the entire Kentucky River Basin.

Soils within this region consist of primarily Lowell, Nicholson, Eden, Elk, McAfee, Faywood, Shelbyville, and Maury series which are generally well drained, moderately deep, silty loams interspersed with clay. Interbedded fragments of limestone and sandstone exist throughout the region. In most of the soil series, permeability is moderately slow to slow, which is consistent with silty loams and clayey soils. Soil hazards include landslides due to poor slope stability (USDA, 2006).

Bedrock consists of primarily Ordovician-aged siltstones, shales, and limestones in the northern portion of the Outer Bluegrass region. Lexington Limestone is interspersed

throughout Garrard Siltstone and shale. Alluvium deposits are located around the banks of the Kentucky River. The southern portion of the Outer Bluegrass region primarily consists of shale and limestone. The region is subject to moderate karst potential due to the dissolution of limestone (Campbell, 1996; Currens et al., 2012; KGS, 2012). Silurian aged rocks are sparsely found at the edge of the Outer Bluegrass region in a narrow belt. These rocks originate from marine environments and are approximately 440 million years old. Primarily, the Silurian outcrop in the Kentucky River Basin consists of dolomite, shale, and minor amounts of limestone and chert. The dolomite and limestone are composed of skeletons of animals that lived in warm, shallow seas. The thickness of Silurian outcrops ranges from 0 to 300 feet thick (McGrain, 1983; McDowell et al. 1986; Andrews, 2004; Kentucky Department of Fish and Wildlife Resources, 2013).

Land use in the Outer Bluegrass region consists of primarily agricultural and forested areas, as shown previously in Figure 4.8. Approximately 48% of the region consists of agricultural land and 45% of the region consists of forested land, with the remaining 7% urban areas (NLCD, 2006). Within the stream corridors of the Outer Bluegrass, sediment sources include stream bank erosion, streambed erosion, and erosion of the surficial fine-grained laminae. In the uplands of the Outer Bluegrass, sediment sources include construction sites, agricultural lands, concentrated flow paths from roadways, and deforestation (Blanford, 2017; Gumbert, 2017; Smallwood, 2017). Four of the fourteen lock and dams on the Kentucky River are located in the Outer Bluegrass.

4.1.1.3 Knobs Region

The Knobs region makes up a small portion (4%) of the Kentucky River Basin (KYAPED, 2014). The region gets its name from the hundreds of conical, isolated hills,

which separate the Eastern Coal Fields from the Bluegrass plateau. The Knobs were once a part of the Mississippian Plateau (also called the Eastern Pennyroyal region of Kentucky) and were eventually separated by stream erosion (Campbell, 1996; KGS, 2012). The Knobs (mostly underlain by sandstones and limestones) are less prone to erosion than the previously overlying siltstone and shale, resulting in their formation (Kentucky Department of Fish and Wildlife Resources, 2013). Elevation ranges between 600 feet to 1,600 feet above MSL. Slopes, especially surround the conical hills can be very steep.

Soils consists of Lowell, Faywood, Eden, Cynthiana, Shrouts, Brassfield, Beasley, Robertsville, Nicholson, Lawrence, Lenberg, Garmon, and Fredrick series which are well drained silt loams and clays on ridges and side slopes. These soils are the residuum of shale, siltstone, and limestone. Soil depth ranges from deep to moderately deep in most instances and permeability is moderately low (USDA, 2006).

The majority of the Knobs region consists of Devonian black shales, as well as limestones and sandstones. Shale is typically found at the base of the knobs since it is more erodible than the overlying limestone and sandstone caps, which are Ordovician-age (i.e. over 400 million years old). Silurian, Devonian, and Mississippian limestone outcrops are also associated with the region. The rocks from the Mississippian period indicate extensive shallowing of the seas and are represented by mostly sedimentary rocks that at one point in time were spread across the entire state. Limestones, sandstones, and shales dominate the strata. The Mississippian period lasted from roughly 360 million years ago to 320 million years ago (McGrain, 1983; McDowell et al. 1986; Andrews, 2004; Kentucky Department of Fish and Wildlife Resources, 2013). Karst potential throughout parts of the

watershed underlain by limestone is moderate (Campbell, 1996; Currens et al., 2012; KGS, 2012).

Land use in the Knobs region consists of primarily agricultural and forested areas, as shown previously in Figure 4.8. Approximately 49% of the region consists of agricultural land and 41% of the region consists of forested land, with the remaining 9% urban areas (NLCD, 2006). Within the stream corridors of the Knobs region, sediment sources include stream bank erosion, streambed erosion, and erosion of the surficial fine-grained laminae. In the uplands of the Knobs region, sediment sources include construction sites, agricultural lands, concentrated flow paths from roadways, and deforestation (Blanford, 2017; Gumbert, 2017; Smallwood, 2017). One of the fourteen lock and dams on the Kentucky River are located in the Outer Bluegrass.

4.1.1.4 Eastern Coal Fields Region

The Eastern Coal Fields region, located on the Cumberland Plateau, makes up the southern 52% of the Kentucky River Basin. The elevation of the Eastern Coal Fields ranges between approximately 1,000 feet above MSL in the lowest parts of the region and 3,200 feet above MSL in the uplands (KYAPED, 2014). The region is characterized by steep, narrow ridges and narrow valleys. Prior to human disturbance and mining, the highest elevation in the state was 4,145 feet above MSL located in the Eastern Coal Fields (Newell, 2001). Slopes in this region are the steepest in the state. Pine Mountain, in the eastern most part of the region, is a 125-mile long mountain range that formed around 230 million years ago (Kentucky Department of Fish and Wildlife Resources, 2013).

Major soil series within the region are Steinburg, Shelocta, Gilpin, Latham, Shrouts, and Rigley silt loams and clays. These soils form in very steep areas and are

typically deep to very deep. In most instances, the soil is well drained and moderately permeable. The soils are the residuum of shale, siltstone, sandstone, or colluvium (USDA, 2006).

Pennsylvanian rocks comprise the majority of the geology of the Eastern Coal Fields. Pennsylvanian strata compose nearly 50% of the Kentucky River Basin, located east of the Knobs region in the Basin. This deposit is part of the Appalachian basin, and is characterized by coal seams buried beneath the Cumberland Plateau. Some researchers believe that Pennsylvanian strata were once continuously deposited across central Kentucky. However, it is believed that large portions of the strata have been removed through erosive processes. Pennsylvanian rocks are predominantly sandstone, siltstone, and shale. Marine shale and limestone are also widespread throughout the region. This indicates that during the formation of Pennsylvanian deposits, swamps, shallow bays, and estuaries likely covered Kentucky. The deposition of the strata resulted from piedmont, alluvial, and costal-plain environments spread across the state during the Pennsylvanian age. The origin of the Appalachian Mountains found in the eastern portion of the Kentucky River Basin date back to nearly 480 million years ago. During the Ordovician period, an oceanic tectonic plate began to submerge beneath the North American tectonic plate thus forcing land upwards. The subduction of the oceanic plate lead to the formation of volcanoes – thus warping previously deposited sedimentary rock. Several other mountain building series existed following the Ordovician period until the Pennsylvanian period as tectonic plates continued to submerge beneath the North American tectonic plate. During the Mesozoic period, erosion and weathering began to wear the mountains away (McGrain, 1983; McDowell et al. 1986; Andrews, 2004).

Moderate karst potential exists in the northwest portion of the Eastern Coal Fields, but is not as concentrated as the other physiographic regions (Campbell, 1996; Currens, 1998; KGS, 1998; Newell, 2001). Devonian strata is also found in the eastern most portion of the Kentucky River Basin and comprises of limestones, dolostones, and a deposit of shale ranging in thickness from 4 feet to over 1,000 feet. Devonian rocks of the Kentucky River Basin are assumed to have accumulated in a gradually deepening sea. Organic-rich muds were deposited from this sea that lead to the formation of the thick shale layer. This period spanned roughly 420 to 360 million years ago (McGrain, 1983; McDowell et al. 1986; Andrews, 2004; Kentucky Department of Fish and Wildlife Resources, 2013).

Land use in the Eastern Coal Fields region consists of primarily forested and agricultural areas, as shown previously in Figure 4.8. Approximately 78% of the region consists of forested land and 14% of the region consists of agricultural land, with the remaining 8% urban areas (NLCD, 2006). Within the stream corridors of the Eastern Coal Fields region, sediment sources include stream bank erosion, streambed erosion, and erosion of the surficial fine-grained laminae. In the uplands of the Eastern Coal Fields region, sediment sources include construction sites, agricultural lands, concentrated flow paths from roadways, deforestation, and mining processes (Blanford, 2017; Gumbert, 2017; Smallwood, 2017). Three of the fourteen lock and dams on the Kentucky River are located in the Outer Bluegrass.

4.1.3 Kentucky River Basin Climate

The Kentucky River Basin's climate is classified as humid subtropical (Ulack et al., 1998). According to the National Oceanic and Atmospheric Administration (NOAA), on average, the Basin receives 45 to 50 inches (1140 to 1270 mm) of precipitation, 10 to

12 inches (250 mm to 300 mm) of which are snow. The average annual temperature ranges between 54°F to 58°F (12.2°C to 14.5°C). The minimum average temperature is approximately 32.9°F (0.5°C) in January and the maximum average temperature is approximately 76.2°F (24.5°C) in July.

4.2 Study Watershed

The probability of (dis)connectivity model was applied to only a portion of the Kentucky River Basin due to the availability of sediment flux data and to reduce computation complexity of the numerical model. The Upper South Elkhorn watershed (65.1 km^2), located in the Inner Bluegrass physiographic region of Kentucky near the city of Lexington and the University of Kentucky is shown in Figure 4.10. The Upper South Elkhorn is a mixed land use watershed, consisting of primarily agricultural lands (55%) and urban areas (45%) as shown in Figure 4.11 (NLCD, 2006). The Upper South Elkhorn watershed was chosen for model application because of (i) the dominance of instream and upland sediment transport processes contributing to sediment flux; (ii) past studies conducted on the watershed including sediment source tracing via fingerprinting (Davis, 2008), sediment transport modeling (Russo, 2009), instream organic carbon fate and transport (Ford, 2011), and surficial fine-grained laminae control on stream carbon and nitrogen cycles (Ford, 2014); (iii) on-going data collection and research conducted by the University of Kentucky, Lexington-Fayette Urban County Government (LFUCG), and USGS; and (iv) the proximity of the watershed to the University of Kentucky.

4.2.1 Study Watershed Physiography

The South Elkhorn Creek is a lowland stream with an initial elevation of 297.3 meters above MSL. At the watershed outlet, the elevation of the channel is approximately

36

254.4 meters above MSL. The stream drops nearly 42.7 meters over the 16.9-kilometer path from the headwaters to the watershed outlet; thus, the slope of the channel is approximately 0.00254 m/m. The South Elkhorn Creek primarily conveys flow year-round. The channel consists of bedrock, weeds, sands, fine sediments, and stones. The Upper South Elkhorn watershed is located in the Inner Bluegrass region of Kentucky, which is characterized by gently rolling hills and relatively mild slopes.

Headwaters of the South Elkhorn Creek originate in southwestern Lexington, within urban areas. There is one active United States Geologic Survey (USGS) gage located near the watershed outlet. Discharge data is available between 10-01-2007 until the present. Flowrate, precipitation, and turbidity data have been collected since 10-18-2015 until the present. The flowrate, as measured at the USGS gaging site, is less than approximately 0.06 CMS during low flows, between 0.28 CMS during normal conditions, and greater than 2.26 CMS during high flows.

The National Oceanic and Atmospheric Administration (NOAA) maintain a precipitation and temperature monitoring station at the Lexington Bluegrass Airport, which is northeast of the watershed. Data has been collected and published between 1981 and 2010, recording the temperature, rainfall, and snowfall averages. Temperatures range between, on average, 32.9°F (0.5°C) in January to 76.2°F (24.5°C) in July. The average yearly rainfall for this region is approximately 45.2 inches (1148 mm). The average yearly snowfall for this region is 13.0 inches (330 mm). The Upper South Elkhorn's climate is classified as humid subtropical (Ulack et al., 1998).

Bluegrass-Murray silt loams primarily make up the South Elkhorn watershed's soil matrix. Bluegrass-Murray silt loams are categorized under the hydrologic soil group "B",

are very deep, well drained, and have moderate permeability (NRCS, 2011). The large amounts of underlying Lexington Limestone that heavily compromise the bedrock in the Upper South Elkhorn watershed attribute to a moderate karst potential (Currens, 1998).

4.2.2 Study Watershed Sediment Transport Processes

Sediment particles are sourced from various agricultural and urban land uses within the Upper South Elkhorn watershed. Within the stream corridor, primary sediment transport processes include streambank erosion, streambed erosion, surficial fine-grained laminae erosion, and mass wasting (Russo and Fox, 2012). Based on visual observation, eroding streambanks are prominent throughout the watershed and are a primary source of instream erosion. Urbanization in the Upper South Elkhorn watershed is a suspected cause of the exacerbated streambank erosion (Russo, 2009). Upland erosion production occurs primarily through rill erosion, ephemeral gully erosion, and concentrated flow pathways, while diffusional erosion processes (i.e. sheet and interrill erosion) are believed to provide a minor contribution to the overall sediment flux at the watershed outlet (Blanford, 2017; Gumbert, 2017; Smallwood, 2017). Livestock and construction sites in the uplands exacerbate the detachment rates of sediment particles through the removal of protective vegetation and exposure to excessive eolian and fluvial shear stresses (Evans, 2017). The Upper South Elkhorn watershed is also characterized by long, flat floodplains adjacent to the stream network. Based on studies conducted by Fryirs et al., (2007) and the authors' observations from field visits, these floodplains are suspected to force sediment to fall out of suspension and be deposited prior to entering the stream network, causing sediment disconnectivitiy. Connectivity to the floodplains generally occurs one to two times per year when bankfull flow is breached and the floodplains are inundated.

Figure 4.1: Kentucky River physiographic regions

Legend

REGION
- Eastern Coal Field
- Eastern Pennyroyal
- Inner Bluegrass
- Knobs
- Outer Bluegrass

Lexington

N

0 10 20 40 60 80
KM
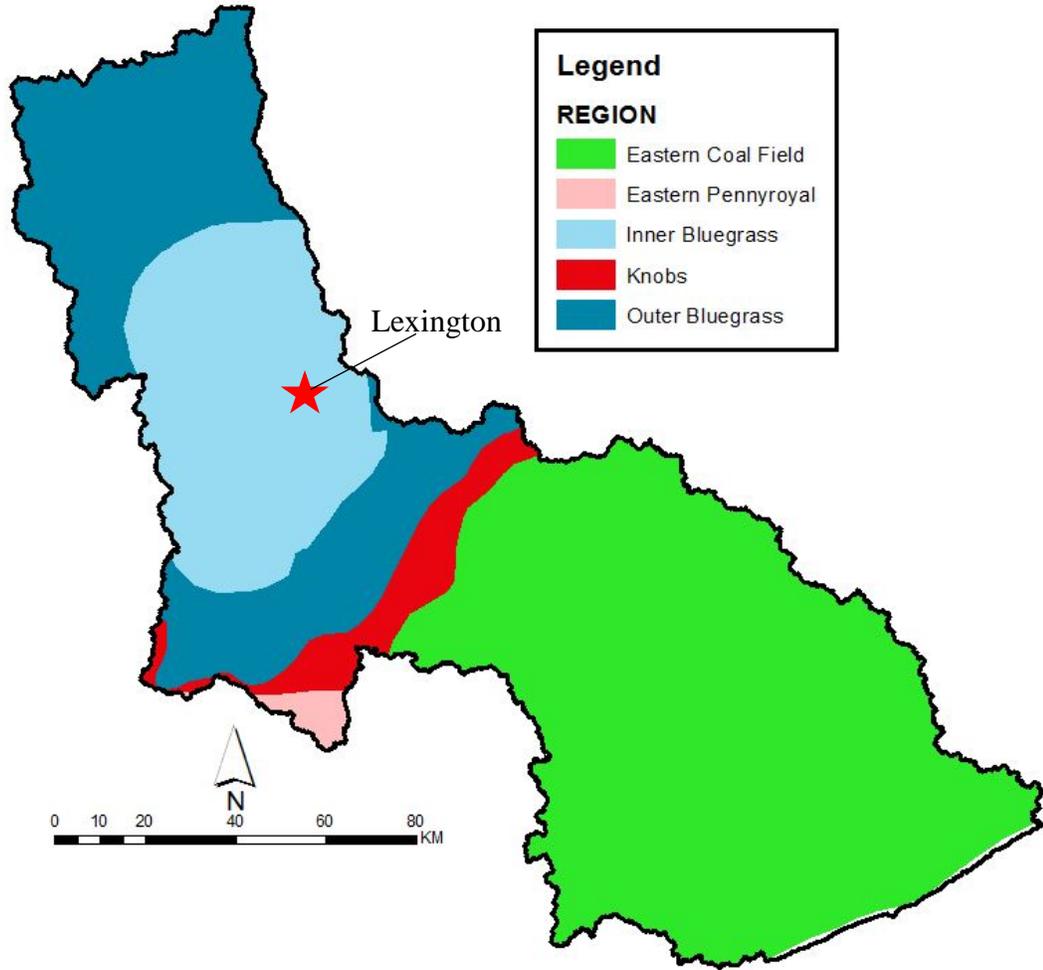
Figure 4.2: Kentucky River Basin location
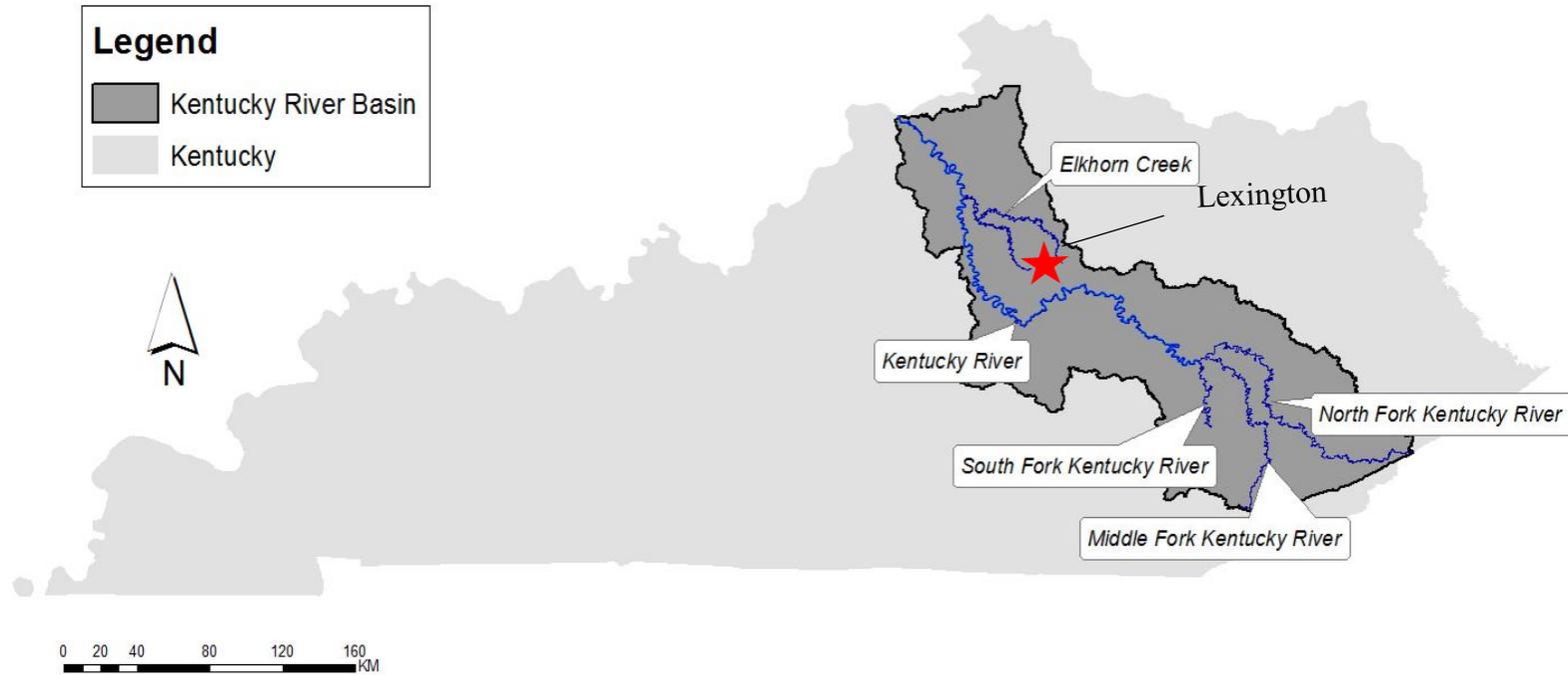
Figure 4.3: Kentucky River Basin elevation (KYAPED, 2014)
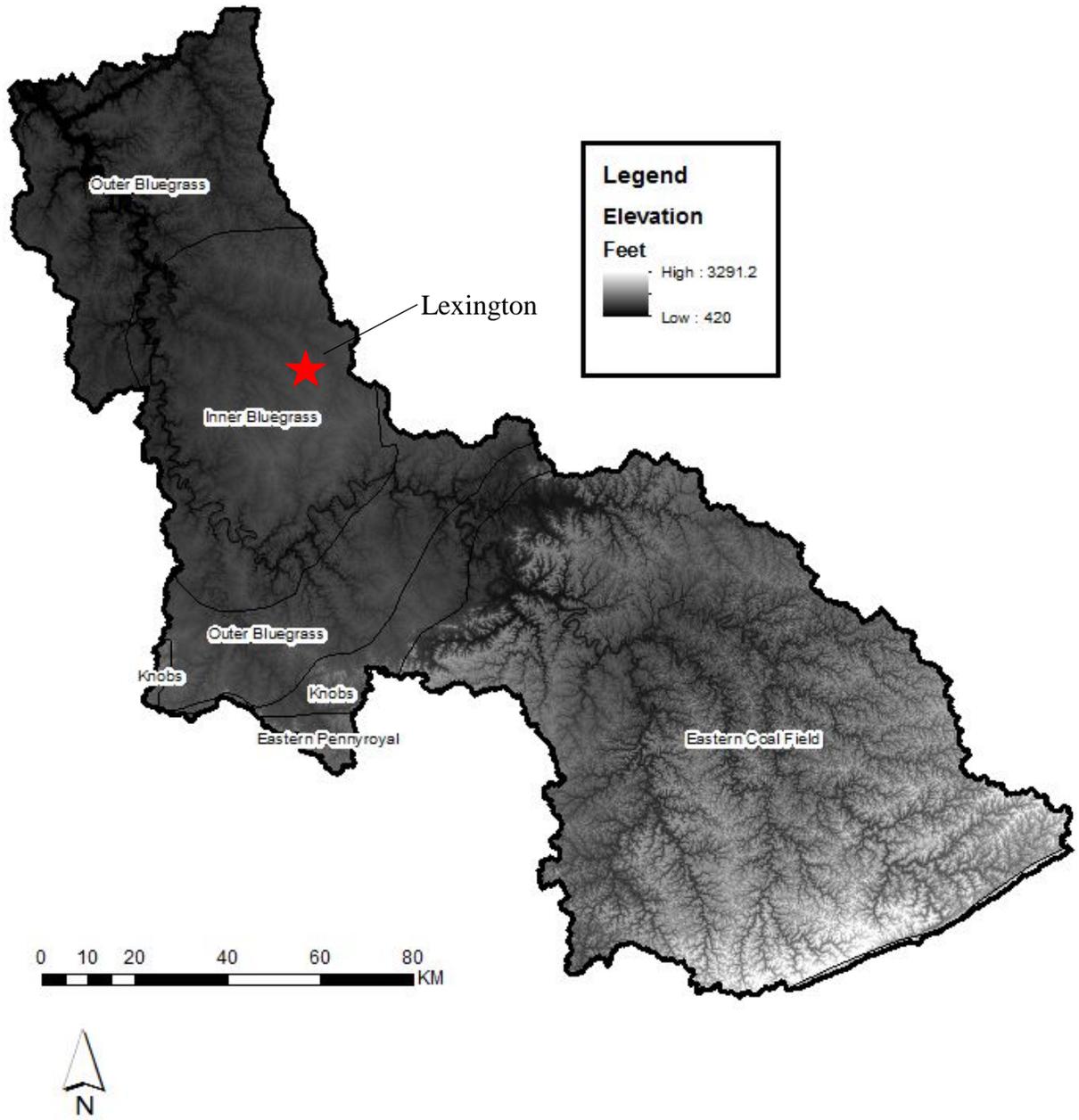
Figure 4.4: Kentucky River Basin slope (KYAPED, 2014)
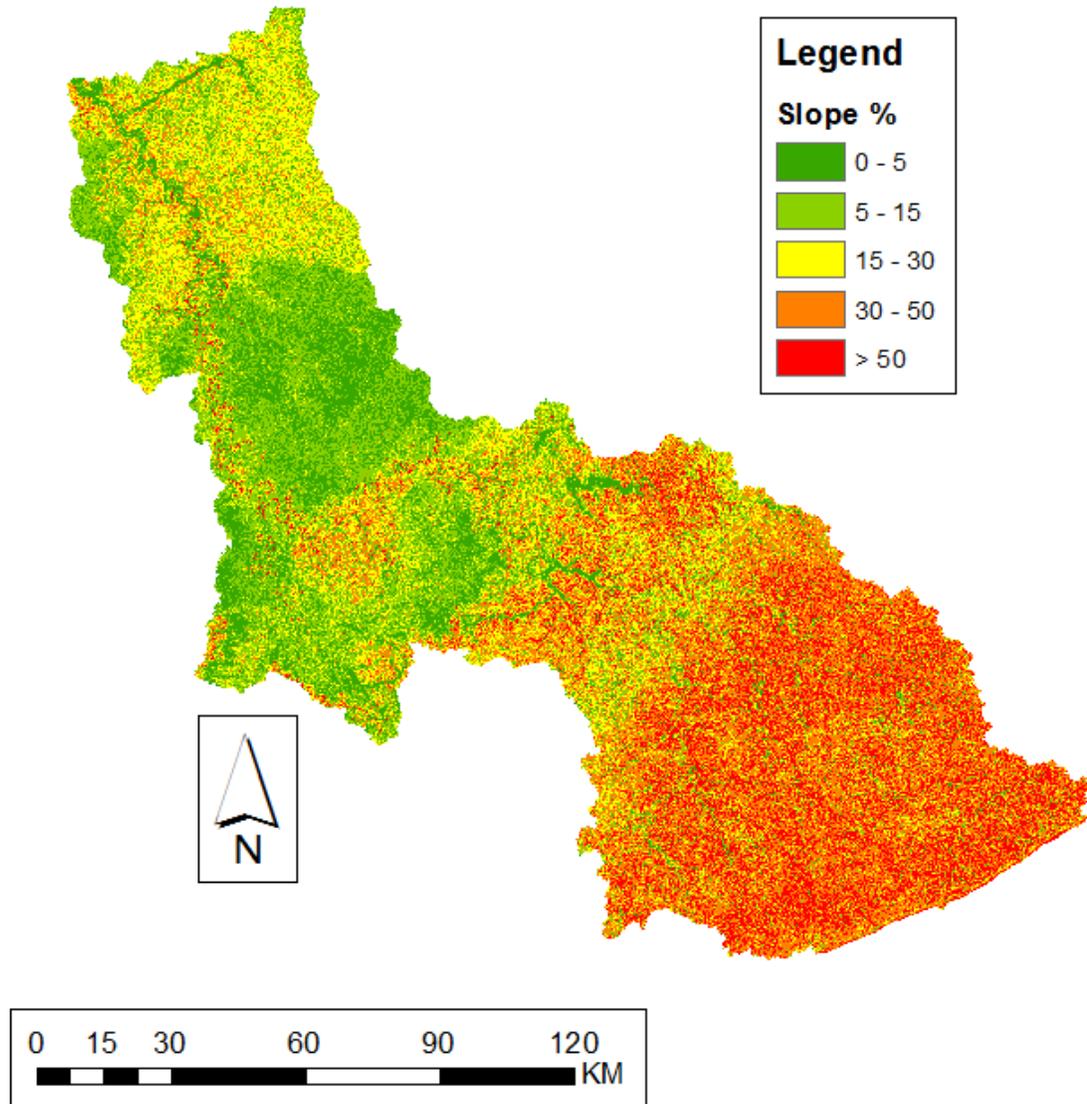
Figure 4.5: Kentucky River Basin geology (Kentucky Geologic Survey, 2012)
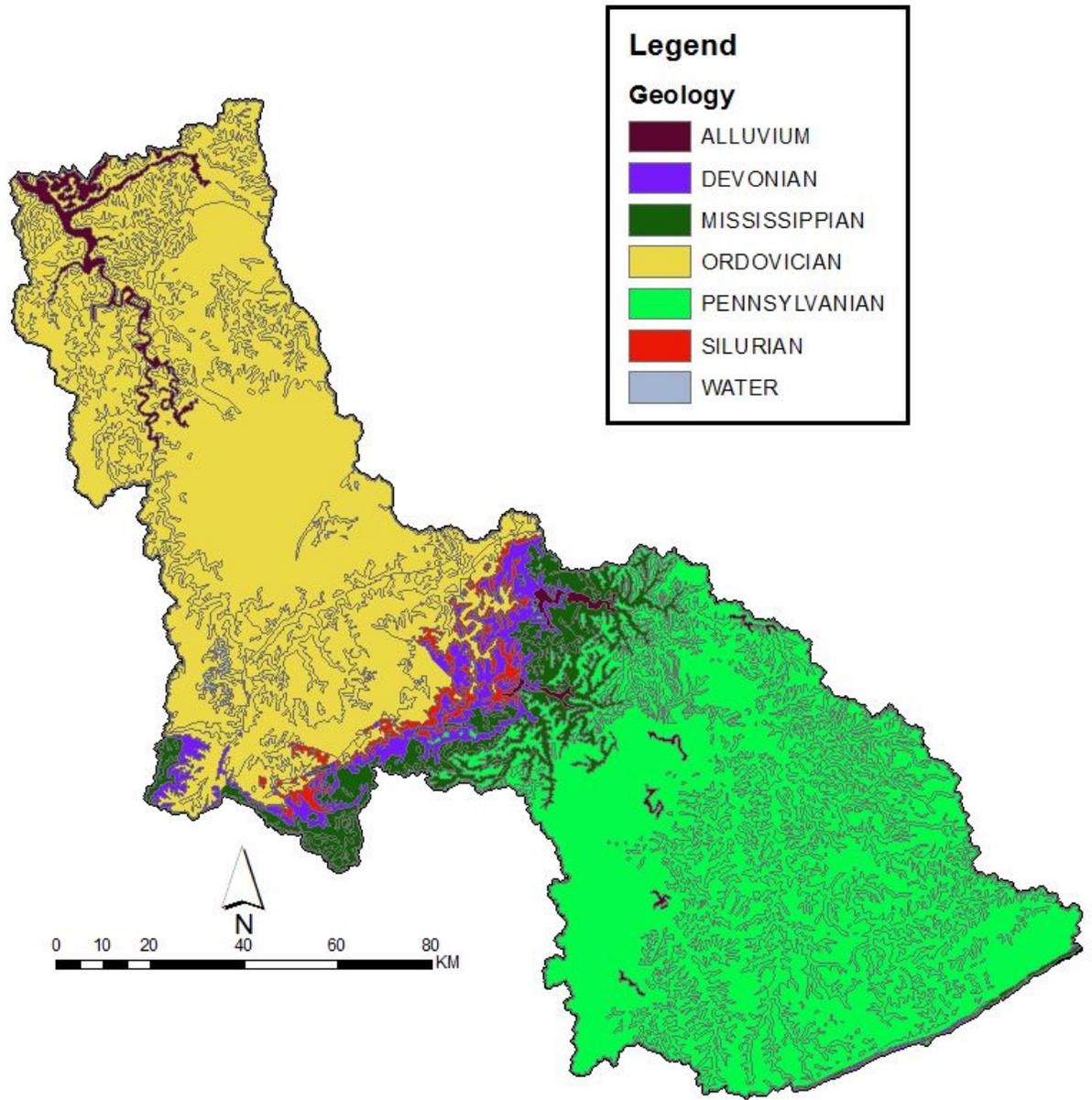
Figure 4.6: Kentucky River Basin soils (USDA, 2016)
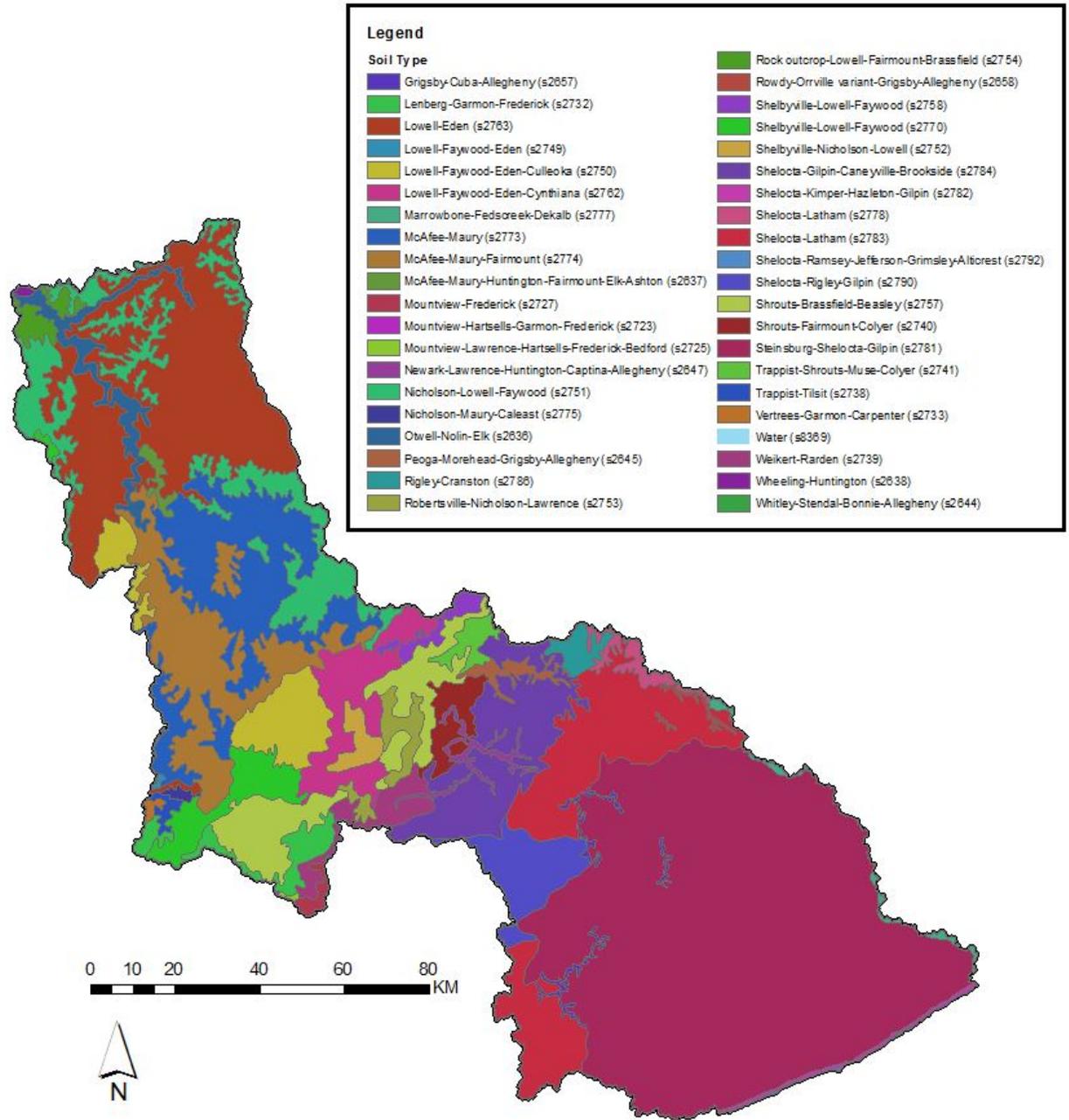
Figure 4.7: Kentucky River Basin karstic landscapes (Currens et al., 2012)
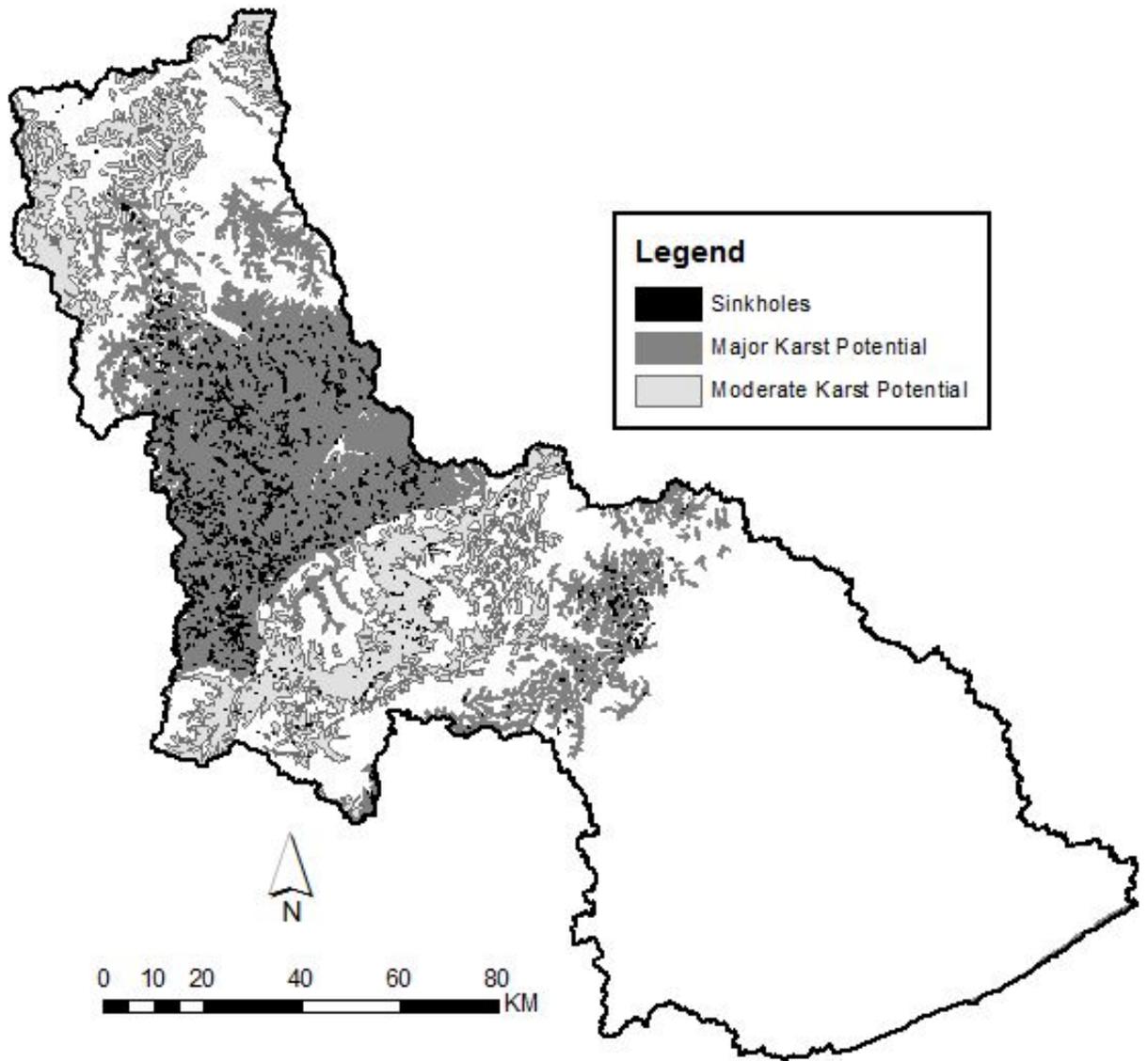
Figure 4.8: Kentucky River Basin land use
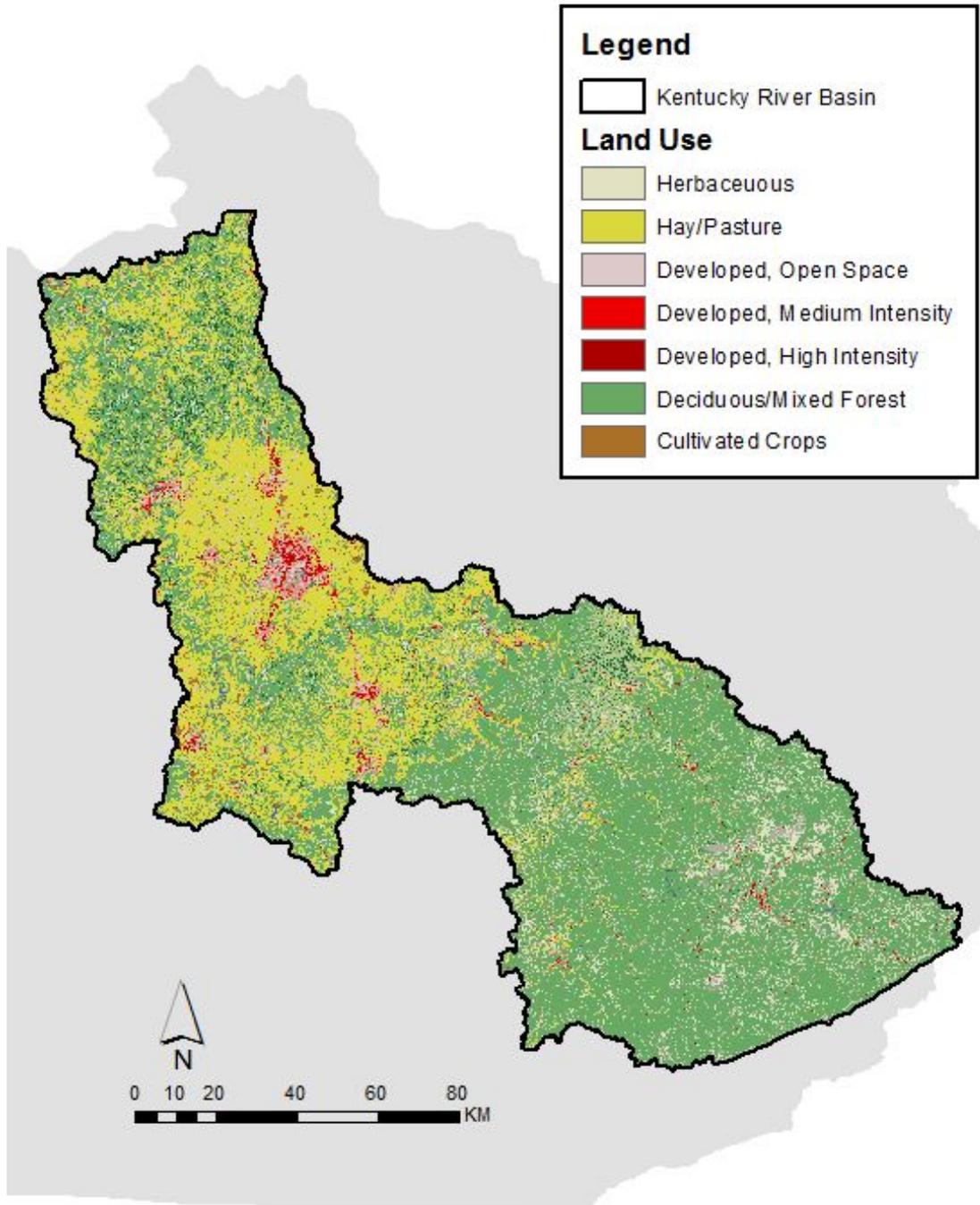
Figure 4.9: Kentucky River Basin lock and dam system (KRA, 2016)
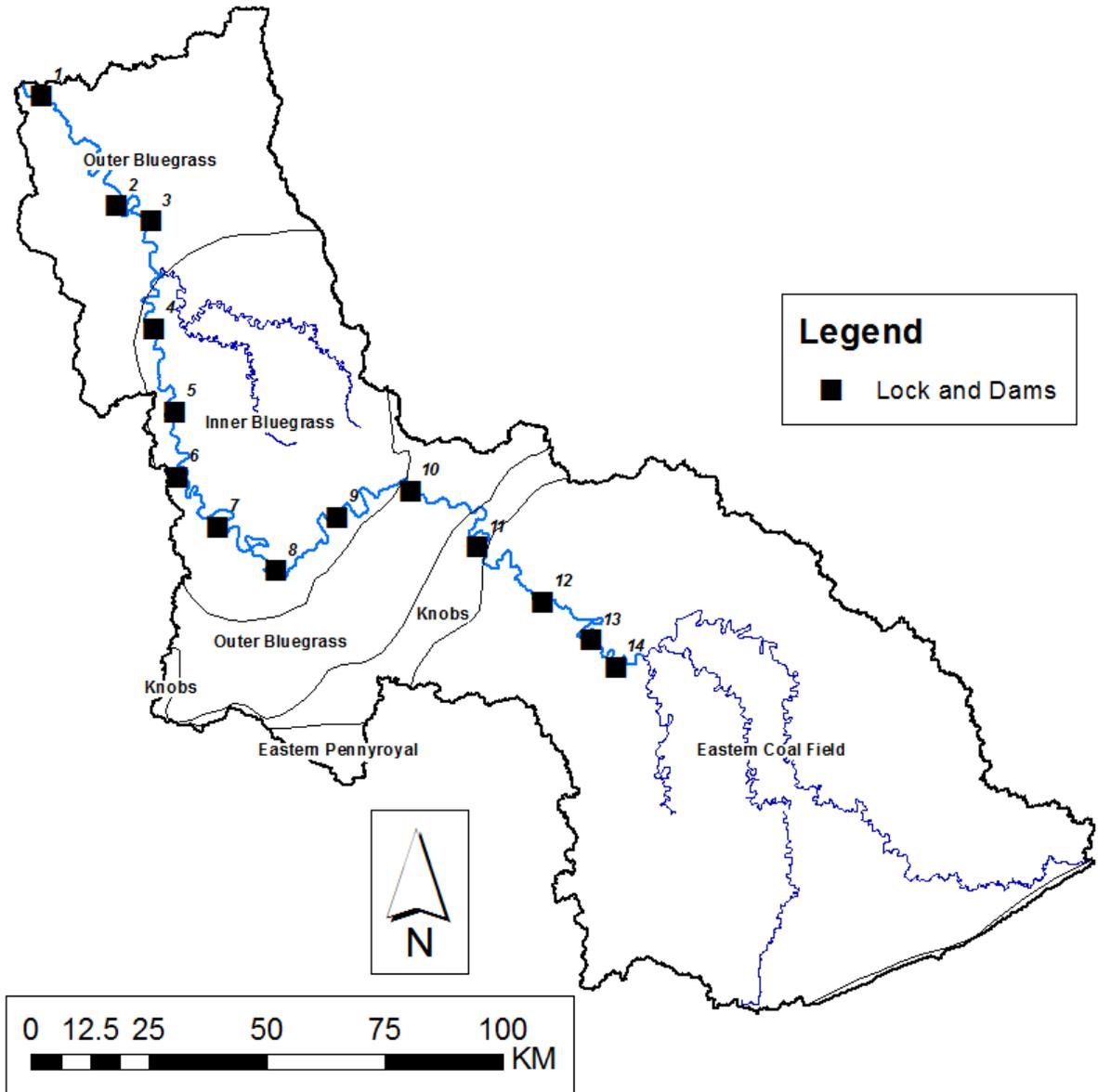
Figure 4.10: Study watershed location within the Kentucky River Basin
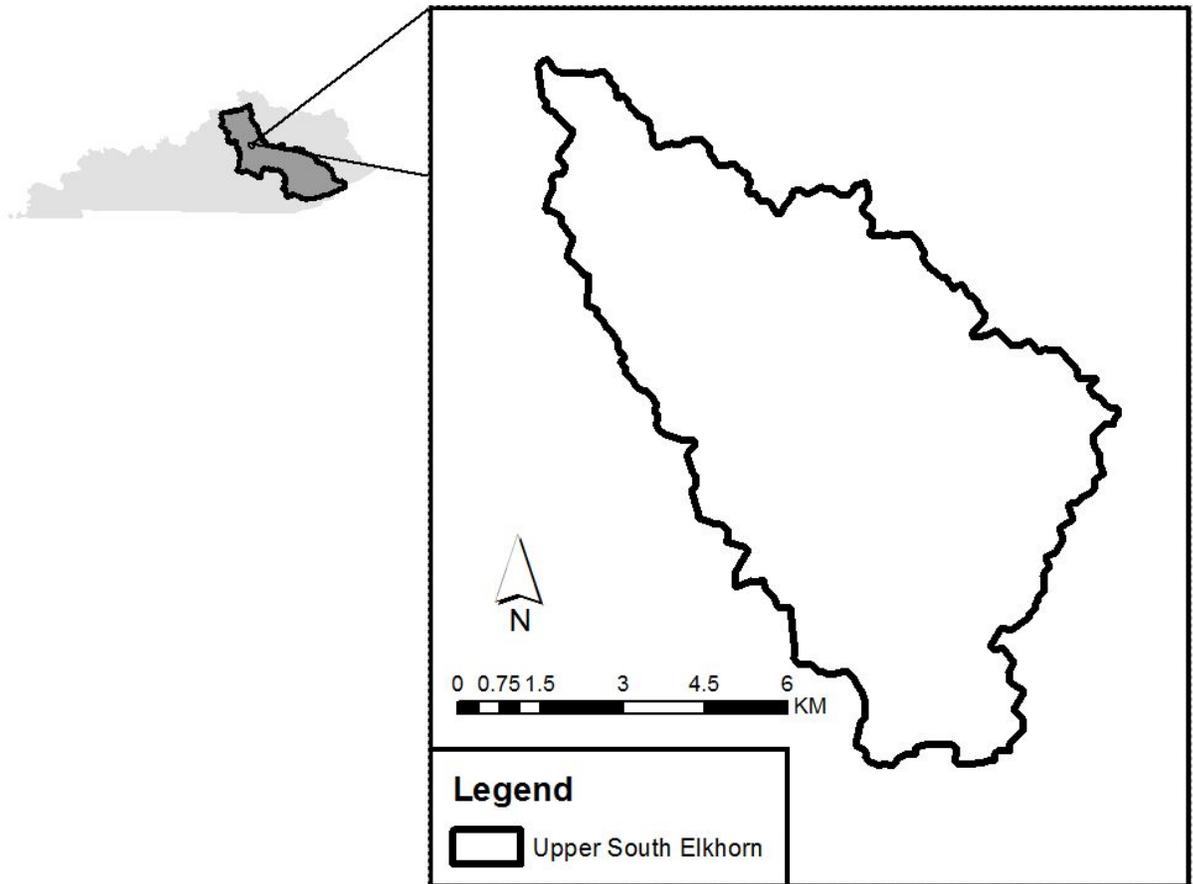
Figure 4.11: Study watershed land use
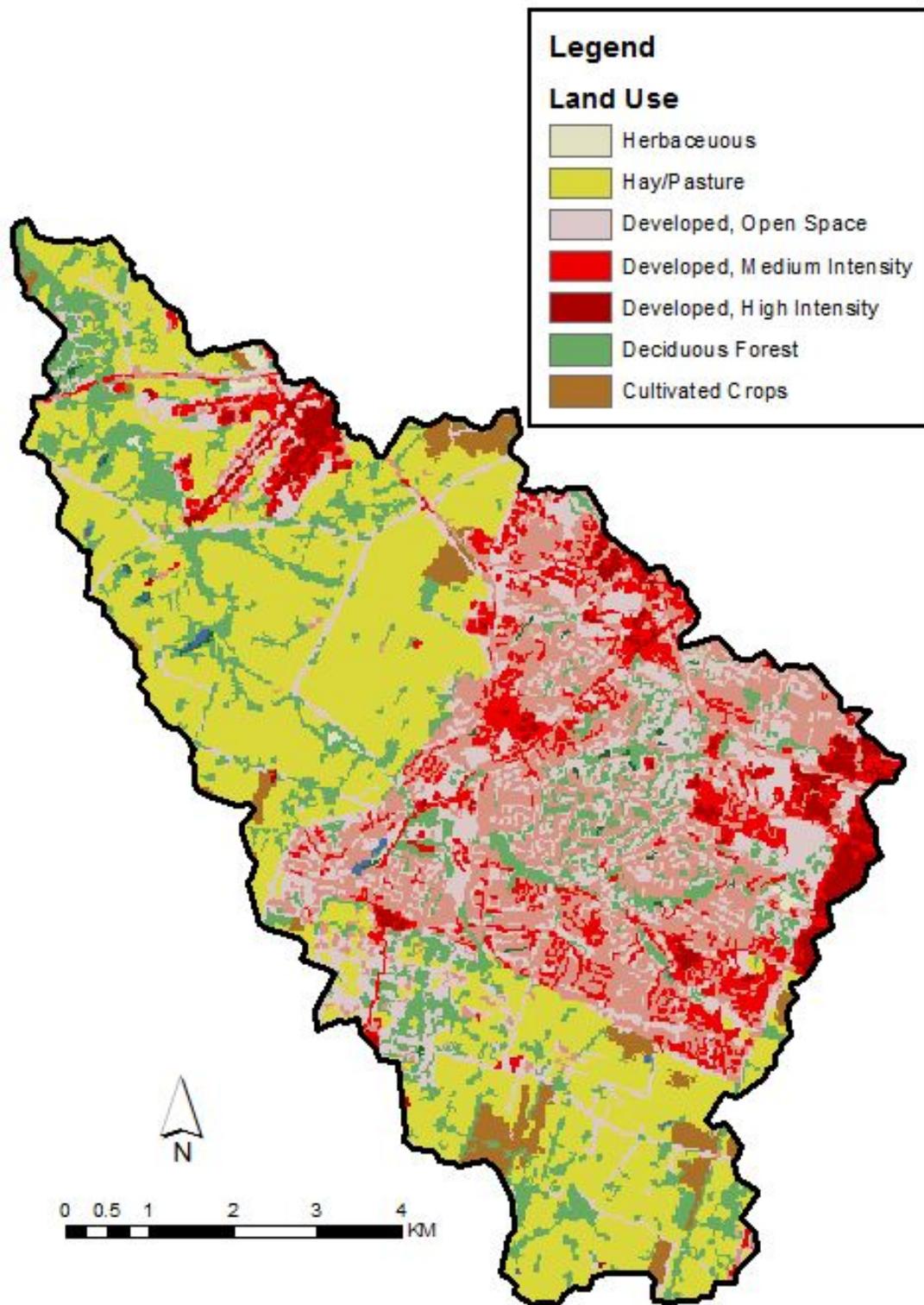
Chapter 5 Watershed Assessment and Visualization of Erosion and Sedimentation (WAVES) Protocol

5.1 WAVES Protocol Introduction and Objectives

The Watershed Assessment and Visualization of Erosion and Sedimentation (WAVES) Protocol is a comprehensive field assessment methodology that was designed to qualitatively elucidate the perceptible conditions of a watershed and the overall governing processes controlling watershed sedimentation and sediment connectivity in the field. The study of sedimentation in watersheds is particularly important because of the harmful impact sediments can have on aquatic life, algae, civil infrastructure (e.g. reservoirs), water supply, and water quality (Wood and Armitage, 1997; FISRWG, 1998; USEPA, 2004; Morris and Fan, 1998; USEPA, 1999; Zappou, 2001). Sediment (dis)connectivity, defined as the detachment and transport of sediment from source to sink between geomorphic zones, controls sediment transport rates but is rarely the focus of watershed field assessments. As mentioned, the quantification of watershed sedimentation has proven to be precarious over years due to what Walling (1983) has defined as the sediment delivery problem. Prior to formulating and applying a connectivity model to predict sediment flux, the author's first saw importance in gaining field-based knowledge of the conditions of the watershed: which is the main purpose of the WAVES Protocol. The utility of gaining field-based knowledge of the catchment's connectivity has been recognized by many researchers (e.g. Brierly and Fryirs, 2005; Fryirs et al., 2007; Borselli et al., 2008; Lexartza-Artza and Wainwright, 2009).

The overall objective of WAVES is threefold: (1) to qualitatively understand hydrological and sedimentological processes occurring within the watershed (i.e. sheet,

50

rill, and gully erosion, instream sediment storage, channel morphology, etc.); (2) to obtain field-based knowledge of the watershed's (dis)connectivity; and (3) to identify sediment sources, sinks, and pathways in the field (such as erosional scars, point bars, and tributaries, respectively). The collection of field data allowed for a comprehensive understanding of the geospatial coverages of erosion sources, sinks, and sediment (dis)connectivity. The post-processing of data collected from the WAVES Protocol lead to an assessment of the overall lateral disconnectivity of the watershed, as is outlined in Chapter 6 of this thesis.

5.2 Method Development

With these objectives in mind, the WAVES method was developed by the authors through the review of contemporary methods to visually assess watersheds and streams, consulting methods pertinent to the physiographic region of the Inner Bluegrass, and literature on sediment connectivity to tailor an assessment towards sediment transport processes within the watershed. Aspects of the following five sources were used as a basis for the methodology of the WAVES Protocol: (1) the *Stream Visual Assessment Protocol (SVAP) Version 2*, developed as a part of the *National Biology Handbook* by the Natural Resources Conservation Service (NRCS, 2009), which provides a basic level of stream health evaluation; (2) the *Bank Erosion Hazard Index (BEHI)*, which evaluates the conditions of stream banks, developed by David Rosgen of Wildland Hydrology, INC. (Rosgen, 2001); (3) the *Rapid Bioassessment Protocol (RBP),* developed to evaluate aquatic organism health by the United States Environmental Protection Agency (USEPA, 1999); (4) the *Visual Stream Assessment for the South Elkhorn Watershed*, prepared for the Lexington-Fayette Urban County Government (LFUCG) of Lexington, Kentucky by Third Rock Consultants, LLC (Third Rock Consultants, 2006); and (5) literature and research

conducted by Fryirs et al. (2007) for the insight gained relative to watershed sediment connectivity. Important definitions pertinent to the WAVES Protocol are shown in Table 5.1. The resulting WAVES Protocol sheets used to complete the visual assessment are shown in Figure 5.1.

5.3 Method Description

Methods for the completion of the WAVES Protocol are broken into three phases: (1) prior to the site visit, (2) during the site visit, and (3) post-site visit. Each stage of the assessment involves preparation and special procedures. This section outlines the developed and accepted methods involved in the WAVES Protocol.

5.3.1 Prior to the Site Visit

Several tasks were completed prior to visiting the field with the intention of completing the *WAVES* Protocol. Prior to the visit, researchers created maps in ArcGIS showing the stream corridor and surrounding land use/land cover, as well as tributaries with contributing areas greater than approximately 0.5 km^2. Aerial imagery and Digital Elevation Model (DEM) analyses were used to delineate stream networks and identify land use/land cover. These maps were used to identify reaches assessed during each site visit, and to spatially identify features of the watershed worth noting. Prior to the visit, researchers predetermined access points to the stream via ArcMap and other mapping services. Access points were chosen based on their proximity to nearby roads that may run parallel to or intersect the stream corridor. Before departure for the field visit, researchers prepared the WAVES binders, which contain maps of the stream, copies of the WAVES Protocol sheets, and extra pens and paper. Finally, before departure, researchers ensured that any relevant and necessary equipment and materials were available and brought to the

field. Potential useful equipment to complete the WAVES Protocol include a GPS connected digital camera, sufficient assessment protocol sheets, surveying rod(s), pencil and extra paper, and prepared maps of the stream. If possible, researchers should take preliminary trips to the field to walk and divide the stream into reaches (i.e. geomorphologically similar lengths of the stream). The start and end points of each reach should be recorded on the field maps brought in the WAVES binder. These points can be mapped through the geolocation features of a smart phone. Note that the WAVES Protocol sheets should not be filled out upon preliminary visits.

5.3.2 During the Site Visit

Five general parameters are assessed through the WAVES Protocol for subreaches: (1) connectivity, (2) streambanks and floodplains, (3) streambed, (4) upland land use, and (5) miscellaneous qualities. These parameters were chosen based upon their suspected influence on sediment delivery at the watershed outlet. Connectivity is assessed by identifying source to sink pathways of sediment and impedances which may cause disconnectivity within the subreach. The condition of the streambanks and floodplains are assessed by observing the density of vegetation surrounding the stream, the structure of the banks, and human infrastructure which may impact sediment transport. The streambed is assessed through the determination of bed bathymetry, morphology, instream sediment storage, and the type of sediment stored. Upland land use conditions are assessed through identification of the type of land use, evidence of historic upland erosion, and upland human interferences that may accelerate sediment transport. Finally, miscellaneous aspects of the subreach that may further contribute to or yield evidence of sediment transport are assessed through the identification of karst features, water quality, and ecosystem quality.

It should be noted that the WAVES Protocol requires a minimum of two researchers to be present and actively assessing the stream condition for each site visit. This is to help eliminate subjectivity when filling out the WAVES Protocol sheets and for safety purposes. During each site visit, researchers arrived at the predetermined access point with WAVES binders, camera, surveying rods, and other necessary materials. Starting at the downstream end of each reach, researchers walked upstream and observed the qualities of the subreach, keeping in mind the five aforementioned parameters. While assessing each reach, geolocated photographs were taken of many features within the stream corridor. Images were taken of (1) the left bank and right bank angle and height at the downstream end, middle, and upstream end of the reach, or wherever significant alterations occurred; (2) hotspots of bank erosion throughout the reach, as well as in-stream sediment storage (i.e. by placing a surveying rod into the sediment); (3) bed material at the beginning, middle, and end of the storage zone; (4) any and all inflowing tributaries and outfalls. Where possible, researchers also walked tributaries and noted bank angles, heights, bed material, erosional hotspots, and upstream land use/land cover. Pictures were also taken of sources of (dis)connectivity within the stream: i.e. check dams, bed rock outcrops, point bars, depositional zones, armoring zones, connected hillslopes, floodplains, in-stream features (riffles, runs, and pools) as well as upland features (land use, human or livestock interference, erosion). At the end of the reach, researchers filled out the WAVES Protocol sheets. This was done individually to minimize subjectivity. While completing the assessment sheets, researchers noted the features separating one reach from another on the *Intermediate Reach* form. Unique features of the reach, weather, flow rate, and other

conditions were noted on this form as well. This process was completed for each reach assessed during each site visit.

5.3.3 Post Site Visit

After completing the site visit, reach information was post-processed and stored for further use. Photos and additional data were uploaded into an ArcGIS database. Assessment sheets were organized and safely stored for future reference. Data was post-processed after completing the visual assessment in the field.

5.4 Data Post Processing

5.4.1 Conglomerate Scoring Procedure

Further refinement of the data collected in the field was necessary because of the subjective nature of the WAVES Protocol. Data were manipulated using a weighting and averaging technique developed by the authors to qualitatively score several watershed sedimentation parameters. Scored parameters included erosion, deposition, and lateral and longitudinal (dis)connectivity. The resulting conglomerate numerical score is a qualitative means of comparing prevalent watershed sedimentation processes in each subreach. These conglomerate scores were ultimately used in the development of hotness/coolness maps, which provide a qualitative means of displaying the results of the data collected in the field.

5.4.1.1 Erosion

The qualitative conglomerate score of erosion severity of subreaches is shown in Equation (5.1) as

$$Erosion = \frac{\sum(avg\ extent + avg\ density)*(value\ weight)}{\sum(value\ weight)} \qquad \text{(Eq. 5.1)}$$

where *Erosion* is the qualitative erosion severity score, *avg extent* is the average extent of erosion within the reach (rated subjectively from 1-10), *avg density* represents the severity of erosion in the subreach (rated subjectively from 1-10), and *value weight* is a qualitative weighting coefficient based on the type of erosion developed by the authors. The average extent and density of erosion were calculated using the arithmetic means of the scores from the WAVES Protocol sheets.

5.4.1.2 Deposition

The conglomerate score assessing the severity of deposition for a subreach is shown in Equation (5.2) as

$$Deposition = \sum \left(\frac{longitudinal\ extent}{10} * lateral\ extent * weight \right) \qquad \text{(Eq. 5.2)}$$

where *Deposition* is the qualitative deposition severity score, *longitudinal extent* is the longitudinal extent of deposition per subreach as qualitatively determined from the WAVES Protocol (rated subjectively from 1-10), *lateral extent* is the lateral extent of deposition per subreach (rated subjectively from 1-10), *weight* is the qualitative weighting coefficient based on the type of deposition type and severity developed by the authors, and the value of 10 is a normalization parameter so the longitudinal and lateral extents of deposition can be related.

5.4.1.3 Lateral (Dis)connectivity

The presence of buffers within subreaches was used to qualitatively determine lateral (dis)connectivity. In this particular watershed, floodplains, farm dams, and terraces were identified as the primary lateral disconnecting features in the Upper South Elkhorn basin. Therefore, the conglomerate score for lateral (dis)connectivity was simply a score

(1-10) representing the extent of lateral disconnectivities found in a particular sub-reach. If no disconnectivites were observed, the subreach was given a lateral disconnectivity score of zero. If there was more than one score given for floodplains (for example, the floodplain extent was different on the left side of the bank than on the right side), a simple arithmetic average was used to produce the lateral disconnectivity score.

5.4.1.4 Longitudinal (Dis)connectivity

The longitudinal disconnectivity conglomerate scoring is based upon observed barriers and blankets, as well as the deposition score calculated in Equation 5.2. The overall equation developed for longitudinal disconnectivity is as shown as

$$Long. Disconnectivity = \frac{BB\ Avg + Deposition}{2}$$ (Eq. 5.3)

where *Long. Disconnectivity* is the conglomerate score for longitudinal disconnectivity per sub-reach, *BB Avg* is the average score for the barriers and blankets within a subreach, and *Deposition* is the conglomerate score for deposition, as previously calculated in Equation 5.2. The average score for barriers and blankets is simply the average of the extent of all recorded barriers and blankets without including any values for floodplains within the calculation. This average was calculated first, then paired with the deposition score from Equation 5.2 to determine an overall arithmetic average for longitudinal disconnectivity as a function of both attributes.

5.4.2 Field Assessment Analysis

The authors recognize the subjectivity of the WAVES Protocol. In order to eliminate some subjectivity, multiple researchers individually scored each parameter of the subreaches and the average of the researchers' scores was used to create the conglomerate

hotspot maps for the major parameters assessed in WAVES. The main utility of the WAVES Protocol is to understand qualitatively where erosion, deposition, and (dis)connectivity are most pronounced to help infer the governing processes of watershed sedimentation prior to creating a model to assess connectivity and sediment flux. This can later serve as a qualitative validation to a connectivity model. Another utility of this Protocol is that disconnectivity features, such as floodplains, were geospatially mapped, and thus can be parameterized in a connectivity model with a high degree of certainty. Finally, the geospatial database of geo-located photographs serves as useful tool for performing other types of visual assessments without having to go into the field. For example, it was intended that the multitude of pictures taken should allow researchers to perform an analysis like the BEHI without having to go back into the field.

The hotspot maps for erosion, deposition, and lateral disconnectivities can be seen in Figures 5.2a through 5.2d. The color of each reach indicates the severity of the parameter in the subreach. For example, in Figure 5.2a, red suggests that a high amount of erosion and green suggests that a low amount of erosion were observed at particular location. A red subreach in Figure 5.2b indicates that intense amounts of longitudinal deposition were observed in that particular location. A red subreach in Figure 5.2c indicates that the reach was suspected to be highly disconnected due to lateral disconnectivities. Finally, a red subreach in Figure 5.2d indicates that the reach was suspected to be highly disconnected due to longitudinal disconnectivities.

Table 5.1: WAVES Definitions

Term	Definition
Active Floodplain	Floodplain that is well connected to the channel and regularly inundated
Agriculture	Land used for the production of crops and/or rearing of livestock; farm land
Algae	Aquatic primary producers
Available Cover	Logs, boulders, swallets that may be used as potential refuge for aquatic life
Bank Angle	Slope of the incline connecting the streambed to the floodplain
Bank Erosion	The abrasion of stream banks, typically due to fluvial forces
Bank Stability	A stream bank's capacity to transport water and sediments without failure
Bankfull Discharge	The flowrate at which water will begin to spill onto a channel's floodplains; this typically occurs every 1-2 years
Barrier	A blockage disrupting longitudinal connectivity within a catchment
Baseflow	Streamflow resulting from natural storage of precipitation; flow is maintained because of baseflow even when there has been no precipitation
Bed Rock	Solid rock underlying soils and alluvium
Bed Width	The width of the bottom of the stream; i.e. the lateral confine of water within the channel
Benthos	Organisms living within the organic material on the bed of the stream channel
Blanket	A blockage disrupting vertical connectivity within a catchment
Buffer	A blockage disrupting lateral connectivity within a catchment
Buffer Strip	Vegetative coverage with efficient means of filtering runoff prior to entering streams
Channel	The lateral and longitudinal confines of streamflow
Channel Depth	The vertical distance from the channel bed to the top of the stream bank
Channel Dimensions	The top and bottom width, depth, and slope of the medium conveying water

Channelization	The process of straightening a channel with the purpose of increasing flow velocity and decreasing sinuosity
Check Dam	A small dam constructed across a tributary, ditch, or stream, with the purpose of counteracting erosion and reducing stream velocity
Cobble	A rock within a stream having a diameter greater than approximately 2.5 inches and less than 10 inches
Connectivity	The physical transfer of sediment from a source to a sink controlled by sediment transport processes
Coverage	The lateral extent within a streambed which an object is present
Culvert	A conduit conveying water from one side of a road or railroad to another
Dam	A hydraulic structure used to retain water for flood control, water supply, and hydroelectric production
Deep Sediment Layer	Deep deposit of sediment found along the bed of a stream
Disconnected Floodplain	Flat surface adjacent to the channel which may rarely become inundated
Embeddedness	The degree which an cobbles/gravels are surrounded by fine sediment within the stream
Erosion Scar	Exposed soil elucidating locations of historic erosion
Extent	The longitudinal span of a substance along the stream corridor
Fine Sediment	Sediments with very small diameters (< 0.074 mm)
Floodplain	Land adjacent to the channel where water will spill onto once the channel's capacity is breached
Fluvial Morphology	The alteration of a landscape due to the water in a stream
Gabion Basket	Wired-cages that hold rocks with the purpose of stabilizing stream banks
Grain Size	The diameter of the sediments found within the streambed
Gravel	Rocks, smaller than cobbles, with a diameter between 0.825 to 2.5 inches
Gully Erosion	A form of soil erosion resulting from the confluence of rills and formed by surface water runoff

Habitat	An ecological area home to certain flora and fauna
Headcut	An actively eroding section of stream noted by an abrupt vertical drop in gradient. Typically headcuts can migrate upstream over time
Incision	The process of lowering the bed of a channel from its original elevation with respect to its floodplains
Intake	A device used to abstract water from a water body
Irrigation	A method of regularly providing water to agricultural lands
Irrigation Ditch/Channel	A canal that is built to carry water from its source to an agricultural land
Karst	Lands underlain by eroded limestone characterized by sink holes, springs, caves, and fissures
Land Use	The characterization of a land by the arrangements and activities undertaken on it
Detritus	Material from vegetation in the uplands/riparian zones of a watershed that enter the stream corridor; i.e. leaves, branches, bark
Land Management	Methods enacted to lessen the impact humans have on surrounding ecosystems
Outfall	The location where a drain, sewer, or pipe empties into another waterbody
Pasture	Land used for the production of hay and suitable for the grazing livestock
Pool	The longitudinal area in the riffle-run-pool sequence with the deepest, slowest moving water
Riffle	A shallow area of a stream where water moves quickly and produces surface agitation
Rill Erosion	The formation of concentrated shallow channels via soil removal
Rip Rap	Large, angular rocks used to prevent erosion
Riparian Buffer	A vegetated area with efficient means of filtering runoff and stabilizing stream banks
Root Density	The distribution, thickness, quantity, and length of roots along a stream bank
Root Depth	The depth of roots along a stream bank
Roughness	The coarseness of the bed, bank, and floodplain of a stream
Row Crop	Land use designated for the production of crops planted in rows

Run	The transition between a riffle and pool designated by fast moving water and little surface disturbance
Sand	Sediment smaller than gravel but larger than fine particles
Sand/Sediment Bar	A deposit where sediment is actively stored within a channel
Sediment Sheet	A widespread sediment deposit disconnecting subsurface sediments
Sediment Slug	A sediment deposit that laterally covers an entire channel bed causing aggradation
Sediment Storage	A location of stored sediment within a watershed which may or may not actively contribute to a catchment's sediment yield
Shade/Coverage	The degree to which a stream is shaded by surrounding trees and vegetation
Shrubs	Plants and bushes found within riparian zones
Sink Hole	A hollow area created from the erosion of lime stone via water, acting as a conduit for water to travel
Species Density	The quantity of a certain species found within a reach or plot of land
Species Diversity	The quantity of different species found within a reach or plot of land
Spring	The emergence of water from an underground aquifer
Stormwater Outlet	The location where a stormsewer system empties into a water body
Stream Corridor	A stream and its floodplains
Stream Restoration	The restoration of a water way to combat erosion and water quality degradation
Surface Fine Grained Laminae	Fine sediment layer associated with the bed surface of a stream approximately 5 mm thick and easily erodible
Swallet	An opening in the ground that transports surface water to the subsurface
Terrace	The remnant of historic floodplains that are formed by downcutting of streams over time
Tile Drain	Outlet emptying into a waterbody that drains excess water from soil, especially in agricultural areas
Turbidity	The cloudiness of water due to suspended sediments, algae, detritus, and other particles
Urban - Commercial	Land use comprising primarily of building offices, shops, and restaurants

Urban - Industrial	Land use comprising primarily of industrial spaces, i.e. manufacturing
Urban - Residential	Land use comprising primarily of residential neighborhoods and houses
Water Quality	The condition of water with respect to chemical, physical, and biological characteristics
Watershed	The cumulative land area draining to an outlet or pour point

Figure 5.1: WAVES Protocol Sheets including: (a) Field sheet key and (b) Acronyms
and WAVES Protocol Field Sheets

(a) Field Sheet Key

The following key shows the colors of different parameters which are to be assessed in the
field.

Color	Field Assessment Parameter
	Sediment Connectivity
	Stream Banks and Floodplains
	Stream Bed
	Upland Land Use
	Miscellaneous
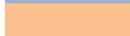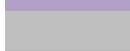
(b) Acronyms and WAVES Protocol Field Sheets

Connectivity		Erosion	**SCAR**	Erosion Scar
			RL	Rill Erosion
			GL	Gully Erosion
			BE	Bank Erosion
		Buffers, Barriers, Blankets	**CD**	Check Dam
			TR	Terrace
			FP	Disconnected Floodplain
			SLUG	Sediment Slug
			BAR	Sand/Sediment Bar
			SFGL	Surface Fine Grain Laminae
			OT	Limestone Outcrop
			SS	Sediment Sheet
Streambanks and Floodplains		Outfalls	**CUL**	Culvert
			STRM	Stormwater Outlet
			TD	Tile Drain
			P	Misc. Pipe
		Restorative Measures	**RIP**	Rip Rap
			GAB	Gabion Baskets
			REST	Other Restoritive Methods
		Vegetation/Riparian Buffer	**S**	Shrubs
			T	Trees
			G	Grasses
			BST	Buffer Strip
			FR	Forrest
Streambed		Sediment Storage in Streambed	**SFGL**	Surface Fine Grain Laminae
			BAR	Sand/Sediment Bar
			THIN	Thin Sediment Layer on Channel Bottom
			DEEP	Deep Bed Deposit
		Bed Material	**FINE**	Fine Material (Clay, Silt)
			SAND	Sandy Material
			GRV	Gravel Material
			COB	Cobble Material
			HCM	Hard Consolidated Material
			BR	Bed Rock
Watershed Land Use	Noticed Upstream Erosion & Agriculture		**UR**	Urban - Resdiential
			UI	Urban - Industrial
			UC	Urban - Commercial
			AG	Agriculture
			PAST	Pasture
			RC	Row Crop
	Irrigation		**IN**	Intake
			DIT	Irrigation Ditch/canal
Misc.	Karst Features		**SP**	Spring
			SW	Swallet
			SI	Sink hole

Reach:	Subreach:	Subreach Length:		

Connectivity

Erosion Scars, Rills, Gullies, Banks				
Type	Extent (1 = Few)	Density	Number of Hotspots	
SCAR RL GUL BE OTHER	1 2 3 4 5 6 7 8 9 10	1 2 3 4 5 6 7 8 9 10		
SCAR RL GUL BE OTHER	1 2 3 4 5 6 7 8 9 10	1 2 3 4 5 6 7 8 9 10		
SCAR RL GUL BE OTHER	1 2 3 4 5 6 7 8 9 10	1 2 3 4 5 6 7 8 9 10		

Buffers, Barriers, Blankets				
Type		Extent (1 = Few)	Disconnecting	Comments
CD TR FP SLUG BAR SFGL SS OT		1 2 3 4 5 6 7 8 9 10	Y N	
CD TR FP SLUG BAR SFGL SS OT		1 2 3 4 5 6 7 8 9 10	Y N	
CD TR FP SLUG BAR SFGL SS OT		1 2 3 4 5 6 7 8 9 10	Y N	

Stream Banks and Floodplains

Outfalls				
Type	Active	Effluent	Diameter (inch)	Comments
CUL TD STRM P OTHER	Y N	Y N		
CUL TD STRM P OTHER	Y N	Y N		
CUL TD STRM P OTHER	Y N	Y N		

Vegetation/Riparian Buffer				
Type	Root Depth (1 = Shallow Roots)	Density (1 = Few)	Extent	Comments
S T G BST FR	1 2 3 4 5 6 7 8 9 10	1 2 3 4 5 6 7 8 9 10		
S T G BST FR	1 2 3 4 5 6 7 8 9 10	1 2 3 4 5 6 7 8 9 10		
S T G BST FR	1 2 3 4 5 6 7 8 9 10	1 2 3 4 5 6 7 8 9 10		

Streambank Condition					
Extent	Bank Angle	Bank Cover (1=bad)	Bank Stability	Incision	Comments
	< 15 30 45 60 75 > 90	1 2 3 4 5 6 7 8 9 10	1 2 3 4 5 6 7 8 9 10	Y N	
	< 15 30 45 60 75 > 90	1 2 3 4 5 6 7 8 9 10	1 2 3 4 5 6 7 8 9 10	Y N	
	< 15 30 45 60 75 > 90	1 2 3 4 5 6 7 8 9 10	1 2 3 4 5 6 7 8 9 10	Y N	

Restorative Measures				
Type	Effectiveness (1 = Ineffective)	Extent (1=Sparse)	Comments	
RIP GAB REST	1 2 3 4 5 6 7 8 9 10	1 2 3 4 5 6 7 8 9 10		
RIP GAB REST	1 2 3 4 5 6 7 8 9 10	1 2 3 4 5 6 7 8 9 10		

Shade/Coverage		
Extent	Shade Coverage (1 = Poor)	Comments
	1 2 3 4 5 6 7 8 9 10	
	1 2 3 4 5 6 7 8 9 10	

Livestock in Stream Corridor				
Interference	Coordinates	Livestock Type	Number	Comments
Y N		Cow Goat Horse Other		

Entering Tributaries			
Tributary Bank Angle	Trib Incision	Bank Erosion	Comments
< 15 30 45 60 75 > 90	Y N	1 2 3 4 5 6 7 8 9 10	
< 15 30 45 60 75 > 90	Y N	1 2 3 4 5 6 7 8 9 10	
< 15 30 45 60 75 > 90	Y N	1 2 3 4 5 6 7 8 9 10	

Stream Bed

Sediment Storage in Streambed				
Storage Type	Lateral Extent	Long Extent	Diversity	Depth (cm)
SFGL BAR THIN DEEP OTHER	1 2 3 4 5 6 7 8 9 10	1 2 3 4 5 6 7 8 9 10	1 2 3 4 5 6 7 8 9 10	
SFGL BAR THIN DEEP OTHER	1 2 3 4 5 6 7 8 9 10	1 2 3 4 5 6 7 8 9 10	1 2 3 4 5 6 7 8 9 10	
SFGL BAR THIN DEEP OTHER	1 2 3 4 5 6 7 8 9 10	1 2 3 4 5 6 7 8 9 10	1 2 3 4 5 6 7 8 9 10	

66

(b) Acronyms and WAVES Protocol Field Sheets (Continued)

Stream Bed

Bed Material

Bed Material	Extent	Depth (1=thin)	Roughness (cm)	Comments
FINE SAND GRV COB BR HCM OTHER		1 2 3 4 5 6 7 8 9 10	< 1 2 4 6 8 > 10	
FINE SAND GRV COB BR HCM OTHER		1 2 3 4 5 6 7 8 9 10	< 1 2 4 6 8 > 10	
FINE SAND GRV COB BR HCM OTHER		1 2 3 4 5 6 7 8 9 10	< 1 2 4 6 8 > 10	

Channel Dimensions

Extent	Approx Width (m)	Approx Depth (m)	Comments

Algae

Type	Lateral Extent	Long Extent	Comments
Benthic Bloom Other	1 2 3 4 5 6 7 8 9 10	1 2 3 4 5 6 7 8 9 10	
Benthic Bloom Other	1 2 3 4 5 6 7 8 9 10	1 2 3 4 5 6 7 8 9 10	

Comments:

Leaves and Detritus

Lateral Coverage (%)	Longitudinal Coverage (%)	Type	Comments
10 20 30 40 50 60 70 80 90 100	10 20 30 40 50 60 70 80 90 100		

Morphology

Riffles	Runs	Pools	Diversity (1=Homogenous)	Comments
			1 2 3 4 5 6 7 8 9 10	

Upland Land Use

Noticed Upstream Erosion

Type	Extent (1 = Few)	Density	Land Use
SCAR RL GUL BE OTHER	1 2 3 4 5 6 7 8 9 10	1 2 3 4 5 6 7 8 9 10	UR UI UC AG PAST RC

Irrigation

Type	Coordinates	Comments
INT DIT		

Agriculture

Extent	Type	Management	Comments
	RC PAST OTHER	1 2 3 4 5 6 7 8 9 10	
	RC PAST OTHER	1 2 3 4 5 6 7 8 9 10	

Miscellaneous

Karst Features

Type	Coordinates	Comments
SP SW SI OTHER		
SP SW SI OTHER		
SP SW SI OTHER		

Habitat/Ecosystem

Available Cover (1= Bad Cover)	Aquatic Life (1 = None)	Extent	Comments
1 2 3 4 5 6 7 8 9 10	1 2 3 4 5 6 7 8 9 10		
1 2 3 4 5 6 7 8 9 10	1 2 3 4 5 6 7 8 9 10		

Water Quality

Appearance (1 = Poor)	Turbidity (1 = Turbid)	Comments
1 2 3 4 5 6 7 8 9 10	1 2 3 4 5 6 7 8 9 10	

Misc.

Item	Location	Comments

(b) Acronyms and WAVES Protocol Field Sheets (Continued)

Reach:	Intermitten Reach:	Length:		
Downstream Controls	**Bed Rock Outcrop**			
	Longitudinally Connected	Approx Lenth (m)	Approx Width (m)	Comments
	Y N			*Get up and downstream coordinates
	Debris			
	Longitudinally Connected	Approx Lenth (m)	Extent (1 = Few Debris)	Comments
	Y N		1 2 3 4 5 6 7 8 9 10	*Get coordins.
	Check Dam			
	Longitudinally Connected	Dam Type	Sed. Buildup (1 = Little Sed)	Comments
	Y N		1 2 3 4 5 6 7 8 9 10	*Get coord
	Misc. Downstream Control			
	Longitudinally Connected	Comments		
	Y N	*Get Coordinates		

Notes: (i.e. Weather, flow rate, etc.)

Figure 5.2: WAVES post-processing including: (a) instream erosion hotspot map, (b) instream sedimentation hotspot map, (c) lateral disconnectivity hotspot map, and (d) longitudinal disconnectivity hotspot map

(a) Instream erosion hotspot map
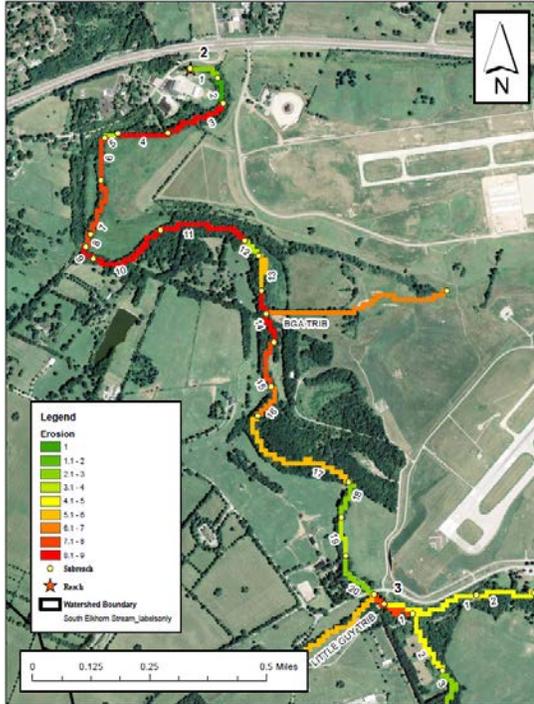
(b) Instream sedimentation hotspot map
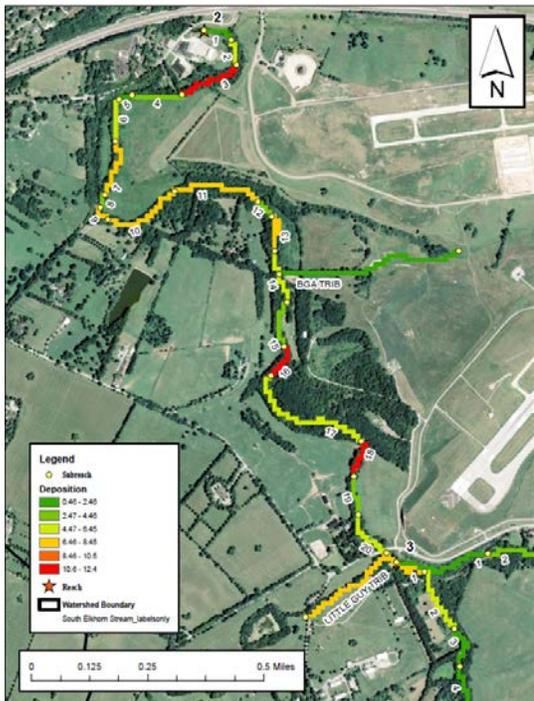
(c) Lateral disconnectivity hotspot map
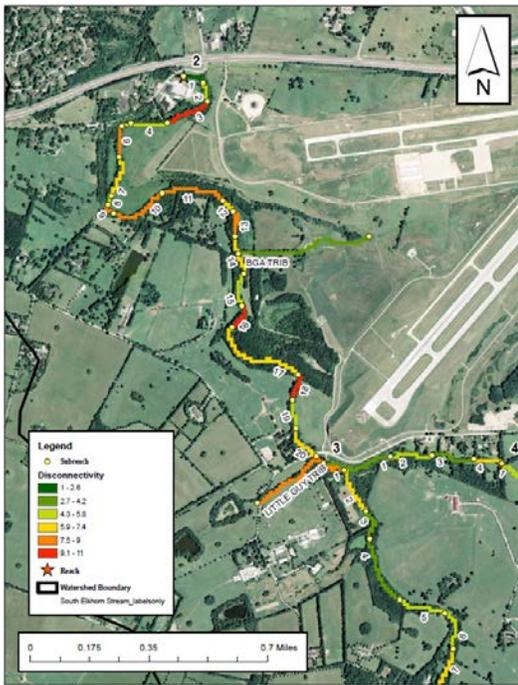
(d) Longitudinal disconnectivity hotspot map
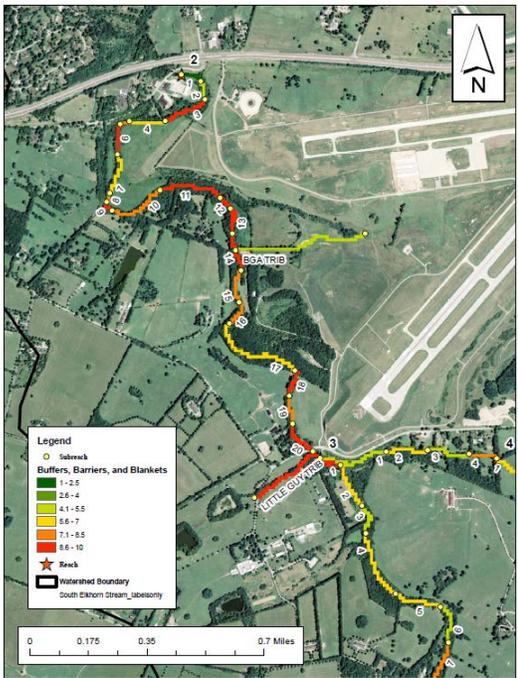
Chapter 6 Probability of Connectivity and Erosion Model Set Up, Input Data, and

Parameterization

6.1 Probability of Sediment Connectivity Model Set Up and Input Data

The probability of sediment connectivity model coupled with the upland erosion model was applied to the Upper South Elkhorn watershed. Model inputs include geospatial data, disconnectivities as assessed in the field and via a geographic information system (GIS), and hydrologic modeling outputs. The upland erosion model was applied only to the active contributing area at a particular time step as predicted by the probability of sediment connectivity model. Figure 6.1 summarizes the application of the probability of sediment connectivity model and the upland erosion model.

6.1.1 Geospatial Input Data

Geospatial data used to determine the probability of connectivity model include land use data, soil type data, and a digital elevation model (DEM). These data were used both as an input to the Soil and Water Assessment Tool (SWAT) to determine hydrologic parameters of the watershed at a daily time step and as a surrogate of the energy gradient of runoff during storm events to predict fluvial shear stress. The land use map, as shown previously in Figure 4.11, is coupled with soil survey data, as determined by the United States Department of Agriculture (USDA), Natural Resources Conservation Service (NRCS), as shown in Figure 6.2, to predict runoff during storm events.

The resolution of the DEM used to predict the Probability of Connectivity is 5 feet by 5 feet and was created by the Kentucky Aerial Photography and Elevation Data Program (KYAPED) in 2014 (KYAPED, 2014). This is shown in Figure 6.3.

6.1.2 Field Disconnectivity Assessment Input Data

Disconnectivities, such as buffers, barriers, and blankets, impede sediment movement in the lateral, longitudinal, and vertical directions, respectively (Fryirs et al., 2007) and decouple land from contributing to the sediment cascade. In order to determine disconnectivities in the watershed, a comprehensive, in-house watershed visual assessment protocol was developed. The WAVES Protocol was designed to qualitatively elucidate the perceptible conditions of a watershed and the overall governing processes controlling watershed sedimentation in the field. See Chapter 5 for more information on the WAVES Protocol. One of the main objectives of the WAVES Protocol is to obtain field-based knowledge of lateral and longitudinal disconnectivitiy within the watershed. Lateral connectivity, which measures the connectedness of uplands and hillslopes to the stream network (Fryirs et al., 2007), was evaluated by assessing the extent of buffers such as floodplains, terraces, and dams at the reach scale. Geolocated photographs denoted the extent of each buffer and then were loaded into ArcMap in post-processing for further review.

Lateral disconnectivities are assumed to cause all suspended sediment to deposit prior to entering the stream network. Therefore, all lands upstream of buffers are also assumed to be disconnected from the stream network, thus not contributing to sediment flux at the watershed outlet. Disconnected lands were digitized by delineating buffers through the WAVES Protocol and remote sensing techniques. Next, the delineated buffer features were converted into a series of approximately 5,200 points for which the upstream contributing area would be determined through ArcHydro, which is a set of data models that delineate and characterize watersheds in ArcMap (ESRI, 2013). The *Batch watershed*

delineation tool, made available by ArcHydro, determined the upstream area of each point. As discussed by Friyrs et al. (2007), lateral disconnections may become connected when floodplains are inundated. However, for this analysis, buffers are assumed to always prevent sediment from entering the stream network. Laterally disconnected land is shown in Figure 6.4.

6.1.3 Hydrologic Modeling Input Data

Results from the Soil and Water Assessment Tool (SWAT) predict subcomponents of the Probability of Sediment Connectivity. SWAT is a lumped-parameter, physically based hydrologic model developed for the watershed or river basin scale. SWAT can be run at monthly, daily, and sub-daily time steps; however, the model is not designed to simulate detailed flood routing at the event-scale. Inputs to SWAT include land cover data, soil data, topology, climatology data, and watershed routing information (Neitsch et al., 2011). Land cover data is available from the USGS's National Land Cover Dataset (NLCD) starting in 2006. Soil data is available from the United States Department of Agriculture (USDA) Natural Resources Conservation Service (NRCS). The STATSGO2 database developed by the NRCS represents soil conditions used in the SWAT model. Topography data is also provided by the USGS as a DEM. The resolution of the DEM used in the SWAT model is 30 meters by 30 meters. The National Oceanic and Atmospheric Administration (NOAA) provides climatology data used in SWAT, i.e. precipitation, temperature, solar radiation, wind speed, humidity, and potential evapotranspiration. A NOAA weather station is present to the northeast of the Upper South Elkhorn watershed at the Bluegrass Airport. The SWAT hydrologic model was calibrated and validated with average flowrate data collected near the watershed outlet at USGS Gage 03289000.

Hydrologic response units (HRUs) group landscapes with similar land uses, soil types, and slopes. SWAT outputs runoff, soil water content, and many other parameters for each HRU at the indicated time step. SWAT results used to predict the Probability of Sediment Connectivity were specified at the daily time step. Results for each HRU in the Upper South Elkhorn watershed exist from 2006 to 2013. The Probability of Connectivity for the Upper South Elkhorn watershed was computed for years 2006, 2007, and 2008.

To predict the Probability of Connectivity, each of the 62 HRUs within the Upper South Elkhorn were spatially mapped in ArcMap and model results were assigned as attributes. Output parameters from SWAT used in the Probability of Connectivity model include daily runoff and daily curve number for each HRU. Rasters for daily runoff and daily curve number were the inputs used for the Probability of Connectivity model. Daily runoff for each HRU is determined using the NRCS Curve Number equation (NRCS, 1972), which is

$$Q = \frac{(R_{day} - I_a)^2}{R_{day} - I_a + S} \qquad \text{(Eq. 6.1)}$$

where Q is the accumulated runoff depth (mm of water), R_{day} is the rainfall depth for the day (mm of water), I_a is the initial abstractions, i.e. surface storage, interception, and infiltration prior to runoff (mm of water), and S is the retention parameter (mm of water). The retention parameter is defined as

$$S = 25.4 * \left(\frac{1000}{CN} - 10\right) \qquad \text{(Eq. 6.2)}$$

where CN is the curve number for the day.

Daily Curve Number is a function of daily soil water content, which can be determined by the water balance equation

$$SW_t = SW_0 + \sum_{i=1}^{t}(R_{day} - Q_{surf} - E_a - w_{seep} - Q_{gw})$$ (Eq. 6.3)

where SW_t represents the final soil water content at the specified time step (mm of water), SW_0 represents the initial soil water content at time step i (mm of water), R_{day} represents the amount of precipitation at time step i (mm of water), Q_{surf} is the amount of surface runoff at time step i (mm of water), E_a is the evapotranspiration at time step i (mm of water), w_{seep} is the amount of water entering the vadose zone from the soil water profile at time step i (mm of water), and Q_{gw} is the amount of return flow at time step i (mm of water). The retention parameter thus is calculated using the following equation

$$S_i = S_{max} * \left(1 - \frac{SW}{[SW + \exp(w_1 - w_2 * SW)]}\right)$$ (Eq. 6.4)

where S_i is the retention parameter at a given time step (mm of water), S_{max} is the maximum value the retention parameter can achieve on any given day (mm of water), SW is the soil water content of the entire profile exluding the amount of water held in the profile at wilting point at a given time step (mm of water), and w_1 and w_2 are shape coefficients.

Figure 6.5 shows the runoff production for every HRU as predicted by the SWAT hydrologic model in the Upper South Elkhorn watershed at day 72 of 2006, which along with daily curve number determines several subcomponents of the probability of connectivity. Day 72 is used as an example here because day 72 was determined to have the most connected land during 2006. As seen in Figure 6.5, larger amounts of runoff are predicted to be produced from southeast and northwest portions of the watershed. Higher runoff in the southeast portion of the watershed is attributed to the higher curve number

assigned to the urban areas found in this portion of the watershed. Engineering properties

of the soils shift lower in the watershed from 64% hydrologic soil group B, which indicates

a moderate rate of water transmission according to the NRCS (1986), 30% hydrologic soil

group C, which indicates a low rate of water transmission, and 6% hydrologic soil group

D, which indicates a very low rate of water transmission to 26% hydrologic soil group B,

45% hydrologic soil group C, and 29% hydrologic soil group D. The shift in the

engineering properties of the soil is attributed to the decrease in percent sand and increase

in percent fine clay in the lower portion (northwest portion) of the watershed (NRCS,

2006). This attributes to the high amounts of runoff predicted in the northwest portion of

the watershed.

6.2 Parameterization of the Probability of Sediment Connectivity

The Probability of Sediment Connectivity is expressed mathematically as

Equation (3.2), as seen in Chapter 3.1

$$P(C) = \{P(S)\} \times \{P(D_H) + P(D_{NH}) - P(D_H)P(D_{NH})\} \times \{P(T_H) + P(T_{NH}) -$$

$$P(T_H)P(T_{NH})\} \times \{1 - P(D_C)\} \tag{Eq. 3.2}$$

In the present study, the individual probabilities within Equation (3.2) were

parameterized as a set of discrete, piecewise distributions to represent small regions, or

geospatial cells, of a watershed. The four subcomponents of the Probability of Connectivity

were parameterized including: (1) the probability of sediment supply, (2) the probability

of sediment detachment, (3) the probability of sediment transport, and (4) the probability

of disconnectivitiy. It was intended that information, via either predictive sediment

transport formula or observation, be estimated for each geospatial cell for application

across the watershed. At the same time, it was realized that the discretized results could be

integrated spatially and temporally to provide continuous distributions applicable to the entire watershed.

6.2.1 Probability of Sediment Supply Parameterization

The probability of sediment supply models the occurrence of a sediment surface that can be eroded. In the present application, the probability of sediment supply was predicted for a geospatial cell using a simple piecewise function as

$$P_i(S) = \begin{cases} 1, & \text{if sediment is present within the cell} \\ 0, & \text{if sediment is absent within the cell} \end{cases} \qquad \text{(Eq. 6.5)}$$

where i is an index representing a geospatial cell. Equation (6.5) was parameterized through observations, both from field visits and remote sensing, of the occurrence of a sediment surface that might be eroded. For the Upper South Elkhorn watershed, the probability of sediment supply was parameterized via observation. Erodible surfaces were considered to be any pervious surface in the watershed. Therefore, if the surface was impervious, it was assumed that no sediment was present within the cell and thus the probability of sediment supply equaled zero. Impervious surfaces were digitized using aerial imagery provided by the USDA National Agriculture Imagery Program (NAIP) in 2010. The probability of sediment supply for the Upper South Elkhorn watershed is shown in Figure 6.6. The digitization of the probability of sediment supply was converted into a raster with resolution of 5 feet by 5 feet.

6.2.2 Probability of Sediment Detachment Parameterization

The probability of sediment detachment models the union of the probabilities of hydrologic sediment detachment and non-hydrologic sediment detachment. The probability of sediment detachment models the likelihood that a sediment particle can be

eroded within a geospatial cell. In the present study, the probability of hydrologic detachment was expressed using an excessive shear stress approach as

$$P_{ij}(D_H) = \begin{cases} 1, & \text{if } \tau_{f\,ij} - \tau_{cr\,i} > 0 \\ 0, & \text{if } \tau_{f\,ij} - \tau_{cr\,i} \leq 0 \end{cases} \qquad \text{(Eq. 6.6)}$$

where j is an index representing a time step. Equation (6.6) evaluates the shear stress of the fluid in the geospatial cell, τ_f, with respect to the critical shear stress. The shear stress of the fluid (in Pascals) was approximated via the fluid momentum equation considering one-dimensional uniform flow of runoff (Jain, 2001) as

$$\tau_{f\,ij} = \gamma H_{ij} S_i \qquad \text{(Eq. 6.7)}$$

where γ is the specific weight of the fluid (kN/m^3), H is the runoff depth of the geospatial cell for a given time step as produced from the SWAT hydrologic model (mm of water), and S is the landscape slope assumed equal to the energy gradient (m/m). The landscape slope was determined in ArcMap using the *Slope* tool. The critical shear stress of the sediment to resist erosion was parameterized by considering the soil characteristics and land management characteristics that control the binding of particles into aggregates (Tisdall and Oades, 1982; Alberts et al., 1995; Foster et al., 1995; Lal, 1999; Fox et al., 2015). Critical shear stress in the Upper South Elkhorn was predicted using the empirical critical shear stress equation for rangeland soil found in Chapter 7 of the Water Erosion Prediction Project (WEPP) manual (Alberts et al., 1995) as

$$\tau_{cr} = 3.23 - 5.6 * sand - 24.4 * orgmat + 0.9 * \frac{\rho_d}{1000} \qquad \text{(Eq. 6.8)}$$

where τ_{cr} is the critical shear stress of the flow necessary to detach soil (Pa), *sand* is the fraction of sand in the surface of the soil (0 to 1), *orgmat* is the fraction of organic material

in the surface of the soil (0 to 1), and ρ_d is the dry soil bulk density (kg/m³). These soil

characteristics are listed in the soil surveys for the Upper South Elkhorn watershed

provided by the USDA. Equation (6.7) parameterizes the probability of hydrologic

detachment in Equation (6.6) as a temporally varying probability because the runoff depth

changes with time as function of the distribution of precipitation and soil conditions. As an

example, the probability of hydrologic detachment for day 72 of year 2006 is shown in

Figure 6.7. The probability of non-hydrologic detachment considers the presence of natural

or anthropogenic disturbance agents, other than fluvial processes, that might initiate

sediment detachment as

$$P_i(D_{NH}) = \begin{cases} 1, & \text{if a disturbance agent exists} \\ 0, & \text{if a disturbance agent is not present} \end{cases} \quad \text{(Eq. 6.9)}$$

Equation (6.9) was parameterized by considering field or remote sensing observations of

non-hydrologic disturbances that would detach sediment from the soil surface. Such

examples could include livestock that trample and dislodge soil particles and aggregates

and mechanized detachment such as that which would occur from construction or mining

equipment. The extent and severity of non-hydrologic detachment in the Upper South

Elkhorn watershed was determined via remote sensing and in the field via the

aforementioned WAVES Protocol. Farms with livestock nearby the stream corridor and

construction sites were digitized in ArcMap and assumed to detach sediment. The result of

the digitization is shown in Figure 6.8. The probability of hydrologic detachment and non-

hydrologic detachment were joined to form the overall probability of sediment detachment

for the Upper South Elkhorn watershed.

6.2.3 Probability of Sediment Transport Parameterization

Equations (6.5) through (6.9) estimate controls on sediment connectivity including

sediment supply and initiation for sediment detachment, but it is well recognized that

fluvial or non-fluvial energy is also needed to allow sediment transport and thus

connectivity in a watershed (Borselli et al., 2008). The probability for hydrologic transport

was parameterized by considering that fluid and its energy must be supplied from upstream

to a geospatial cell, which is termed upstream hydrologic energy for transport or $T_{H\text{-}up}$, and

energy must exist within a geospatial cell such that sediment does not fall out of suspension

and deposit, which is termed $T_{H\text{-}dwn}$. The authors' parameterization of the probability of

hydrologic transport adopts the theory behind the now fairly widely cited index of sediment

connectivity (Borselli et al., 2008). In this manner, the probability of hydrologic transport

was parameterized as

$$P_{ij}(T_H) = P_{ij}\big(T_{H-up} \cap T_{H-dwn}\big) \qquad\qquad \text{(Eq. 6.10)}$$

which is equivalent to

$$P_{ij}(T_H) = P_{ij}\big(T_{H-up}\big)P_{ij}\big(T_{H-dwn}\big) \qquad\qquad \text{(Eq. 6.11)}$$

The probability for upstream energy for hydrologic transport represents the

likelihood that a sediment particle is transported from flow accumulated from the upstream

contributing area (Borselli et al., 2008). It is theorized that the probability for upstream

energy for hydrologic transport reflects the geomorphic threshold conditions for ephemeral

gully and rill incision, which have been identified as a dominant sediment source in

catchments (Auzet et al., 1993; Baade et al., 1993; Vandaele, 1993; Vandaele and Poesen,

1995; and Vandaele et al., 1996). Interrill and diffuse erosional processes were not

considered to contribute to the probability of upstream energy for hydrologic transport after

discussions with several experts in the soil science field and field visits where erosional

processes were observed (Blanford, 2017; Gumbert, 2017; Smallwood, 2017). The

probability for upstream energy for hydrologic transport was parameterized with the

following piecewise function as

$$P_{ij}(T_{H-up}) = \begin{cases} 1, & \text{if } S_{ac\,i} - S_{cr\,ij} > 0 \\ 0, & \text{if } S_{ac\,i} - S_{cr\,ij} \leq 0 \end{cases} \qquad \text{(Eq. 6.12)}$$

where S_{ac} indicates the slope of geospatial cell i and is assumed equal to the energy gradient

and S_{cr} represents the critical slope required to initiate ephemeral gully incision of

geospatial cell i (Vandaele et al.,1996).

Past literature (Montgomery and Dietrich 1994; Vandaele et al., 1996; Torri and

Poesen, 2014) has focused particularly on the relationship between the upstream drainage-

basin area and the critical slope gradient of ephemeral gully initiation. By plotting the

critical slope of ephemeral gullies measured in the field against the upstream drainage area

of the ephemeral gully, Vandaele et al. (1994) showed the critical relation between critical

slope and upstream drainage area is a power function, above which ephemeral gullying has

the potential to occur. Thus, the critical slope required to initiate ephemeral gully incision

here is represented as

$$S_{cr\,i} = a_i A_i^{-b} \qquad \text{(Eq. 6.13)}$$

where a is a coefficient representative of the local climate and specific land use and soil

characteristics of geospatial cell i, A is the upstream drainage area of geospatial cell i, and

b is an exponent. Upstream drainage area is used as a surrogate for the volume of runoff

contributed to the ephemeral gully, which reflects the theory that the location and size of ephemeral gullies is controlled by concentrated surface runoff of sufficient magnitude and duration to initiate and sustain erosion (Vandaele et al., 1994). The entirety of the upstream drainage area contributing to geospatial cell i is assumed to be hydrologically connected; i.e. all land within the upstream drainage area of geospatial cell i contributes runoff to geospatial cell i.

Torri and Poesen (2014) empirically derived a critical slope-upstream drainage area relationship for geospatial cells after extensively reviewing ephemeral gully initiation data collected by many researchers from 1983 to 2011 across six continents. The empirical relationship between critical slope and upslope area is parameterized as

$$S_{cr\,i\,j} = 0.73c_i e^{1.3RFC_i}\big(0.00124S_{0.05\,ij} - 0.37\big)A_i^{-0.38}$$ (Eq. 6.14)

where $S_{0.05}$ represents the maximum potential loss to runoff as determined from the NRCS Curve Number method for a geospatial cell at a particular time step, RFC is the rock fragment cover of the soil, which affects the infiltration rate of runoff, and c represents other sources of the variation of the coefficient a from Equation (6.13) in geospatial cell i not accounted for by the Curve Number approximation. The Curve Number method here models the effect that vegetation, land use, and soil type have on runoff abstraction. Initial abstraction is predicted using the empirical equation developed by Hawkins et al. (2009)

$$S_{0.05} = 0.819\left(25.4\left[\frac{1000}{CN_{ij}} - 10\right]^{1.15}\right)$$ (Eq. 6.15)

where CN_{ij} represents the Curve Number of cell i at time step j. The daily curve number output for individual HRUs via the SWAT hydrologic model represents CN_{ij}. Equation

(6.15) aims to consider both the quantity of water transporting sediment and the energy of water through the inclusion of the upstream contributing area and flow depth of runoff, respectively. The probability of upstream hydrologic transport for day 72 of year 2006 is shown in Figure 6.9.

The probability of hydrologic transport shown in Equation (6.11) also must consider the potential for sediment to fall out of suspension within the geospatial cell or remain suspended and transport through the geospatial cell downstream to the next region of the watershed. The probability for downstream hydrologic transport can be parameterized for a geospatial cell by considering the capacity of the fluid to transport sediment in cell i relative to the capacity of the fluid to transport sediment in the contributing area upstream of cell i. The probability for downstream hydrologic transport can be expressed with a discrete piecewise function as

$$P_{ij}(T_{H-dwn}) = \begin{cases} 1, & \text{if } T_{C\,ij} - T_{C-up\,ij} > 0 \\ 0, & \text{if } T_{C\,ij} - T_{C-up\,ij} \leq 0 \end{cases} \tag{Eq. 6.16}$$

where T_C is the transport capacity of the fluid to carry sediment in geospatial cell i and T_{C-up} is the transport capacity of the fluid to carry sediment upstream of cell i. In order to provide expressions for T_C and T_{C-up}, the authors consider a power associated definition for the transport capacity (Russo and Fox, 2012; Ford and Fox, 2014) as

$$T_C = k_t \tau_f^{1.5} \tag{Eq. 6.17}$$

where k_t is a coefficient and τ_f is defined in Equation (6.7). Considering Equations (6.17) and (6.7) via substitution, it is realized that Equation (6.16) can be simplified when assuming that a representative runoff depth for the watershed can be substituted for the

spatially explicit runoff depth in Equation (6.7). The assumption removes the temporal dependence of Equation (6.16) placing the probability of downstream transport upon the relative energy gradient. The assumption is reasonable when considering that upstream contributing area was already accounted for within the spatially explicit runoff depth in Equations (6.10) and (6.11). The probability of downstream hydrologic transport thus is representative of the static connectivity of the watershed when surrogating slope for the energy gradient of the fluid. It should be noted that disconnected cells downstream of connected cells do not necessarily cause deposition. Rather, the authors imply that disconnected cells downstream of connected cells simply do not have the capacity to pick up more sediment that is contributable to the stream network. The authors believe this to be a reasonable assumption considering the realization that fine sediments and colloidal particles (less than 53 microns in diameters), once entrained, can take hours, or even days to settle (Jin and Romkens, 2001; Jin et al., 2002; Le Bissonnais et al., 2004; Owens et al., 2007; Liu et al., 2008; Rienzi, 2017). In order to consider the upstream energy gradient that might be compared with the energy gradient in the geospatial cell i, the authors suggest the spatial mean upstream energy gradient as reasonable. Therefore, the probability for downstream hydrologic transport can be expressed as

$$P_i(T_{H-dwn}) = \begin{cases} 1, & \text{if } S_i - \frac{\sum S_{up}}{N} > 0 \\ 0, & \text{if } S_i - \frac{\sum S_{up}}{N} \leq 0 \end{cases} \qquad \text{(Eq. 6.18)}$$

In this manner, the fluid energy to transport sediment in cell i is compared to the incoming fluid energy. S_i, representative of the slope in a particular geospatial cell, is found by applying the *Slope* tool in ArcMap to the Upper South Elkhorn DEM. N is representative of the number of upstream cells that flow into cell i. This is determined via the *flow*

accumulation tool, which determines the number of cells flowing into a downstream cell. $\sum S_{up}$ is the sum of the slopes of each cell upstream of cell i. This is determined by weighting the flow accumulation raster by the slope raster. The probability of downstream hydrologic transport is shown in Figure 6.10.

The probability of non-hydrologic transport represents processes such as eolian transport from wind, mass wasting, and land sliding. However, the present application of this thesis focuses on a fluvial-dominated system only, thus non-hydrologic transport was not parameterized for the Upper South Elkhorn watershed.

6.2.4 Probability of Sediment Disconnectivity Parameterization

Finally, the probability of sediment disconnectivity (Fryirs et al., 2007, Fryirs, 2013) via morphologic features and anthropogenic obstacles and revetments is explicitly included into the probability-based modeling framework primarily through observations from remote sensing and field assessments. The probability of disconnectivity is parameterized as

$$P_i(D_C) = \begin{cases} 1, & \text{if disconnectivity exists} \\ 0, & \text{if disconnectivity does not exist} \end{cases} \qquad \text{(Eq. 6.19)}$$

Features causing sediment disconnectivitiy were identified via observations. If features do exist, the entire upstream region of the watershed that was disconnected should be parameterized with $P(D_C) = 1$. The present study focuses primarily on the contribution of sediment from the uplands of the watershed, thus only lateral disconnectivities were digitized in the parameterization of the probability of disconnectivitiy for the Upper South Elkhorn watershed. Disconnectivities and the regions upstream of disconnectivities were digitized using the method previously discussed in Section 6.1.3 of this thesis. The inverse

of the probability of disconnectivitiy $(1 - P(D_C))$ is intersected with the other aforementioned probabilities and is shown in Figure 6.11.

6.3 Probability of Sediment Connectivity Calibration and Validation

The union of the subcomponents of the probability of connectivity simulate the active contributing area of a catchment at a particular time step. It was iteratively determined that the parameters that potentially could be calibrated for the probability of connectivity model lacked pronounced sensitivity (see Chapter 7.1.3). For this reason, and because the authors believed the parameterized probability of connectivity model best represented the processes occurring in the catchment intuitively and according to the literature, the probability of connectivity model was not calibrated.

The authors performed a qualitative validation of the probability of connectivity model by comparing the land found to actively contribute to the sediment cascade at a particular time step to the actual processes known to occur within the Upper South Elkhorn watershed. Upland erosion production in the Upper South Elkhorn occurs primarily through rill erosion, ephemeral gully erosion, and concentrated flow pathways, while diffusional erosion processes (i.e. sheet and interrill erosion) are believed to provide a minor contribution to the overall sediment flux at the watershed outlet (Blanford, 2017; Gumbert, 2017; Smallwood, 2017). Livestock and construction sites in the uplands exacerbate the detachment rates of sediment particles through the removal of protective vegetation and exposure to excessive eolian and fluvial shear stresses (Evans, 2017). The authors determined through visual observation that, in general, the active contributing area predicted by the probability of connectivity model coincided well with the potential locations where the known dominant processes of the watershed could occur. While the

authors recognize the importance of calibrating and validating parameters of models, the lack of parameter sensitivity and perceived difficulty of collecting functional data that could calibrate and validate the probability of connectivity model lead the authors to believe that the qualitative validation aforementioned was sufficient.

6.4 Erosion Model Set Up, Input Data, and Parameterization

6.4.1 Erosion Model Set Up

One utility of a highly distributed sediment connectivity model promoted in this research is that it can be coupled with watershed erosion predictive modeling. Such coupling may alleviate the complexity of simulating a spatially explicit, yet over-parameterized and computationally intensive, sediment transport model. A watershed erosion model was simulated in this application by inputting temporally and spatially explicit results of the probability of sediment connectivity application as well as providing inputs and parameterizing sediment transport formula. As previously mentioned, the probability of sediment connectivity provides the active contributing area for sediment transport within any time step. The authors choice of sediment transport formula within actively eroded portions of the landscape relied on an understanding of the dominant sediment transport processes in the watershed as well as information propagated from or already considered within the probability of sediment connectivity results. In the present study site, it was recognized that fluvial erosion of concentrated flow pathways including gullies and rills provided the major source of upland eroded sediment to the stream network (Blanford, 2017; Gumbert, 2017; Smallwood, 2017). For this reason, fluvial erosion of fines, in this case primarily gully erosion of silt loam, estimated via the classical Partheniades (1965) approach was pertinent. The initiation and hence existence of rills and

ephemeral gullies across the landscape was already explicitly considered in the probability

of sediment connectivity model, and for this reason it was not necessary to re-map the

distribution of rills and gullies when calculating the sediment transport loads. In addition,

the parameterization of the probability of sediment disconnectivitiy subcomponent within

our probability of sediment connectivity model already simulated portions of the landscape

where deposition is pronounced due to the existence of buffers.

The watershed erosion model is simulated by inputting the temporally and spatially

explicit results of the probability of connectivity as well as parameterizing and providing

inputs to the sediment transport formula. The erosion model simulates sediment yield

(tonnes/day) at the watershed outlet by integrating the daily volume of eroded sediment

from the active contributing area predicted by the Probability of Connectivity model at the

specified time step. The yearly sediment yield is predicted by integrating the daily sediment

yield for 365 days. Daily sediment yield is predicted as

$$S_y = \epsilon * \rho_s * t * l * w \tag{Eq. 6.20}$$

where S_y is the sediment yielded at the watershed outlet from the active contributing area

(tonnes), ϵ is the erosion rate (m/s) as predicted by the Partheniades (1965) equation, ρ_s is

the bulk density of the sediment (kg/m^3), t is the amount of time that sediment is contributed

from the active contributing area (s), l is the length of the eroding rill or ephemeral gully

(m), and w is the width of the eroding rill or ephemeral gully (m). It is assumed that the

erosion rate is proportional to shear stress in excess of the critical shear stress of the eroding

surface. Erosion rate, as predicted by Partheniades (1965), is simulated as

$$\epsilon = k_d * (\tau_f - \tau_{cr}) \tag{Eq. 6.21}$$

where ϵ is the erosion rate of the soil (m/s), k_d is the erodibility coefficient (m³/N-s), τ_{cr} is the critical shear stress of the eroding surface (Pa), and τ_f is the effective shear stress (Pa) of the accumulated flow on the eroding surface. The effect shear stress of the accumulated flow on the eroding surface is approximated via the fluid momentum equation considering one-dimensional uniform flow of runoff (Jain, 2001) as

$$\tau_f = \rho g H S \qquad \text{(Eq. 6.22)}$$

where ρ is the density of the fluid (kg/m³), g is the gravitational acceleration constant (m/s²), H is the accumulated runoff depth. Because connected cells within the watershed were found to have a generally steep slope, runoff depth is approximated using the Darcy-Weisbach equation as

$$R = \frac{U^2 * f}{8 * g * S} \qquad \text{(Eq. 6.23)}$$

where R is the hydraulic radius of the channel (m), U is the velocity of the fluid (m/s), f is the Darcy-Weisbach friction factor (dimensionless), g is the gravitational acceleration constant (m/s²), and S is the slope of the channel (m/m), a surrogate of the energy gradient. In the present study, the hydraulic radius R is assumed equal to the runoff depth H. The velocity of the fluid is found using the conservation of mass equation for a rectangular channel as

$$U = \frac{Q}{wH} \qquad \text{(Eq. 6.24)}$$

where Q is the flowrate (m³/s) of the fluid, w is the width of the channel (m), and H is the runoff flow depth (m) .

6.4.2 Erosion Model Input Data

The watershed erosion model was applied to the Upper South Elkhorn watershed at the same time step as the probability of connectivity model. The inputs to the erosion model include the active contributing area that produces sediment, the critical shear stress of the eroding surface, average upstream contributing area, longitudinal channel slopes, channel bathymetries, channel lengths, relative roughness of the channel, bulk density of the eroded sediment, storm length, the time sediment is produced from an eroding channel, and an erodibility coefficient. Table 6.1 shows the input data and parameter values used in the watershed erosion model after calibration and validation.

6.4.3 Erosion Model Parameterization

The storm length and sediment contributing times were parameterized by using three methods to determine time of concentration. The estimation of the routing times of storms is precarious if knowledge of the storm length is unknown. Therefore, representative storm lengths were determined for the erosion model using several widely accepted methods to estimate time of concentration. Time of concentration was used as a surrogate for storm length because (1) time of concentration represents the time needed for water to flow from the hydraulically most remote point in the watershed to the watershed outlet and (2) the time of concentration generally lasts until the inflection point of the falling limb of the hydrograph (NRCS, 2010), thus capturing a majority of the length of the storm event. The three methods used to determine the time of concentration were: (1) the watershed lag method (Mockus, 1973), (2) the velocity method (NRCS, 2010), and (3) the Kirpich equation (Wanielista et al, 1997).

In order to determine the time of concentration, a representative flow length for each bin was first determined using the empirical relationship developed by Mockus (1973) by

$$l = 209 * A^{0.6}$$
(Eq. 6.25)

Where l represents the flow length (ft) and A represents the drainage area of the watershed (acres). The watershed lag method estimates the time of concentration as

$$T_c = \frac{l^{0.8}*(S+1)^{0.7}}{1,140*Y^{0.5}}$$
(Eq. 6.26)

where T_c represents the time of concentration (hr), l is the flow length (ft), Y is the average watershed land slope (%), and S is maximum potential retention (in). S is a function of the curve number of the watershed, found as

$$S = \frac{1000}{CN} - 10$$
(Eq. 6.27)

where CN is the average weighted curve number of the watershed.

The velocity method developed by the NRCS was also used to determine time of concentration. The velocity method breaks up the time of concentration into three separate flow regimes: (1) sheet, (2) shallow concentrated flow, and (3) open channel flow. Typically, 300 feet is the maximum flow length for sheet flow (NRCS, 2010). Sheet flow is represented as

$$T_t = \frac{0.007*(nl)^{0.8}}{P_2^{0.5}*S^{0.4}}$$
(Eq. 6.28)

where T_t is the travel time (hr), n is Manning's roughness coefficient, l is the sheet flow length (ft), P_2 is the 2-year, 24-horu rainfall (in), and S is the slope of the land surface

(ft/ft). To determine the travel time of shallow concentrated flow and open channel flow, the following relationship is used

$$T_t = \frac{l}{3600 * V} \qquad \text{(Eq. 6.29)}$$

Where T_t is the travel time for shallow concentrated flow (hr), l is the shallow concentrated flow length, and V is the velocity of the traveling fluid.

Finally, the Kirpich method was used to determine the time of concentration for each bin, given by

$$T_t = 0.0078 * \left(\frac{L^{0.77}}{S^{0.385}} \right) \qquad \text{(Eq. 6.30)}$$

where T_t is the time of concentration (min), L is the flow length (ft), and S is the slope (ft/ft).

Average rill/ephemeral gully width was empirically parameterized using the equation developed by Nachtergaele et al., (2002) as

$$W = 2.51 * Q^{0.41} \qquad \text{(Eq. 6.31)}$$

where W is the average rill or ephemeral gully width (m) and Q is the peak flow rate. For the present study, however, the average flow rate was used to estimate average rill/ephemeral gully width.

Erodibility, k_d, and critical shear stress, τ_{cr}, of the eroding soil were parameterized via typical literature values. According to Hanson and Simon (2001), minimum and maximum values of k_d were ranged from 0.00 to 1.3 cm^3/N-s in the Yalobusa River System

of Mississippi. Minimum and maximum values of τ_{cr} ranged from 0.38 Pa to approximately 400 Pa in extreme situations.

The friction factor used in the Darcy-Weisbach was empirically determined using the Colebrook-White equation (Colebrook and White, 1937) as

$$\frac{1}{\sqrt{f}} = -2\log\left(\frac{\epsilon}{3.7D_h} + \frac{2.51}{Re*\sqrt{f}}\right) \qquad \text{(Eq. 6.32)}$$

where f is the Darcy-Weisbach friction factor, $\frac{\epsilon}{D_h}$ is the relative roughness of the surface, and Re is the Reynolds number. The relative roughness parameter was assumed to range between 10% and 20%, which is representative of hydraulically rough channels that are found in lowland, bedrock watersheds (Colebrook and White, 1937). For fully turbulent, rough flows, such as most concentrated flows that initiate rill and ephemeral gully erosion, the Colebrook-White equation simplifies substantially to

$$\frac{1}{\sqrt{f}} = -2\log\left(\frac{\epsilon}{3.7D_h}\right) \qquad \text{(Eq. 6.33)}$$

6.4.4 Erosion Model Simulation Method

The erosion model produces sediment flux at the watershed outlet at the daily time step. In order to estimate the erosion rate of the connected cells, cells were separated into three bins based on upstream contributing area. It is assumed that each cell placed in a certain bin will produce the same amount of sediment. To determine the upstream contributing area for each cell, the flow accumulation raster was multiplied with the connectivity raster produced by multiplying the rasters representing the subcomponents of the probability of sediment connectivity together. Connected cells were placed into bin one if their upstream contributing area was less than or equal to 65 cells. Cells were placed into

the bin two if their upstream contributing area was greater than 65 cells and less than or equal to 4,500 cells. Cells were placed into the third bin if the upstream contributing area was greater than 4,500 cells. The average contributing area for each bin was determined in ArcMap on the day of highest connectivity during the first study year, day 72 (March 12) of year 2006. The first bin has an average contributing area of 116 m^2. The second bin has an average contributing area of 951 m^2. The third bin has an average contributing area of approximately 34,079 m^2. To determine the average contributing area of each bin, the average number of contributing cells for the bin was multiplied times the pixel resolution of the raster (5 feet by 5 feet), and converted from square feet to square meters. Bin sizes were iteratively chosen so multiple orders of magnitude of upstream contributing area were represented.

The average slope of the connected cells in each bin was also determined on the most connected day of the first study year, day 72 of 2006. The slope of each cell, as determined by the *Slope* tool in ArcMap, was averaged for the connected cells in each bin. Cells in the first bin with the smallest contributing area were found to have an average slope of approximately 0.16 m/m. Contributing cells in the second bin have an average slope of 0.13 m/m. The cells belonging to the third bin with the largest contributing area have an average slope of 0.12 m/m.

Accumulated flow rate was determined for each cell by multiplying the average upstream contributing area times the runoff depth at the particular time step, and then dividing by a representative storm length, as

$$Q_{avg} = \frac{A_{bin} * H_i}{t_{bin}}$$
(Eq. 6.34)

94

where Q_{avg} represents the average accumulated flow rate produced by cells belonging to a certain bin (cms), A_{bin} is the average contributing area for the connected cells belonging to a certain bin (m²), H_i is the average runoff depth produced across the entire watershed for a day (m), and t_{bin} is the representative length of time that runoff is produced for the connected cells belonging to a certain bin (s). The representative storm lengths were determined for each bin using several widely accepted methods to estimate time of concentration. The three methods used to determine the time of concentration were: (1) the watershed lag method (Mockus, 1973), (2) the velocity method (NRCS, 2010), and (3) the Kirpich equation (Wanielista et al, 1997). The representative flow lengths of the three bins were determined to be 10.8 feet for bin one, 87.7 feet for bin two, and 750. 5 feet for bin three, as determined from Equation (6.25).

A representative slope of 1% was used for each bin to determine the time of concentration rather than the average slope found by averaging the slope of the connected cells in each bin since, by definition, time of concentration is equal to the time it takes for runoff to traverse from the hydraulically most remote point in the watershed to the watershed outlet. The time of concentration using the watershed lag method for each bin was found to be 0.015 hours for bin one, 0.08 hours for bin two, and 0.45 hours for bin three using the watershed lag method.

The velocity method developed by the NRCS was also used to determine time of concentration. A Manning's n of 0.41, corresponding to Bermudagrass, was assumed. Flow length up until 300 feet was assumed to be sheet flow, thus contribution to time of concentration from bins one and two is only from sheet flow. P_2 was determined from the

NOAA Precipitation Frequency Data Server (PFDS) as 3.04 in. The slope of each bin was assumed to also be 1%, or (0.01 ft/ft).

The velocity of shallow concentrated flow used to determine time of concentration is empirically derived (Kent, 1964) for short-grass and pasture as

$$V = 6.962 * S^{0.5}$$ (Eq. 6.35)

where V is the velocity of shallow concentrated flow (ft/s) and S is the slope of the channel (ft/ft). The shallow concentrated flow velocity was determined for connected cells in the third bin. The time of concentration for each bin was found to be 0.08 hours for bin one, 0.45 hours for bin two, and 1.36 hours for bin three.

Finally, the time of concentration using the Kirpich method (Equation (6.30)) for the three bins was 0.7 minutes for bin one, 3.59 minutes for bin two, and 18.8 minutes for bin three. Time of concentration as determined by the velocity method was used as an initial guess for determining storm length. The timing parameter for each bin is a calibration parameter for determining sediment flux at the watershed outlet. Using this information, the average flowrate and the maximum flowrate for each bin was determined for the first study year. The average accumulated flow from cells in bin one is 0.0003 cms, 0.0008 cms for bin two, and 0.014 cms for bin three. The maximum accumulated flow from cells in bin one is 0.025 cms, 0.068 cms for bin two, and 1.23 cms for bin three. Average rill/ephemeral gully width can be empirically determined using the equation developed by Nachtergaele et al., (2002) as

$$W = 2.51 * Q^{0.41}$$ (Eq. 6.31)

where W is the average rill or ephemeral gully width (m) and Q is the peak flow rate. For the present study, however, the average flow rate was used to estimate average rill/ephemeral gully width because the peak flow yielded a predicted gully width that far exceeds the gully widths that the authors have observed in the field. The error in this equation may be attributed to the model used to predict this empirical relationship in Nachtergaele et al.'s study (2002), from the prediction of runoff from SWAT, or because of differences in the climatology and physiology between the regions that Nachtergaele studied and the Upper South Elkhorn watershed.

The authors noticed several discrepancies between the average daily flow rate predicted by the SWAT hydrologic model and the actual flow rate observed at the USGS gage located at fort springs, near the watershed outlet. In general the hydrologic model predicted the average daily flow rate well ($R^2 = 0.65$), but some average daily predicted flow rates differed substantially from the average daily flow rate measured at the watershed outlet. In order to account for this in the probability of connectivity model, days where the predicted average daily flow rate differed by more than 30% of the actual average daily flow rate were assimilated so the model could better reflect the actual hydrologic conditions of the day.

If the predicted daily flow rate needed to be assimilated, the actual measured flow rate at the watershed outlet was used to predict the average runoff over the catchment (mm). This was completed by plotting the predicted runoff (mm) versus the actual observed flow rate (cms) and fitting a regression equation to model the relationship. The actual runoff lead to a new estimation of the predicted daily runoff depth, which was reapportioned to individual hydrologic response units (HRU) based on the average deviation that each HRU

97

experienced from the weighted average of the runoff for the entire catchment. This newly

reapportioned daily runoff depth (mm), as predicted by the actual flow rate at the watershed

outlet, predicted a new probability of hydrologic detachment for the day, which was then

used to predict the overall probability of connectivity. Once a new probability of

connectivity was determined for the watershed for the day, erosivity and thus sediment flux

at the watershed outlet were predicted using the newly apportioned bins of connected cells

and new runoff predicted by the actual flow rate at the watershed outlet.

The average daily curve number parameter was not assimilated because soil water

content is the major predictor of daily curve number, and, generally, the soil water content

estimation operates on a different time scale than the runoff parameter. For example, soil

water content can remain high because of previously active hydrologic events even when

no runoff occurs on a particular day, whereas runoff will generally enter the stream network

in less than a day.

The assimilation of daily flow rate was particularly important when predicting

sediment flux at the daily time step since sediment flux can vary greatly based on the

hydrologic conditions of the watershed. This was particularly important for the calibration

and validation of the erosion model, since daily sediment flux data was used to calibrate

and validate the model. Thus, all days in 2006 with predicted flow rate that deviated by

more than 30% of the actual flow rate, as well as the days with sediment flux data used for

calibration and validation, were assimilated. However, as outlined in the results of this

thesis, it was determined that while some daily discrepancy existed between sediment flux

estimates for assimilated and non-assimilated model runs, the net sediment flux over the

entire year was identical at the end of the 2006 simulation year. For this reason, runoff was

not assimilated for the 2007 and 2008 probability of connectivity results, since only yearly sediment flux was desired for those years.

6.5 Erosion Model Calibration and Validation

Calibration and validation is a vital part of applying a predictive erosion model. In order to calibrate and validate the erosion model, the prediction of daily sediment flux data was compared to the actual sediment flux measured at the watershed outlet. Sediment flux measurements were completed by Russo and Fox (2012), in late 2007 and 2008 using a Teledyne ISCO water sampler. The ISCO sampler was installed at the outlet of the watershed and collected 500 mL samples at the start of a storm event at one- or two-hour intervals until 24 samples were collected. The ISCO sampler collected total suspended solids, and an analysis performed by Russo and Fox (2012) determined the concentration of suspended sediments at the inlet of the sampler. The Einstein approach (1950) determined the sediment yield for each storm event. A total of seven events were sampled with the ISCO device. Table 6.2 summarizes the date, peak flow rate, and sediment yield for each captured event.

After careful consideration of the watershed processes, days 5 and 6 of this data were thrown out of this calibration and validation process. This is because the source of sediment production for this event (during mid-summer), was suspected to only be in-stream sediment transport processes. The current iteration of the probability of connectivity model only accounts for upland erosion, and will later be coupled with an instream connectivity model to predict instream sediment transport processes. Also, it was realized that the flow rate and runoff used to predict the second captured event (2/21/2008) should be assimilated via the processes previously mentioned because the predicted flow rate from

the hydrologic model differed by more than 30% of the actual flow rate measured at the watershed outlet.

Therefore, the model was iteratively calibrated so the predicted daily sediment flux matched as closely as possible with the observed sediment flux. The first three events were used to calibrate the model: days 1 (12/2/2007), day 2 (2/21/2008), and day 3 (4/10/2008). Calibration parameters that were altered included the erodibility coefficient, k_d, the critical shear stress of the eroding surface τ_{cr}, the relative roughness of the channel surface $\frac{\epsilon}{D}$, and the length of storm event and contribution time of sediment from the eroding surface. The contributing time of sediment was assumed equal to the length of the storm event in this instance, since the length of the storm event represents an idealized, average storm as opposed to capturing the length of an individual event. The coefficient of determination (R^2) and the Nash-Sutcliff coefficient (NS) were maximized to calibrate the model

$$R^2 = \left[\frac{\sum_{i=1}^{n}(O_i - O_{avg})(S_i - S_{avg})}{(\sum_{i=1}^{n}(O_i - O_{avg}))^{\frac{1}{2}}(\sum_{i=1}^{n}(S_i - S_{avg}))^{\frac{1}{2}}} \right]^2 \qquad \text{(Eq. 6.36)}$$

$$NS = 1 - \frac{(\sum_{i=1}^{n}(O_i - S_j))^2}{(\sum_{i=1}^{n}(O_i - O_{avg}))^2} \qquad \text{(Eq. 6.37))}$$

where O_j is the observed value at time i, O_{avg} is the average value observed for i, S_i is the simulated value at the time step, and S_{avg} is the average simulated value for the time step.

The remaining two events were used for the validation of the erosion model (days 4 and 7). Then, the same parameters were used to estimate the yearly sediment flux for 2006, 2007, and 2008 and compared to the yearly results of Russo (2009). The R^2 and NS values were determined to be 0.95 and 0.71 respectively for the calibration period, which

subjectively represents good agreement between the predicted and simulated flux. Table 6.3 shows the calibration and validation fluxes. The yearly flux matched well the yearly flux predicted by the model of Russo (2009), which, on average, deviated by just 6%. While it is recognized by the authors that it would be ideal to have more data points to calibrate and validate the model, the efficacy of the model to fairly accurately predict sediment flux at two different time scales lead the authors to believe that the calibration method of the model was sufficient.

Figure 6.1: Probability of connectivity application
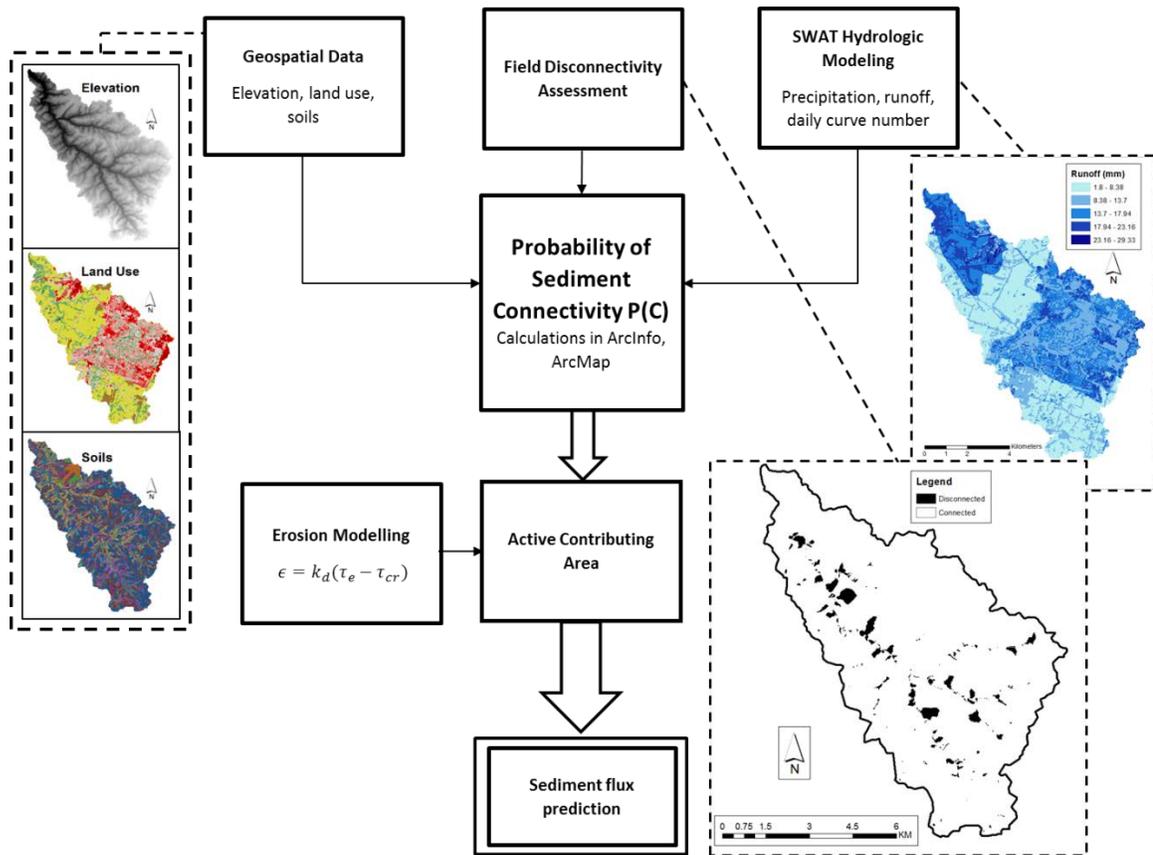
**Figure 6.2:** Study watershed soil types
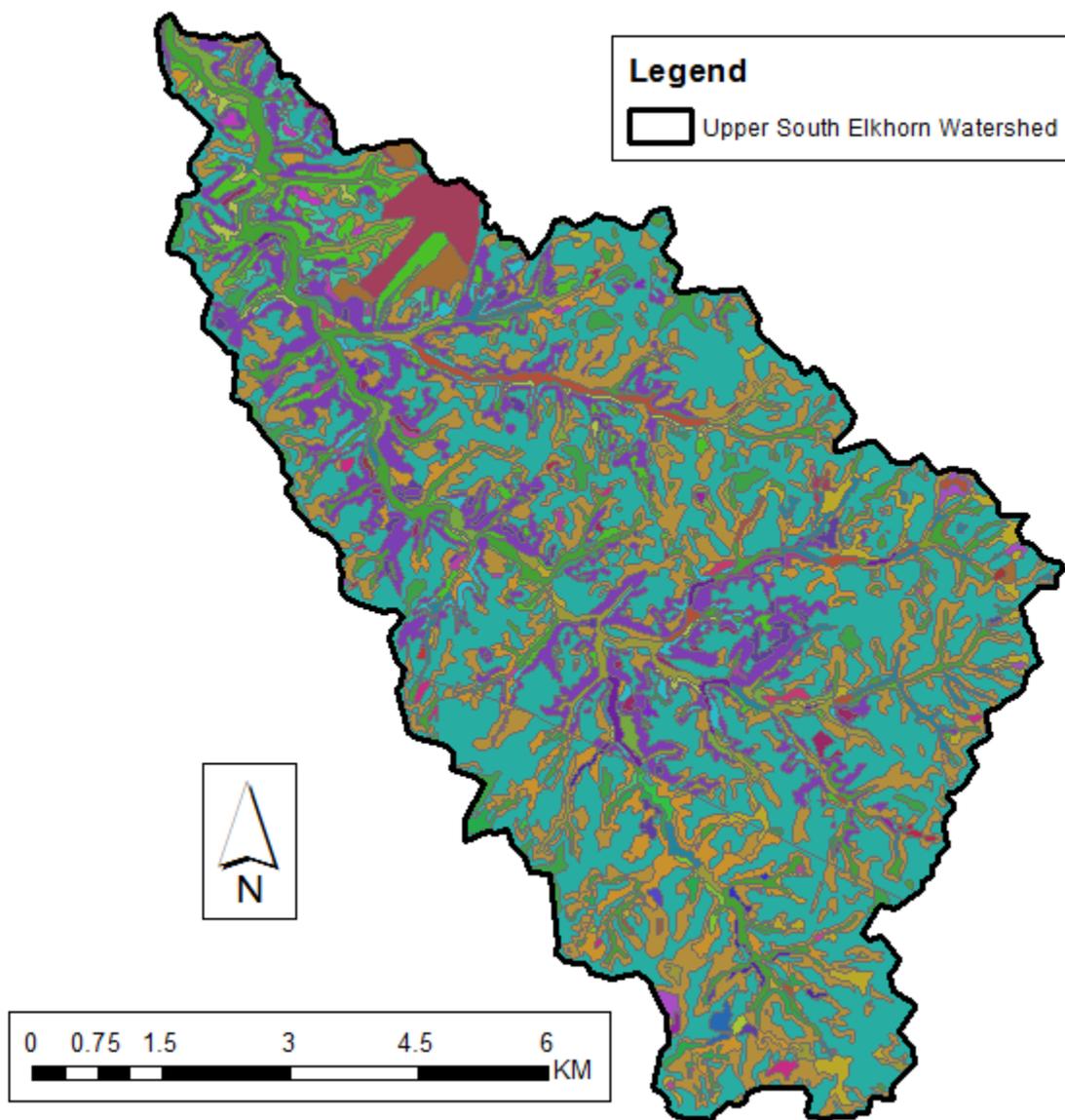
Figure 6.3: Study watershed elevation
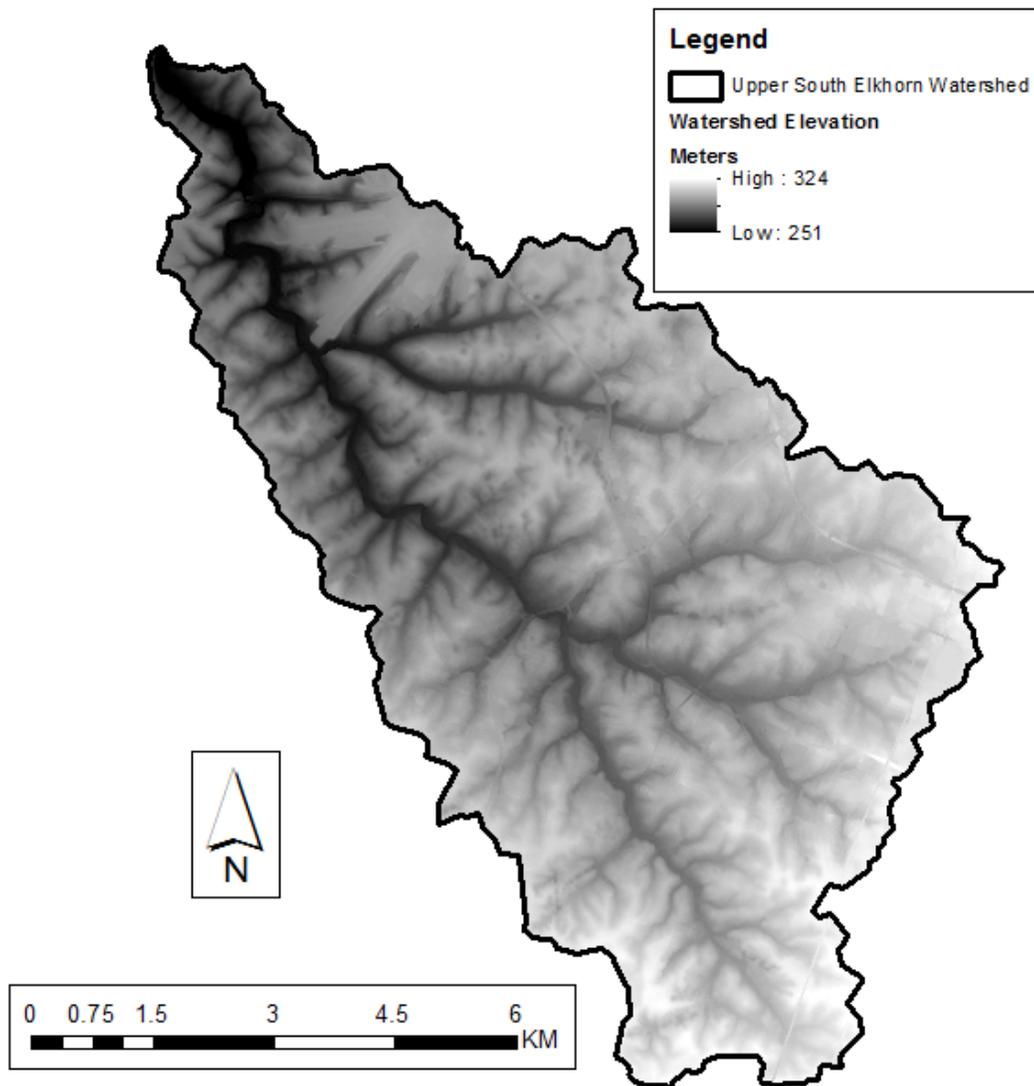
Figure 6.4: Study watershed disconnectivities


Legend
Disconnected
Connected
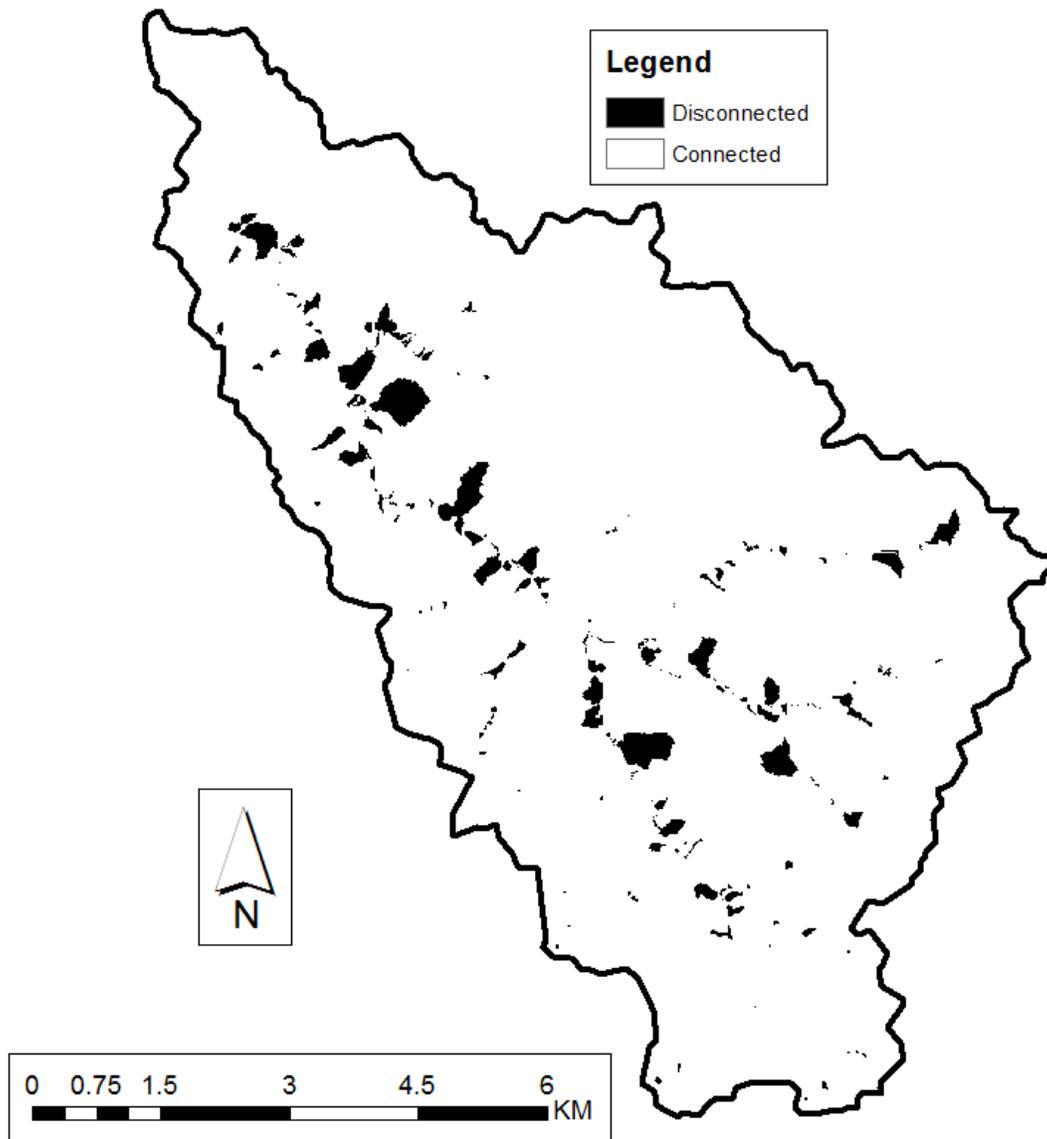
**Figure 6.5:** Predicted runoff for study watershed by the SWAT model on day 72
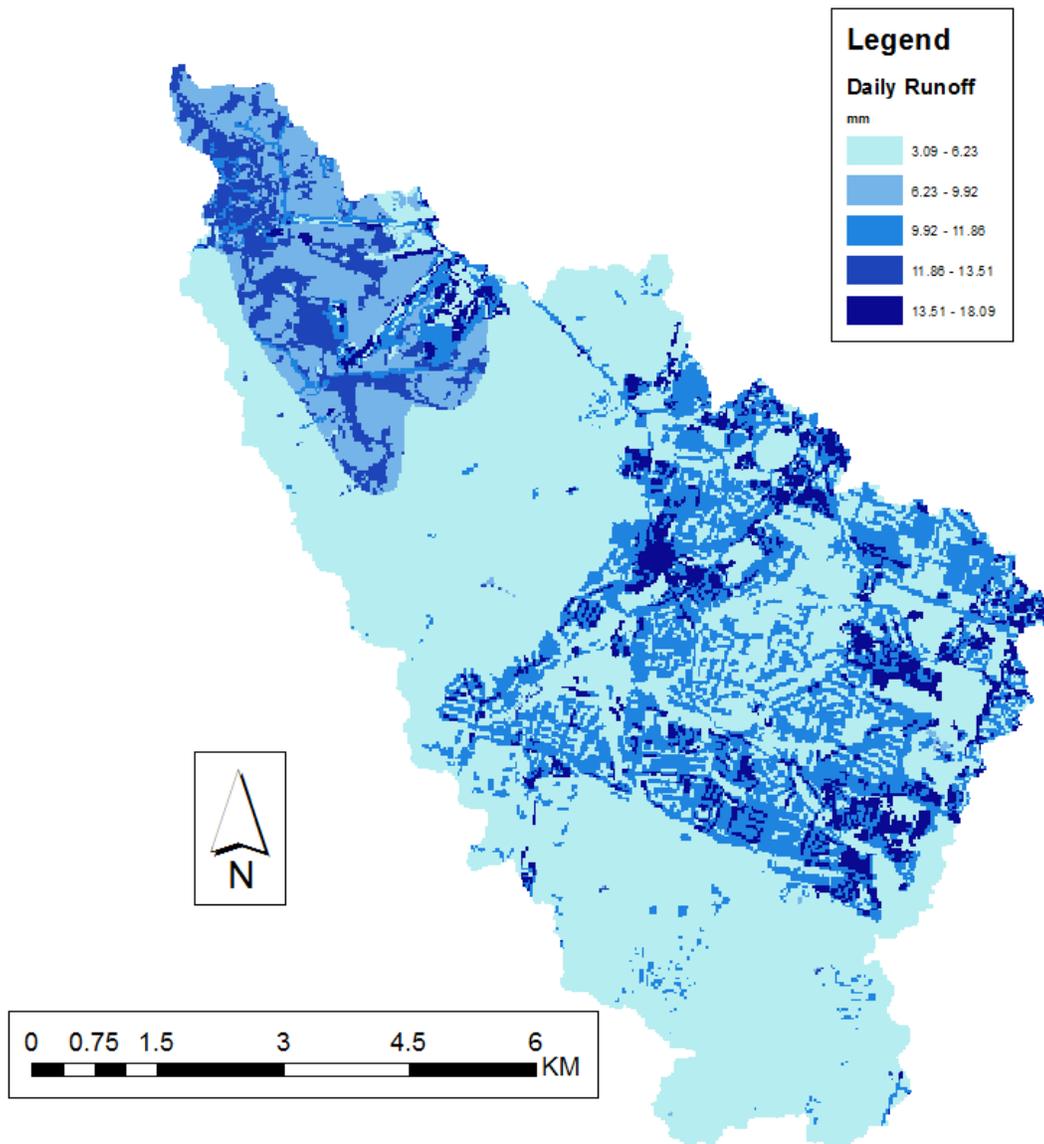
Figure 6.6: Probability of sediment supply
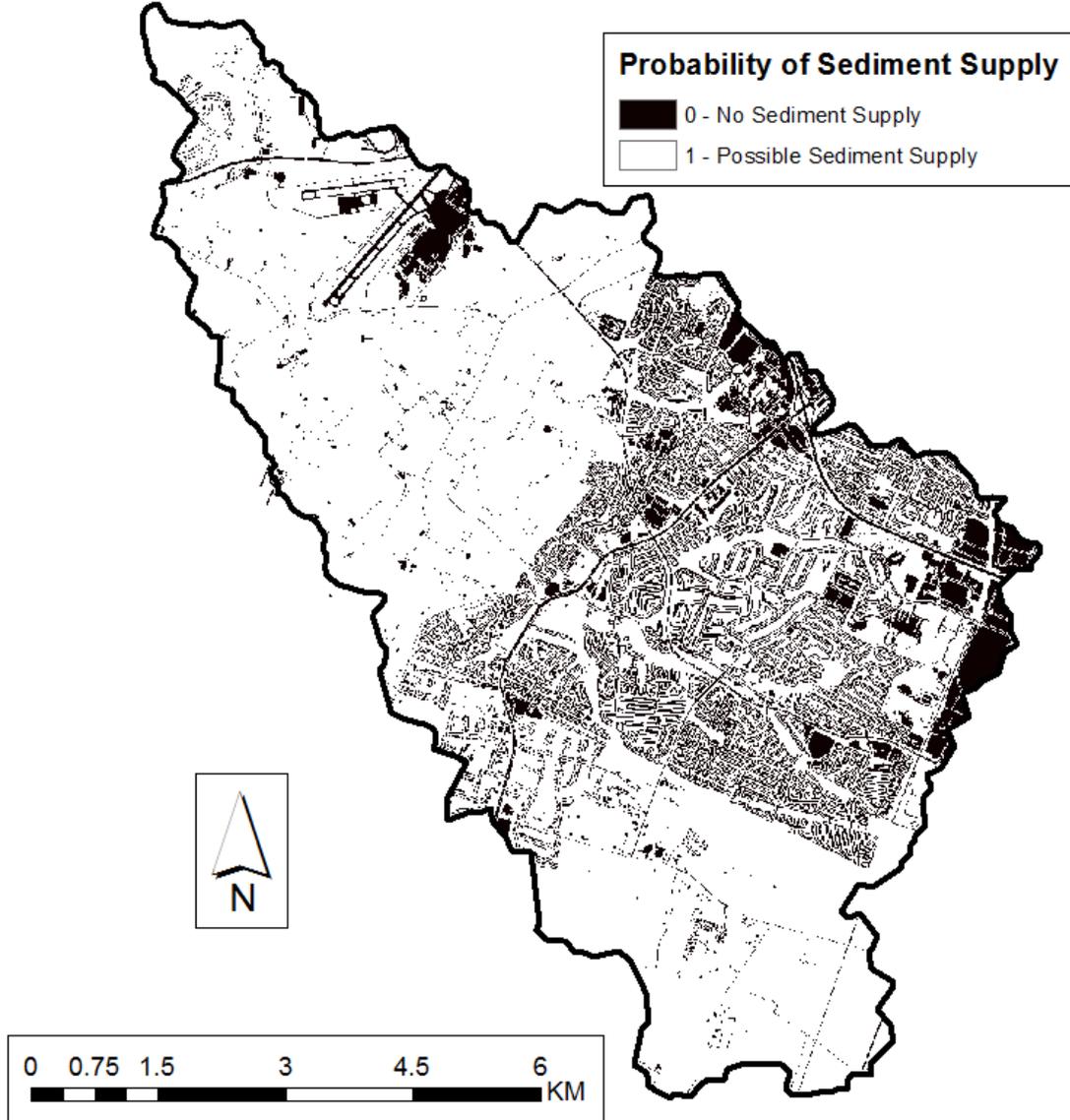
**Figure 6.7:** Probability of hydrologic detachment
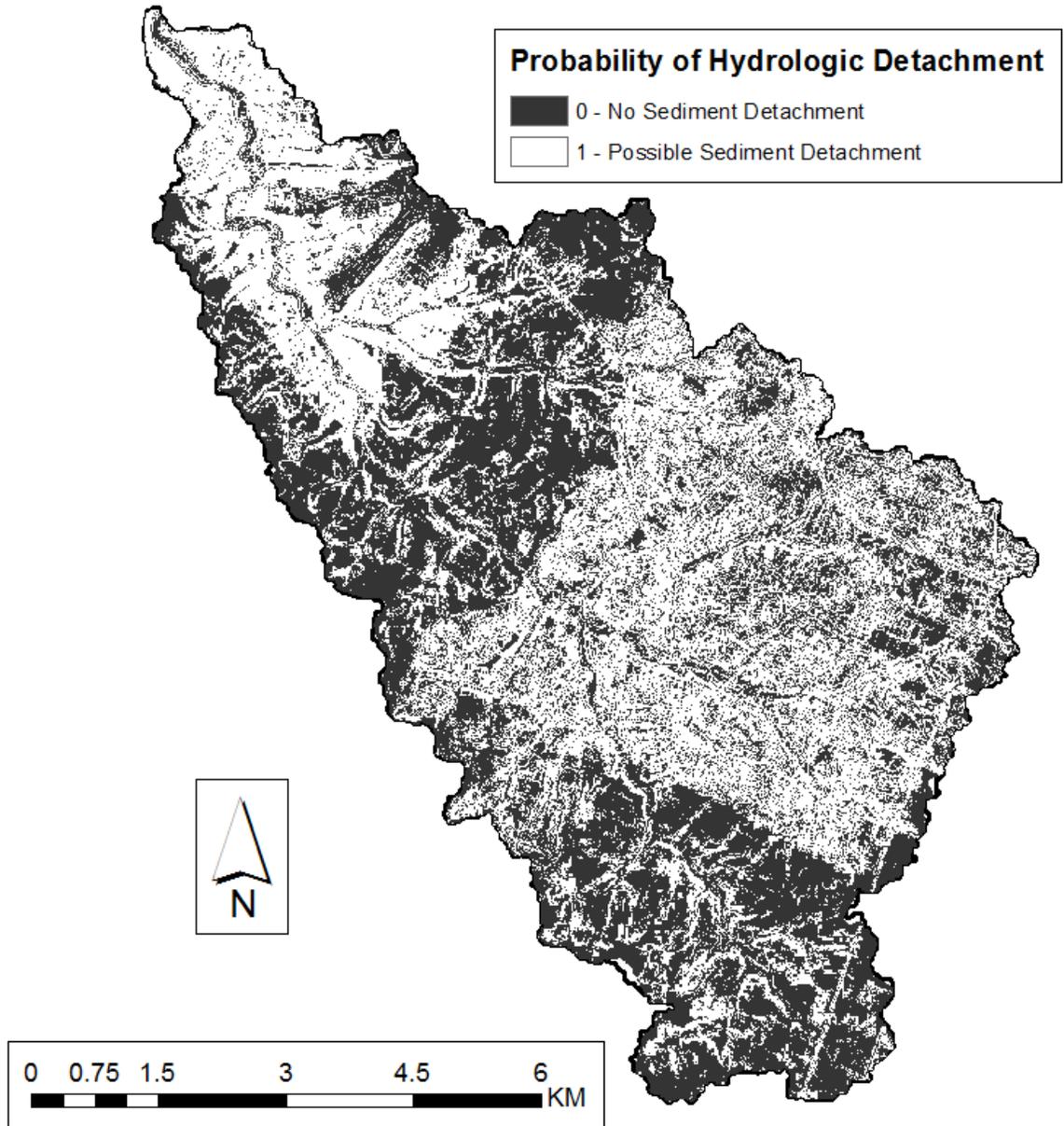
Figure 6.8: Probability of non-hydrologic detachment
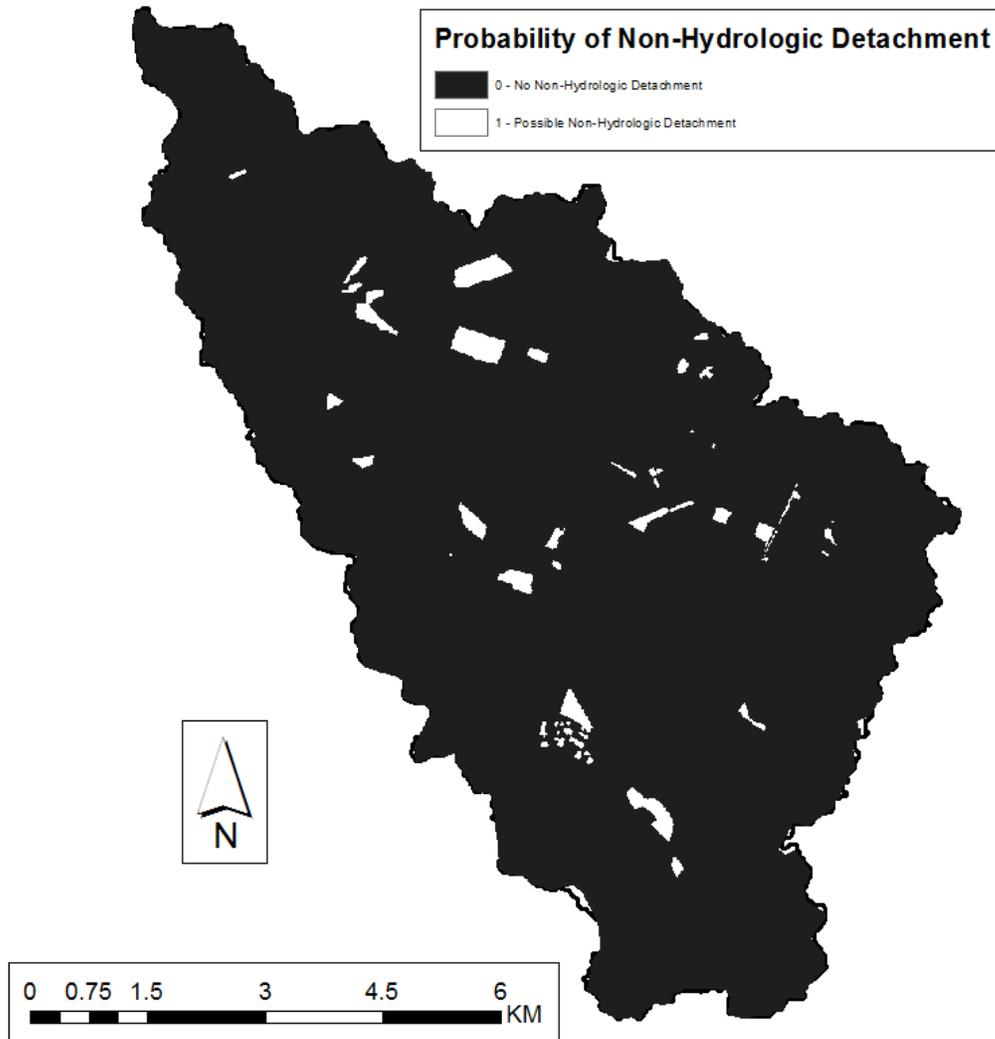
Figure 6.9: Probability of upstream transport

Probability of Upstream Transport

- 0 - No Upstream Transport
- 1 - Potential Upstream Transport

N

| 0 | 0.75 | 1.5 | 3 | 4.5 | 6 |

KM
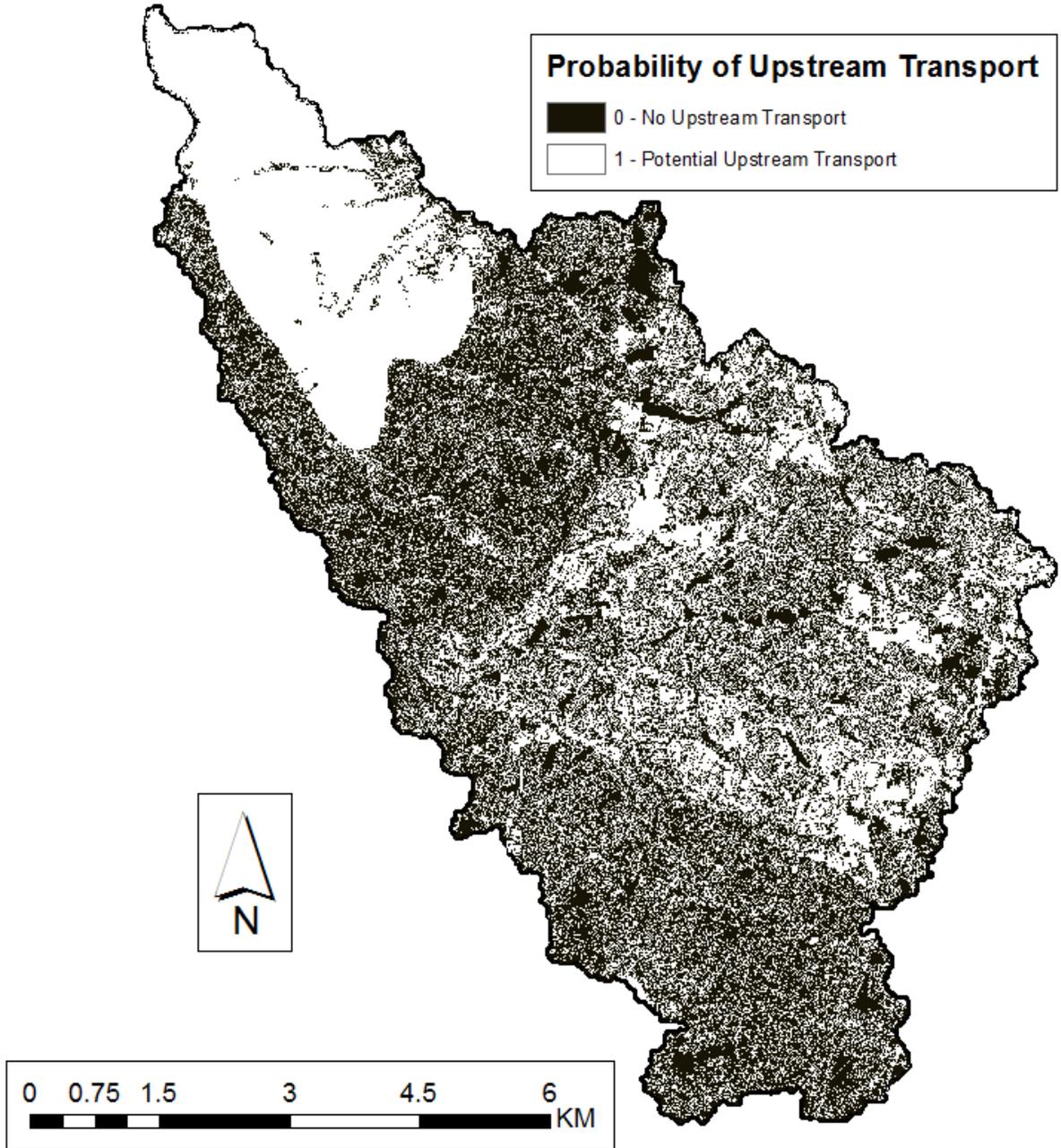
Figure 6.10: Probability of downstream transport
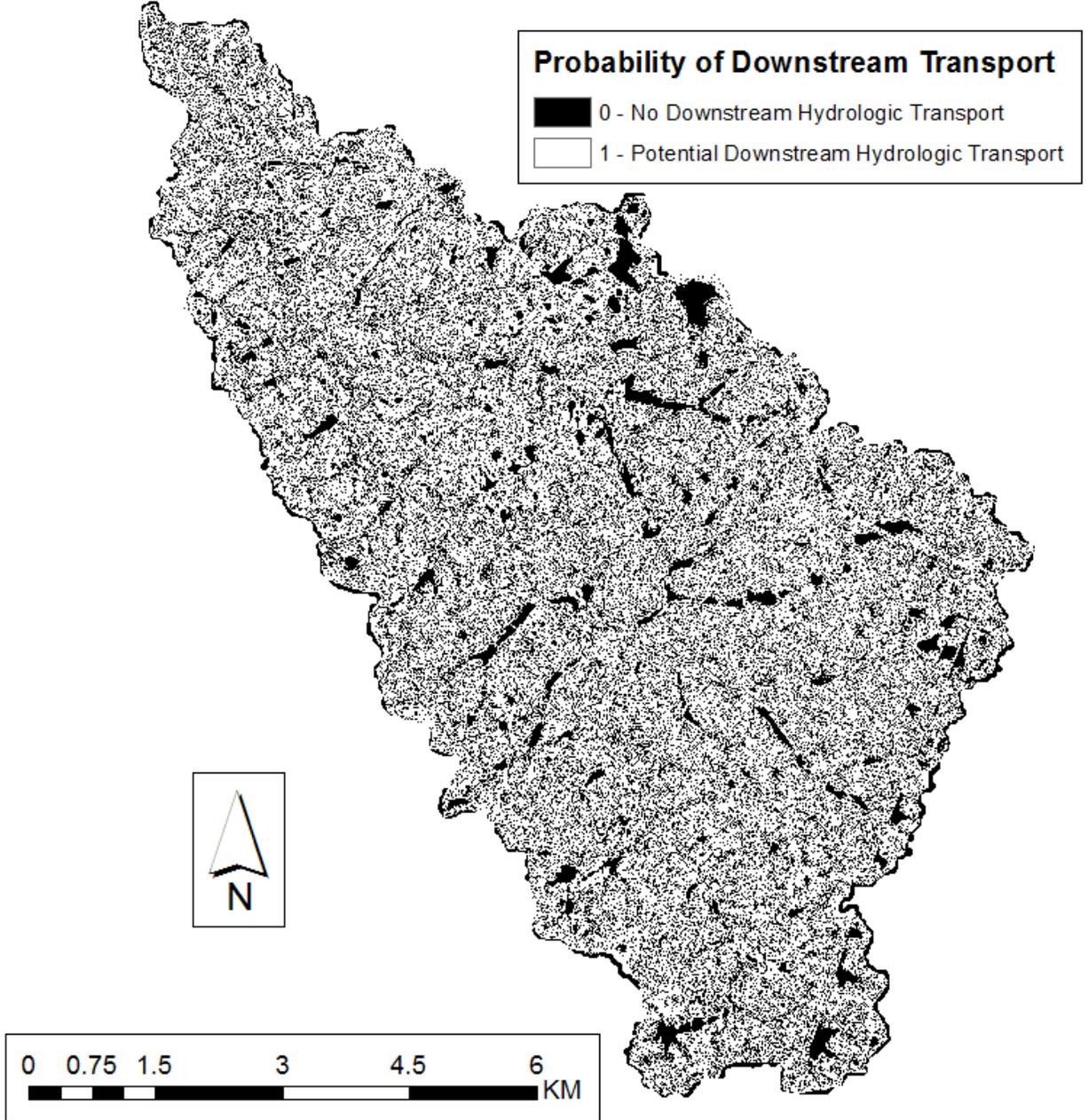
Figure 6.11: Probability of disconnectivity
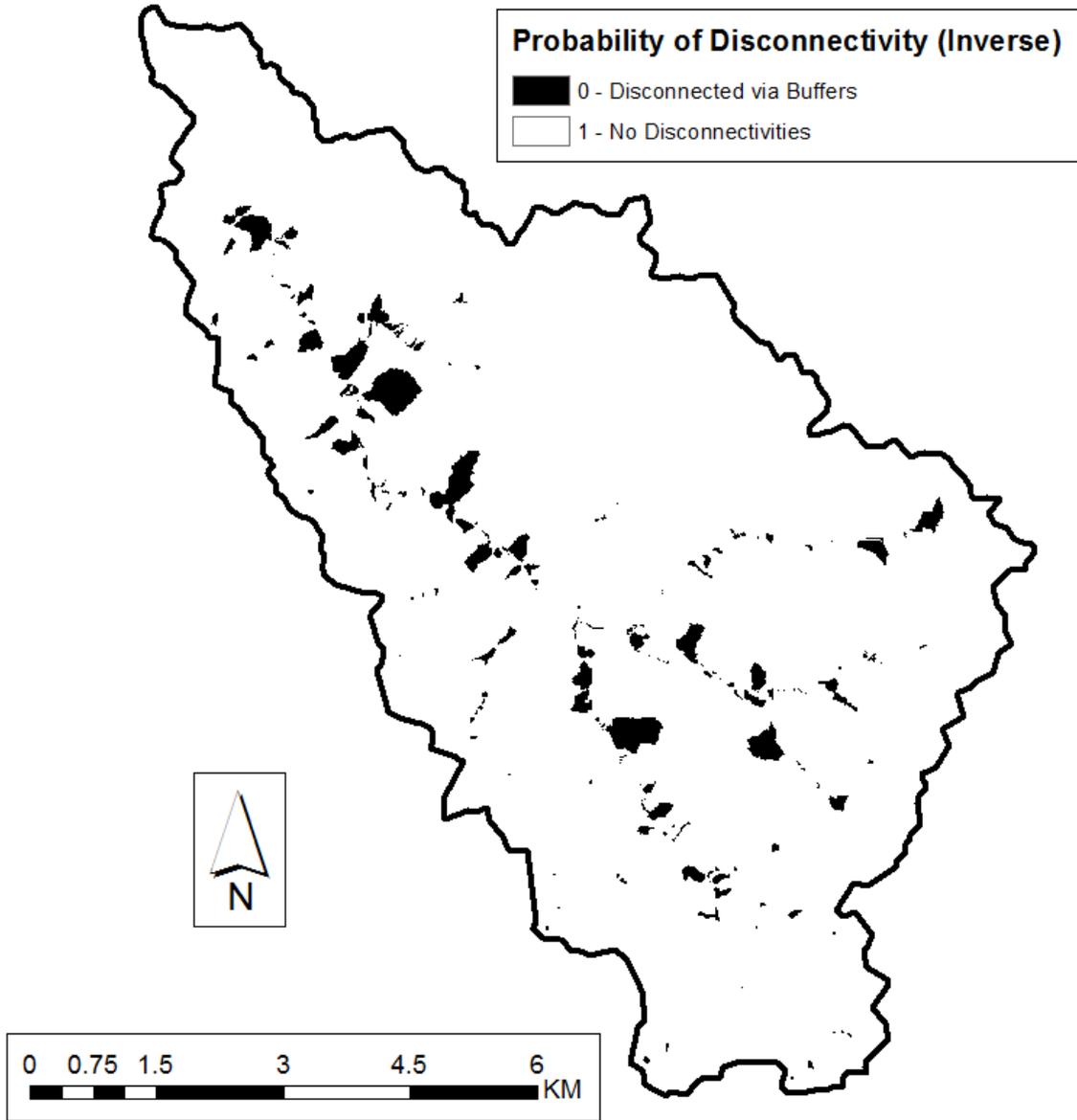
Table 6.1: Erosion model parameters

Parameter	Description	Value	Units
A_1	Contributing Area, Bin 1	116	m^2
A_3	Contributing Area, Bin 2	951	m^2
A_3	Contributing Area, Bin 3	94,079	m^2
τ_{cr}	Critical Shear Stress	3.5	Pa
S_1	Longitudinal Slope, Bin 1	0.16	m/m
S_2	Longitudinal Slope, Bin 2	0.13	m/m
S_3	Longitudinal Slope, Bin 3	0.12	m/m
w_1	Channel Width, Bin 1	0.088	m
w_2	Channel Width, Bin 2	0.13	m
w_3	Channel Width, Bin 3	0.44	m
ε/D	Relative Roughness	0.1	Unitless
f	Darcy-Weisbach Friction Factor	0.102	Unitless
ρ_d	Bulk Density of Eroded Sediment	1,400	kg/m^3
t_1	Storm Length, Erosion Time Bin 1	5	m
t_2	Storm Length, Erosion Time Bin 2	0.25	hr
t_3	Storm Length, Erosion Time Bin 3	0.5	hr
k_d	Erodibility Coefficient	0.0055	cm^3/N-s
L_1	Channel Length, Bin 1	Varies daily	m
L_2	Channel Length, Bin 2	Varies daily	m
L_3	Channel Length, Bin 3	Varies daily	m
ρ_w	Density of Fluid	1,000	kg/m^3

Table 6.2: Calibration and validation data used to predict sediment flux

Day	Date	Q_{peak} (cms)	S_y (t)
1	12/2/2007	9.91	44.5
2	2/21/2008	3.45	3.5
3	4/10/2008	3.45	3.1
4	5/15/2008	7.67	19
5	7/30/2008	3.26	6.4
6	7/31/2008	3.82	11.4
7	10/7/2008	1.3	1.3

Table 6.3: Calibration and validation data used to predict sediment flux

Day	Predicted (t)	Observed (t)	
1	63.48	44.5	Calibrate
2	7.25	3.5	
3	1.50	3.1	
4	15.01	19	Validate
7	1.17	1.3	

Chapter 7 Results

7.1 Evaluation of Probability of Sediment Connectivity Model

7.1.1 The probability of sediment connectivity reflects individual processes

The overall premise of the sediment connectivity model developed herein was to incorporate the probability of occurrence of sediment transport processes as well as morphologic features responsible for sediment connectivity. Therefore, as part of the model evaluation, it was important for the authors to investigate how sediment processes and morphologic characterization (e.g., sediment supply, hydrologic detachment of sediment) included within application of the model influence the net results.

Examples of process impacts on connectivity show that all of the processes included within the probability of sediment connectivity model have some instances where they exhibit importance (see Figure 7.1). For example, as shown in Figure 7.1a, the probability of sediment supply exhibits control on connectivity when impervious surfaces limit the production of sediment and thus have no connectivity. Impervious surfaces shown in the left portion of Figure 7.1a cause the overall probability of connectivity to equal zero, indicating disconnectivity due to a lack of sediment supply. In Figure 7.1b, the probability of sediment detachment exhibits control on connectivity when the predicted shear stress of the fluid is less than the estimated critical shear stress of sediment particles. Since the slope of the land surrogates the energy gradient of the flow, particularly flat surfaces will limit the fluvial shearing ability of the runoff, forcing the probability of sediment detachment to equal zero, thus causing the overall probability of sediment connectivity to equal zero as well, indicating disconnectivity due to the occurrence of no detachment. This is shown by the flat surface in the bottom left corner of Figure 7.1b causing overall disconnectivity.

Figure 7.1c shows the probability of downstream sediment transport by estimating the potential for sediment to be transported through a particular geospatial cell downstream to the next region of the watershed. The probability of downstream sediment transport exhibits control on connectivity when the transport capacity at a particular downstream cell during a particular time step is less than the average upstream transport capacity of the fluid to carry sediment upstream of a particular geospatial cell. When the slope of the downstream cell is less than the average upstream slope, the fluid does not possess enough energy to transport sediment, thus causing downstream disconnectivity of sediment. This is shown by the flat surface in the center of Figure 7.1c causing overall disconnectivity. Figure 7.1d shows the probability of upstream sediment transport by estimating the potential for sediment to be transported from the upstream contributing area. The probability of upstream energy for hydrologic transport reflects the geomorphic threshold conditions for ephemeral gully and rill incision. The probability of upstream sediment transport exhibits control on connectivity when the slope of the geospatial cell is greater than the critical slope required to initiate ephemeral gully incision. The formation of gullies, as shown on the left side of 7.1d, controls the connectivity of the hillslopes, as shown in the right side of 7.1d. Finally, the control exhibited by probability of disconnectivity on the probability of sediment connectivity is shown in Figure 7.1e. In this figure, lateral disconnectivities (buffers) disconnect everything upstream of them in the catchment. In Figure 7.1e, floodplains have been delineated and everything upstream of them has automatically been set to zero, i.e. disconnected.

The results in Figure 7.1 highlight the efficacy of the authors probability of sediment connectivity model to incorporate the different processes and morphologic

features controlling sediment transport and reflect a need called upon in the literature to include hydrologic and non-hydrologic supply, detachment and transport processes (Fryirs, 2013; Bracken et al., 2015). Also, the authors were curious as to the net impact of the individual processes on their control of connectivity. For example, visually it appears that the probability of upstream transport might be the most highly correlated with connectivity results for the examples shown, as the results in Figure 7.1d upstream transport and connectivity spatial results are most similar in comparison to the other features.

The net impact of the individual probabilities is quantified in Figure 7.2 where the probability of connectivity results is shown for the entire watershed for a moderate and extreme hydrologic event, as is the individual process-based probabilities used to calculate net connectivity.

Results in Figure 7.2 suggest that "probability of upstream transport" shows the most agreement with the probability of connectivity. The most dominant control on the results in Figure 7.2 tends to show qualitative agreement with other previous published models of sediment connectivity, thus providing confidence that our approach is consistent with watershed geomorphology theory. For example, the Index of Connectivity model has showed efficacy for hydrologic and sediment connectivity studies (Vigiak et al., 2012; Lopez-Vincent et al., 2013; Messenzehl et al., 2014; Cavalli et al., 2014; Souza et al., 2016), and this model is based primarily on the coupling of upstream and downstream hydrologic transport in a watershed (Borselli et al., 2008). Yet, at the same time, the results in Figure 7.2 highlight the importance of other individual processes upon controlling sediment connectivity for some instances, highlighting a need to explicitly include disconnectivity and account for hydrologic and non-hydrologic processes (Fryirs, 2013;

Bracken et al., 2015). This may occur when soil water content is high because of antecedent moisture, i.e. the upstream transport of connectivity will be high, and a hydrologic event of low magnitude produces a small amount of runoff, as shown in Figure 7.2c for Day 33. In general, however, the most connected days are limited by the probability of upstream transport, as shown by Days 72 and 138 in Figure 7.2.

7.1.2 The probability of sediment connectivity reflects erosion-prone watershed features

The ability of the sediment connectivity model to reflect hydrologic and non-hydrologic detachment and transport perhaps shows the wider utility of the method (e.g., Bracken et al., 2015). Yet the authors contend that the connectivity results should also be represented of site specific, erosion-prone features within an individual watershed. Therefore, the authors evaluated the probability of sediment connectivity results by inspecting regions where it was known that watershed erosion will be pronounced and investigating the sediment connectivity results.

Figure 7.3 shows that the probability of sediment connectivity results tended to produce high connectivity for a number of erosion-prone watershed features in the South Elkhorn Watershed including steep slopes in newly constructed, urban areas, accumulated flow pathways alongside roadways, and gully erosion from concentrated flow pathways in agricultural areas. Figure 7.3a shows the occurrence of connectivity from steep slopes in an urban/newly constructed development. The location within the watershed is circled in red in the bottom-left corner of Figure 7.3a. The imagery at the site of predicted connectivity is the first blown-up image shown in Figure 7.3a. Next, the slope raster created from the DEM of the watershed is shown for the connected site. The steepest slopes are shown in white and the flatter slopes are shown in black. Finally, the right-most image

shows the probability of connectivity for the site. Areas in white are connected, and areas in black are disconnected. Here, the most connected areas are coincident with steeper slopes and on land that is fallow/recently disturbed.

Figure 7.3b shows the occurrence of connectivity from steep ditches and water accumulated from roadways. The location of the site within the watershed is circled in red in the bottom-left corner of Figure 7.3b. The imagery at the site of predicted connectivity is the first blown-up image shown in Figure 7.3b. Next, the slope raster created from the DEM of the watershed is shown for the connected site. The steepest slopes are shown in white and the flatter slopes are shown in black. The steepest slopes are generally found next to roadways. Finally, the right-most image shows the probability of connectivity for the site. Areas in white are connected, and areas in black are disconnected. Here, the most connected areas are adjacent to roadways, where slopes are generally steep and accumulated concentrated runoff is anticipated to flow.

Figure 7.3c shows the occurrence of connectivity from concentrated flow paths in agricultural gullies. The location of the site within the watershed is circled in red in the bottom-left corner of Figure 7.3c. The imagery at the site of predicted connectivity is the first blown-up image shown in Figure 7.3c. Next, the slope raster created from the DEM of the watershed is shown for the connected site. The steepest slopes are shown in white and the flatter slopes are shown in black. Finally, the right-most image shows the probability of connectivity for the site. Areas in white are connected, and areas in black are disconnected. Here, the most connected areas are coincident with the hillslopes adjacent to the stream network, where slopes are generally steep, the land use is pasture, and gully formation may occur.

The site specific results of the probability of sediment connectivity's ability to reflect erosion-prone watershed features in the South Elkhorn Watershed is consistent with historic research and current sentiment of watershed managers and scientists in the South Elkhorn. As previously mentioned, sediment particles are sourced from various agricultural and urban land uses within the Upper South Elkhorn watershed. Within the stream corridor, primary sediment transport processes include streambank erosion, streambed erosion, surficial fine-grained laminae erosion, and mass wasting (Russo and Fox, 2012). Based on visual observation, eroding streambanks are prominent throughout the watershed and are a primary source of instream erosion. Urbanization in the Upper South Elkhorn watershed is a suspected cause of the exacerbated streambank erosion (Russo, 2009). Upland erosion production occurs primarily through rill erosion, ephemeral gully erosion, and concentrated flow pathways, while diffusional erosion processes (i.e. sheet and interrill erosion) are believed to provide a minor contribution to the overall sediment flux at the watershed outlet (Blanford, 2017; Gumbert, 2017; Smallwood, 2017). Livestock and construction sites in the uplands exacerbate the detachment rates of sediment particles through the removal of protective vegetation and exposure to excessive eolian and fluvial shear stresses (Evans, 2017).

7.1.3 Sensitivity analysis results for the probability of sediment connectivity

Sensitivity analysis focused on the sensitivity of individual parameters impacting the sediment connectivity as well as the impact of geospatial resolution upon the results (see Figure 7.4). In general, the parameters used to calculate the probability of sediment connectivity show a lack of pronounced sensitivity within a reasonable range reported in the literature, which adds confidence that the connectivity model can be applied by

incorporating geospatial inputs and hydrologic modeling results for a watershed. Table 7.1 shows the minimum, maximum, and optimal value of the critical shear stress used to determine the probability of connectivity for the Upper South Elkhorn watershed (Hanson and Simon, 2001). The critical shear stress of sediment to resist detachment shows a lack of sensitivity until reaching a value of approximately 15 Pa, as shown in Figure 7.4a. Such an extremely high critical shear stress will generally not be expected for agricultural surface lands (Simon and Thomas, 2002).

The *b* exponent represents the flow condition that initiates rill and ephemeral gully erosion. According to Torri and Poesen (2014), lower values of the *b* exponent represent laminar flow conditions while higher values of the *b* exponent represent turbulent flow conditions. It is anticipated that, in general, fully turbulent concentrated flow is required to breach the threshold required to initiate rill and ephemeral gully erosion (Torri and Borselli, 2003). *b* values were predicted to vary between 0.5 for laminar flows and 0.857 for fully rough, turbulent flow (Montgomery and Dietrich, 1994). Torri and Poesen (2014), however, believe that 0.38 is more representative of turbulent flow conditions because the original study by Montgomery and Dietrich (1994) did not consider hydrologic disconnectivities in their study, thus over estimating the actual value for *b*. Table 7.1 shows the minimum, maximum, and accepted value of *b* found from literature (Vandaele et al., 1996; Torri and Poesen, 2014). Figure 7.4b shows the sensitivity of the probability of connectivity to changes in the *b* factor.

The sensitivity of the probability of connectivity to the *c* factor found in Equation (6.14) was also assessed. The *c* factor is a modification to the *a* factor from Equation (6.13) that represents other sources variation of the *a* factor of Equation (6.13) that are not

represented by the empirical estimation of a via the $S_{0.05}$ estimation of infiltration. a is representative of the climate, soil, land use, and management activities present in the cell at a particular time step. One example of a process not modeled by the k factor is piping (Torri and Poesen, 2014). The c factor can vary between 0.1 and 1 according to Torri and Poesen (2014). A c factor of 0.1 represents conditions where piping is prevalent and 1 represents a situation where no external processes affect the a factor besides those represented in the $S_{0.05}$ infiltration parameter. The physical significance of the c factor has not been intensely investigated in the connectivity literature, but after review of one study completed by Verachtert et al., (2010), a range of 0.1 to 0.4 has been suggested as a c factor representative of piping (Torri and Poesen, 2014). Table 7.1 shows the minimum, maximum, and accepted value of c from literature.

A number of past studies have placed emphasis upon the importance of a sediment connectivity model that can account for sediment transport thresholds associated with fluid energy and sediment resistance (Kirkby et al., 2002; Fryirs et al., 2007; Fryirs, 2013; Nicoll and Brierly 2016; Souza et al., 2016). The overall general sensitivity of the individual parameters in the author's probability of sediment connectivity model tend to suggest that such energy and sediment thresholds can be justifiably represented without substantially skewing the overall results.

On the other hand, the geospatial resolution of the DEM did tend to show substantial sensitivity and impact the results. The 9 m by 9 m (30 ft by 30 ft) DEM tended to produce probability of sediment connectivity results that were nearly two times greater than the 1.5 m by 1.5 m (5 ft by 5 ft) DEM geospatial analysis, as shown in Figure 7.4b. In turn, this reflects a doubling of the active contributing area of watershed erosion to the

stream. Multiple DEM resolutions have been used in the literature. In their analysis, Fryirs et al., (2007) used a 25 m by 25 m DEM to analyze the slope threshold required for land to actively contribute to the sediment cascade. Borselli et al., (2008) used a 5 m by 5 m DEM to create the Index of Connectivity. Cavalli et al., (2013) slightly altered the Index of Connectivity and used a 2.5 m by 2.5 m DEM. Figure 7.4b shows the deviation in the predicted probability of connectivity for 2006 using the 1.5 m by 1.5 m DEM and the 9 m by 9 m DEM. The average deviation between the 1.5 m by 1.5 m and 9 m by 9 m DEM was 80%. The predicted probability of connectivity for highly connected days, in particular, differed greatly between both DEMs. For example, days 71, 22, 292, and 300 of year 2006 were each predicted to have double the amount of connected land when using the 9 m by 9 m DEM when compared to the amount of connected land predicted by the 2.5 m by 2.5 by DEM. The authors believe that this is significant because the days with the highest amounts of connectivity are suspected to coincide with days where the most amounts of sediment will be transported. Thus, sediment flux prediction will likely differ greatly because of DEM resolution.

The authors suggest that the difference in the predicted probabilities of connectivity is attributed to both the size of the DEM pixel and the dissection of the DEM. As shown in Figure 7.4c, areas of predicted connected lands do spatially coincide with one another. However, since the area of the connected cells for the 9 m by 9 m DEM are 36 times greater in area of the 1.5 m by 1.5 m DEM, the overall probability of connectivity for the entire watershed will also be higher. Figure 7.4c shows the size comparison of the connected cells for the 1.5 m by 1.5 m DEM and the connected cells for the 9 m by 9 m DEM. The 1.5 m by 1.5 m DEM better captures the micro-topology of the landscape, better discerning where

locally flat slopes occur. Locally flat surfaces recognizable due to resolution of the 1.5 m

by 1.5 m DEM but not the 9 m by 9 m DEM may increase the amount of disconnectivity

predicted by the probability of connectivity model. At the same time, the 9 m by 9 m DEM

may overestimate the slope of the landscape because of the same lack of DEM precision,

thus causing more cells to be connected.

As mentioned, the 1.5 m by 1.5 m DEM can better capture micro-landscape

dissection due to the micro-contributing areas of very small tributaries. According to

Equation (6.14), the more upstream contributing area that a geospatial cell has, the more

likely it is to be connected. Geospatial cells with no upstream contributing area, i.e those

on the boundary of a watershed or micro-catchment, are automatically assumed to have no

connectivity, which the authors believe to be reasonable considering the lack of

accumulated runoff that can be generated in such a small contributing area. Thus, the more

dissected a DEM is into the landscape's micro-contributing areas, the more the

disconnectivity in the overall catchment. The dissection of the each DEM can be seen in

Figure 7.4d. Black pixels represent areas on the boundary of local micro-catchments that,

because of a lack of upstream contributing area, are assumed to be disconnected. Pink and

green cells represent disconnected and connected cells predicted from the probability of

connectivity model, respectively. The 1.5 by 1.5 m DEM has many more disconnected

cells due to the dissection of micro-catchments as compared to the 9 m by 9 m DEM.

Because higher resolution DEMs better reflect the actual topography of a landscape

(Cavalli et al., 2013), the authors suggest that the 1.5 m by 1.5 m DEM does a better job of

predicting the probability of connected land than the 9 m by 9 m DEM does and reflecting

the actual dissection of the landscape. Hence, always the highest resolution DEM available

should be used to predict the probability of connectivity. For this reason, sediment flux was predicted at the Upper South Elkhorn watershed only for the 1.5 m by 1.5 m DEM.

7.2 Probability of Sediment Connectivity for the South Elkhorn

7.2.1 Net results for the South Elkhorn Watershed

The authors estimated the net probability of sediment connectivity for the South Elkhorn watershed for 2006, 2007 and 2008. Temporally distributed results for 2006 are shown in Figure 7.5 as is the spatial distribution of the probability of sediment connectivity for a wet day in the South Elkhorn Watershed on March 12, 2006, the 72nd day of the year.

For 2006, the probability of sediment connectivity ranges between 0%, during no rainfall, to approximately 13%, during a day with wet soils and high rainfall (Figure 7.5a). This means that on the most connected day of 2006, approximately 13% of the catchment had the potential to contribute to the sediment cascade. 13% connectivity occurred on March 12, 2006, i.e. the 72nd day of the year (time step 72). For the majority of the year, the catchment is disconnected. At least some connectivity (i.e., greater than 0%) of the catchment uplands only occurs during 104 days of 2006 (i.e. only on days when rain produced runoff in the catchment). Rainfall occurred on 132 days of the year, and runoff occurred on 104 days of the year, which highlights the importance of hydrologic connectivity in this watershed system. It is of interest to note that just because rainfall occurs in the catchment, sediment connectivity will not necessarily also occur. However, days where runoff occurred in the catchment correlated with days with sediment connectivity in the catchment.

Figure 7.5b shows the connected areas for March 12 of 2006, where dark gray represents connected areas and white represents disconnected areas. As shown in the

figure, the northern portion of the watershed shows the highest connectivity attributed to a shift in the soil conditions in this portion of the watershed. Engineering properties of the soils shift lower in the watershed from 64% hydrologic soil group B, which indicates a moderate rate of water transmission according to the NRCS (1986), 30% hydrologic soil group C, which indicates a low rate of water transmission, and 6% hydrologic soil group D, which indicates a very low rate of water transmission to 26% hydrologic soil group B, 45% hydrologic soil group C, and 29% hydrologic soil group D. The shift in the engineering properties of the soil is attributed to the decrease in percent sand and increase in percent fine clay in the lower portion (northwest portion) of the watershed (NRCS, 2006). This attributes to the higher connectivity predicted in the northwest portion of the watershed.

The central eastern half of the watershed has connectivity associated with the urban and surburban regions due to an increase in the imperviousness of the landscape in this portion of the catchment. The curve number of this region, which is an empirical measure of the imperviousness and infiltration capacity of the landscape, is higher in this region, and thus produces more runoff. The increase of the production of runoff in this region and the reduced infiltration capacity of the soil are indicative of the prediction of higher amounts of hydrologic detachment and upstream hydrologic transport of sediment than other portions of the watershed.

7.2.2 Comparison of the South Elkhorn Watershed with other Systems

It is not possible to quantitatively compare the sediment connectivity results from this study with that of other studies in the literature due to the fact that the modeling approach here is somewhat unique. Nevertheless, some qualitative comparison is possible

in order to understand the watershed geomorphology of the study system in relation to other studies where the sediment connectivity has been considered.

In general, the South Elkhorn Watershed could be classified as an event-resilient, disconnected system as opposed to a highly connected, event-sensitive landscape (Fryirs et al., 2007). The low connectivity results for the South Elkhorn suggest the relatively low propagation of disturbances within the watershed (Borselli et al., 2008). The fairly well established non-intensive pasture systems (i.e., equine systems) as well as the mild watershed gradients promote a lack of overall connectivity for the watershed. The South Elkhorn results tend to contrast steeper gradient systems where connectivity results are much higher, as in the work of Fryirs et al., (2007). Fryirs et al., (2007) predicted the active contributing area for four landscape units in the upper Hunter catchment in Australia, which have relatively high elevation, deep dissection, and a rugged, hilly landscape. Comparatively, the Upper South Elkhorn watershed, which is within the Inner Bluegrass Physiographic region of Kentucky, has gently rolling hills and relatively mild slopes. For what was assumed to be a moderate-sized storm event, approximately 48% of the catchment was predicted to be connected, which contrasts greatly with the predicted results from the authors' method. Previous research has suggested that in-stream sediment functions within the lowland system substantially contrast in-stream sediment processes of steeper systems (Ford and Fox, 2015), and the results here extend the geomorphologic spectrum to the upland template.

One potentially interesting connectivity feature in the South Elkhorn Watershed was the importance of the accumulated flow pathways alongside roadways (i.e., ditches, roadside gullies) in the urban regions of the watershed. The net result was that urban

regions of the watershed could show net higher connectivity than surrounding agricultural regions. The importance of roadways to induce erosion and sediment connectivity has been discussed previously for mountainous catchments (Latocha et al., 2014), and urban sprawl, i.e., urbanization, has been well understood to induce gully formation and channeling processes (Trimble, 1993). However, few papers to our knowledge have reported the net importance of roadway ditches and gullies in well established urban environments. The coupling of the probability of sediment connectivity model with the 1.5 m by 1.5 m geospatial resolution was able to highlight the importance of the landscape features.

7.3 Spatial and Temporal Distribution of the Probability of Sediment Connectivity

7.3.1 Spatial distribution of connectivity for the South Elkhorn Watershed

The authors also assessed the spatial variability of sediment connectivity longitudinally in the watershed by investigating the probability of sediment connectivity from catchment (~1 km^2) to mid-sized watershed scales (~60 km^2). Spatial variability results identified longitudinally included a weak increase in the probability of sediment connectivity with scale (see Figure 7.6). in addition, the variance of sediment connectivity was highest at the smaller scale and the variance tended to decrease as watershed scale increased.

The longitudinal variability of sediment connectivity tends to be under-investigated in the literature, yet there tends to be competing processes operating at different scales within a watershed configuration (Phillips, 2003; Borselli et al., 2008; Fryirs, 2013). That is, at relatively smaller, hillslope to small catchment scales higher relative landscape gradient is suggested to promote sediment connectivity far from low gradient deposition

zones and floodplains (Fryirs et al., 2007). On the other hand, as the watershed scale increases, upstream flow accumulation has the potential to concentrate fluid providing the hydrologic connectivity for conveying sediment (Borselli et al., 2008). The results in Figure 7.6 tend to suggest the latter process, i.e., flow accumulation, for the South Elkhorn, which is likely attributed to the dominance of gully erosion and erosion within concentrated flow pathways as opposed to sheet erosion processes or mass wasting. In either case, the variance of sediment connectivity seems to be higher at smaller scales, which seems logical. That is, the processes reflecting sediment connectivity might vary from sub-catchment to catchment, in the present case such as the distribution of roadways or previously impacted agricultural sites.

Fryirs (2013) conceptually reviewed the linkages of sediment in an idealized catchment at the headwaters, mid-catchment, and lowland plain zones. In general, the headwaters of a catchment, i.e. catchment areas with steep slopes and low order streams, are well connected between hillslopes and channels and efficiently transfer flow and sediment longitudinally. Further downstream, in the mid-catchment zone, hillslope-channel connectivity becomes irregular, channel-floodplain connectivity is irregular, but there is still efficient transfer of flow and sediment longitudinally. In the lowland plains, hillslope-channel connectivity is limited and sediments are inefficiently transferred longitudinally. Channel-floodplain connectivity, i.e. lateral connectivity, is high, however, since floodplains are generally more easily accessible in the lowlands. As water and sediments flow from the headwaters to the lowland plain, sediment storage is conceptualized by Fryirs to increase, sediment delivery decreases, and there is increased channel-floodplain connectivity. Since the Upper South Elkhorn is a lowland watershed,

130

the spatial distribution of connected land as predicted by the authors' probability of connectivity model compares well with Fryirs' theory.

7.3.2 Temporal distribution of sediment connectivity for the South Elkhorn Watershed

Connectivity is a function of both the geomorphology of the catchment, i.e. structural or static connectivity, and the hydrology of the catchment at a particular time step, i.e. functional or dynamic connectivity (Benda and Dunne, 1997; Bracken and Croke, 2007; Lexartza-Artza and Wainwright, 2009; Fryirs, 2013). Therefore, connectivity will dynamically change on a daily basis. As previously mentioned, for 2006, 104 days have some connectivity. The Probability of Sediment Connectivity model predicted that approximately 13.47% of the catchment had the potential to contribute to the sediment cascade on March 12, 2006 (day 72). The average percent of connected land for the days with some connectivity for the study period is 2.31% and the standard deviation is 0.0362.

Figure 7.7 shows the frequency distribution of the percent of connected land on connected days for the study year. 0% to 1.68% of the catchment was connected for 68 days of the study period. A second frequency distribution was created where days with less than 1% connectivity were neglected. Neglecting days with less than 1% connectivity yielded 38 days where the catchment had some sediment connectivity. The beta distribution best fits the selected data (beta: 0.73, 1.08, 1.13, 13.48; Ch-Sq is 9.71; p-value is 0.137). The beta distribution is a logical choice for temporal representation of the probability of sediment connectivity given that the beta distribution is continuous in nature but bounded by 0 and 1, and therefore is suitable for representing the behavior of percentages.

Dynamically, we see that connectivity reflects a beta-like distribution. While few studies have investigated the dynamic nature of connectivity, the importance of dynamic

131

connectivity within connectivity estimation is well known (Borselli et al., 2008; Bracken et al., 2015). To this end, the probability of sediment connectivity definition presented in this study highlights the potential to couple hydrologic connectivity via the hydrologic model within the sediment connectivity framework. As researchers work towards a better understanding of sediment connectivity across different watershed systems, it is suggested that dynamic connectivity might be included via frequency analyses, e.g., using a beta-like distribution.

7.4 Watershed Erosion Modeling Results

7.4.1 Evaluation of the watershed erosion modeling

As mentioned in the methods section, the authors adjusted the sediment transport parameters within the watershed erosion modelling in order to calibrate and validate the model. The calibration and validation procedure was first performed on a daily basis, and thereafter validation was also performed on an annual basis (Figure 7.8). Predicted and observed sediment flux values for specified days of the study period are shown in Figure 7.8a, and in general good agreement is seen between the data and modeling results (R^2=0.95). Assimilation of hydrologic data was performed in order to reduce the propagation of error from the SWAT hydrologic model to the watershed erosion model at a daily time step and therefore allow isolated daily calibration and validation of the erosion model. The method worked well to reduce the propagation of error. However, the authors were also curious as to the net impact of data assimilation, or lack thereof, upon the watershed erosion model results. As shown in Figure 7.8b, while some daily discrepancy existed between sediment flux estimates for assimilated and non-assimilated model runs, the net sediment flux was identical at the end of the 2006 simulation year. The results

highlight the effectiveness of our data assimilation procedure for calibration purposes but also the annual prediction capabilities of the watershed erosion model for time periods when data assimilation is not possible. Sensitivity analysis of parameters in the calibrated watershed erosion model showed the importance of the erodibility coefficient, which has been found to vary widely in the literature (Hansen and Simon, 2001). The time of concentration also showed moderate sensitivity upon sediment flux while the impact of the friction coefficient and critical shear stress of sediment to resist erosion was marginal upon the sediment yield results. Annual sediment yield for the watershed (see Table 7.2) was just 6% greater than annual sediment yield estimated for the upland contribution estimates reported in Russo and Fox (2012) for the same time period, which provides further validation of the modeling results.

The authors highlight the concept that the spatially explicit probability of sediment connectivity can be used as a precursor to estimating watershed erosion, which can be temporally distributed throughout a year due to the dynamic nature of sediment transport. At the same time, and perhaps somewhat surprisingly, the authors highlight that the probability of sediment connectivity alone is not necessarily a good predictor of sediment flux associated with watershed erosion. This idea is highlighted in Figure 7.9, where both the probability of sediment connectivity and sediment flux are shown for 2006. Obviously, nonzero sediment flux cannot occur unless some sediment connectivity exists in the watershed given the logic assumed in our watershed erosion model. Nevertheless, the probability of sediment connectivity by itself is a poor predictor of sediment flux (i.e., via visual comparison of temporal distributions in Figure 7.9). The results highlight the sentiment that sediment connectivity alone does not provide the research with an estimate

of flux, which has been highlighted in the framework of Bracken et al. (2015). In the present study, the reason for the lack of agreement is attributed to the need for estimating the flow accumulated fluid shear stress via hydraulic formula, as was performed in the watershed erosion modeling. This concept is further mentioned in the discussion chapter.

While sediment flux did not necessarily agree with the probability of sediment connectivity, coupling of the probability of sediment connectivity and erosion formula does a very nice job of providing a spatially explicit estimation of erosion rates across the landscape. Consistent with the probability of sediment connectivity results, erosion-prone watershed features also showed sediment flux and included erosion from newly constructed developments, urban areas, accumulated flow pathways alongside roadways, and gully erosion from concentrated flow pathways in agricultural areas. The result is highlighted for accumulated flow pathways in roadside ditches (see Figure 7.10) where the watershed erosion model results provide an estimate of erosion rates.

Figure 7.1: Examples of how sediment processes and morphology reflected within probability of sediment connectivity results

(a) Probability of sediment supply

Probability of Supply:

$$P_i(S) = \begin{cases} 1, & \text{if is sediment is present within the cell} \\ 0, & \text{if sediment is absent within the cell} \end{cases}$$

Sediment Supply 0 1

Connectivity 0 1

0   0.1   0.2   0.4 Kilometers
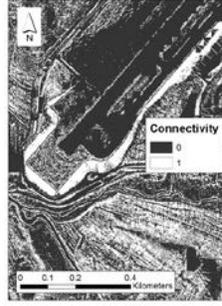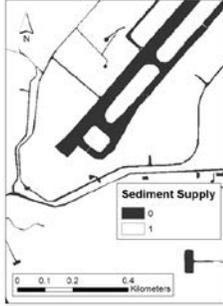
(b) Probability of sediment detachment

Probability of Detachment:

$$P_{ij}(D_H) = \begin{cases} 1, & \text{if } \tau_{f\,ij} - \tau_{cr\,i} > 0 \\ 0, & \text{if } \tau_{f\,ij} - \tau_{cr\,i} \le 0 \end{cases}$$

$$\tau_{f\,ij} = \gamma H_{ij} S_i$$

$$P_{ij}(D_{NH}) = \begin{cases} 1, & \text{if a disturbance agent exists} \\ 0, & \text{if a disturbance agent is not present} \end{cases}$$

Detachment 0 1

Connectivity 0 1

0   0.075   0.15   0.3 Kilometers
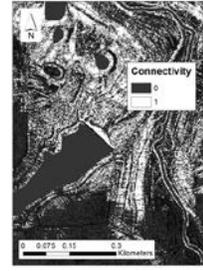
(c) Probability of downstream transport

Probability of Hydrologic Transport – Downstream:

$$P_i(T_{H-dwn}) = \begin{cases} 1, & \text{if } S_i - \dfrac{\sum S_{up}}{N} > 0 \\ 0, & \text{if } S_i - \dfrac{\sum S_{up}}{N} \le 0 \end{cases}$$

Downstream Transport Probability 0 1

Connectivity 0 1

0   0.075   0.15   0.3 Kilometers

(d) Probability of upstream transport

Probability of Hydrologic Transport – Upstream:

$$P_i(T_{H-up}) = \begin{cases} 1, & \text{if } S_{cr} - S_{act} > 0 \\ 0, & \text{if } S_{cr} - S_{act} \le 0 \end{cases}$$

$$S_{cr} = 0.73 * c * e^{1.3RFC} * (0.00124 * S_{0.05} - 0.037) * A^{-0.38}$$

Upstream Transport 0 1

Connectivity 0 1

0   0.075   0.15   0.3 Kilometers

(e) Probability of disconnectivity

Probability of Disconnectivity:

$$P_i(D_C) = \begin{cases} 1, & \text{if disconnectivity exists} \\ 0, & \text{if disconnectivity does not exist} \end{cases}$$

Connectivity Legend Floodplain 0 1

0   0.035   0.07   0.14 Kilometers
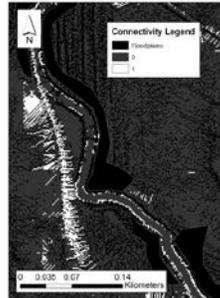
Figure 7.2: Results of net impact of individual probabilities upon the probability of sediment connectivity

Individual Probabilities of Connectivity - Day 72

Individual Probabilities of Connectivity - Day 138

Figure 7.2 (continued)

Individual Probabilities of Connectivity - Day 72

Individual Probabilities of Connectivity - Day 138

Figure 7.2 (continued)

Individual Probabilities of Connectivity - Day 33
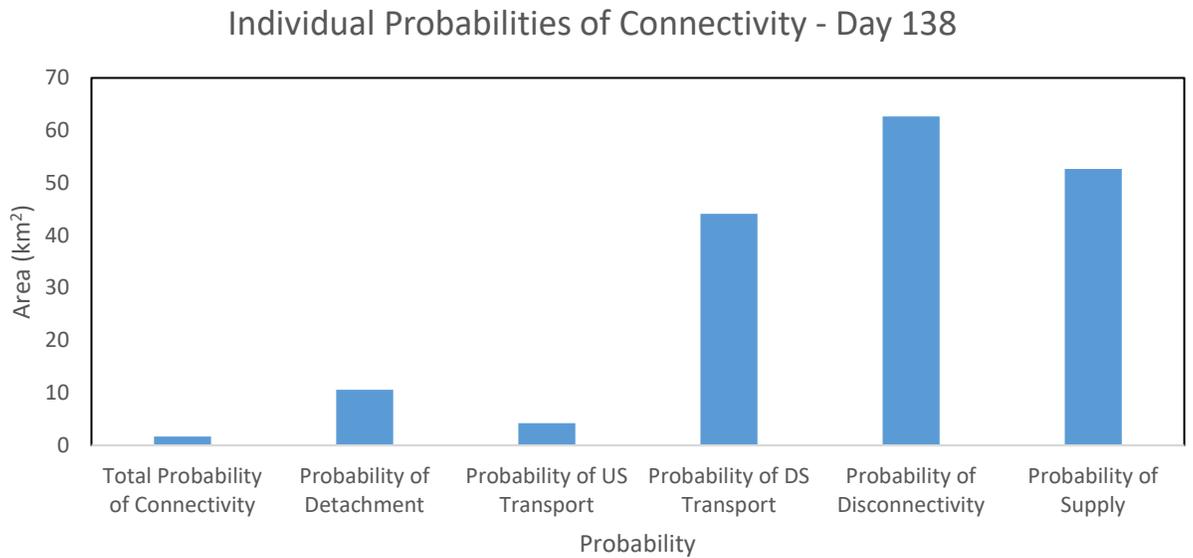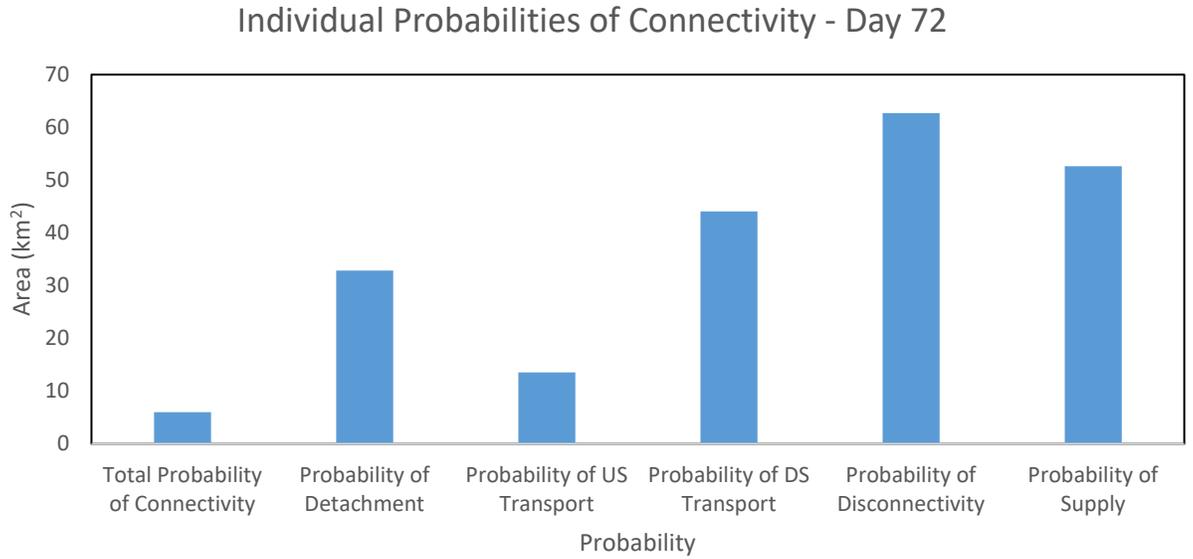


Individual Probabilities of Connectivity - Day 33
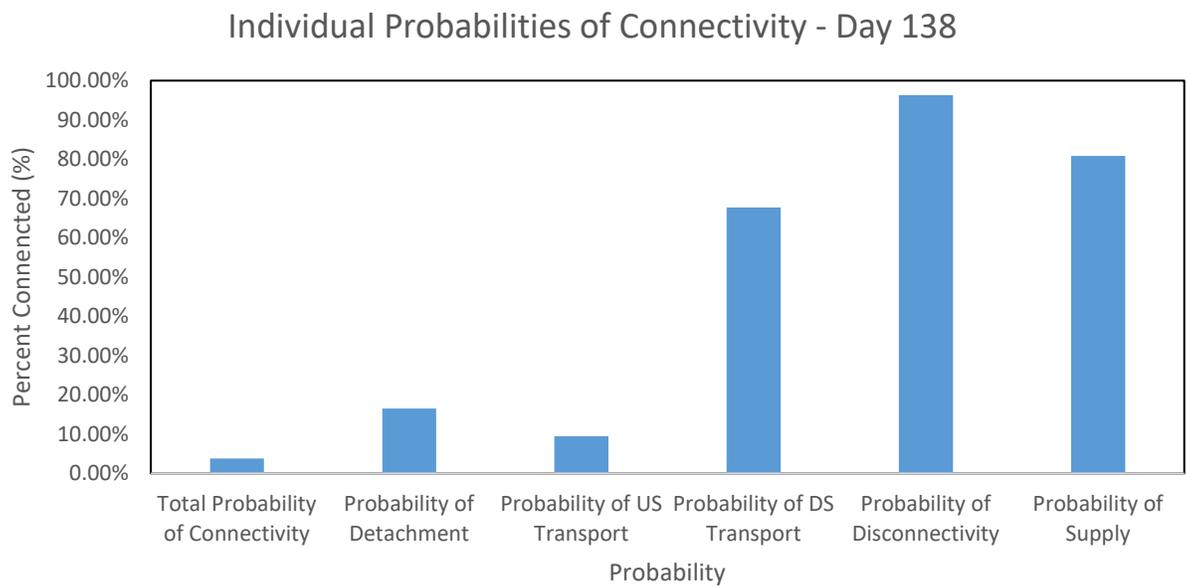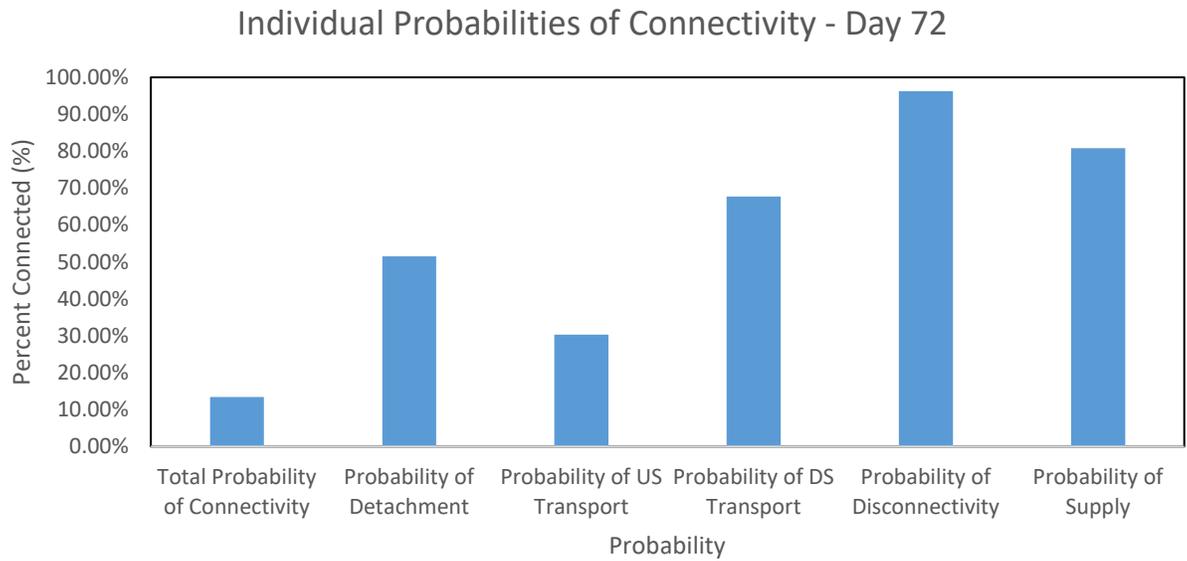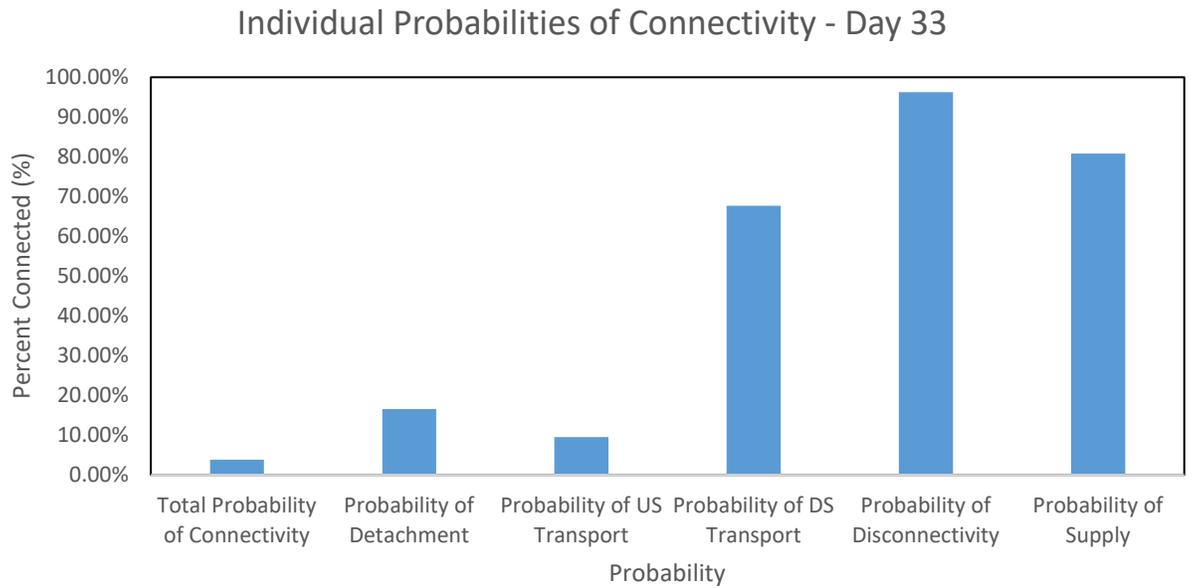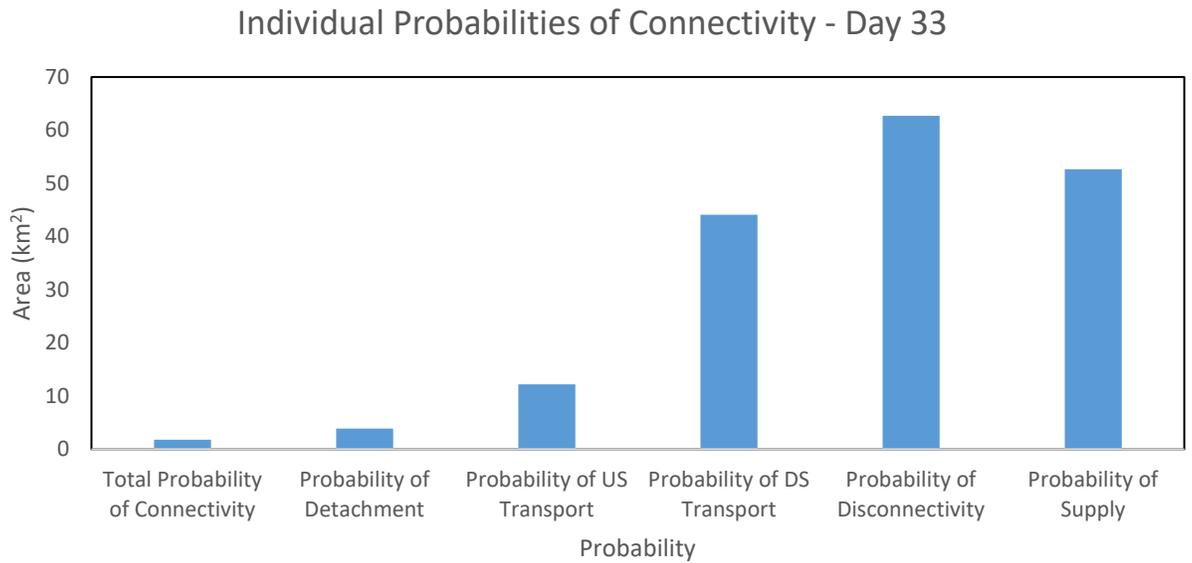
Figure 7.3: Results of net impact of individual probabilities upon the probability of sediment connectivity

Table 7.1: Minimum, maximum, and optimal values of sensitive parameters used in the probability of connectivity model and percent change in the probability of connectivity

Parameter	Unit	Minimum	Optimal	Maximum	% Change, P(C) Min	Max
τ_{cr}	Pa	0.1	3.75	75	14.13	-98.6
b	unitless	0.1	0.38	4	109.3	-34.93
c	unitless	0.1	1	1	105.81	0

Figure 7.4: Sensitivity analysis for the probability of sediment connectivity including: (a) sensitivity of parameters, (b) sensitivity of geospatial resolution, (c) comparison of the 1.5 m by 1.5 m DEM and the 9 m by 9 m DEM, and (d) a comparison of the dissection

(a) Sensitivity of individual parameters
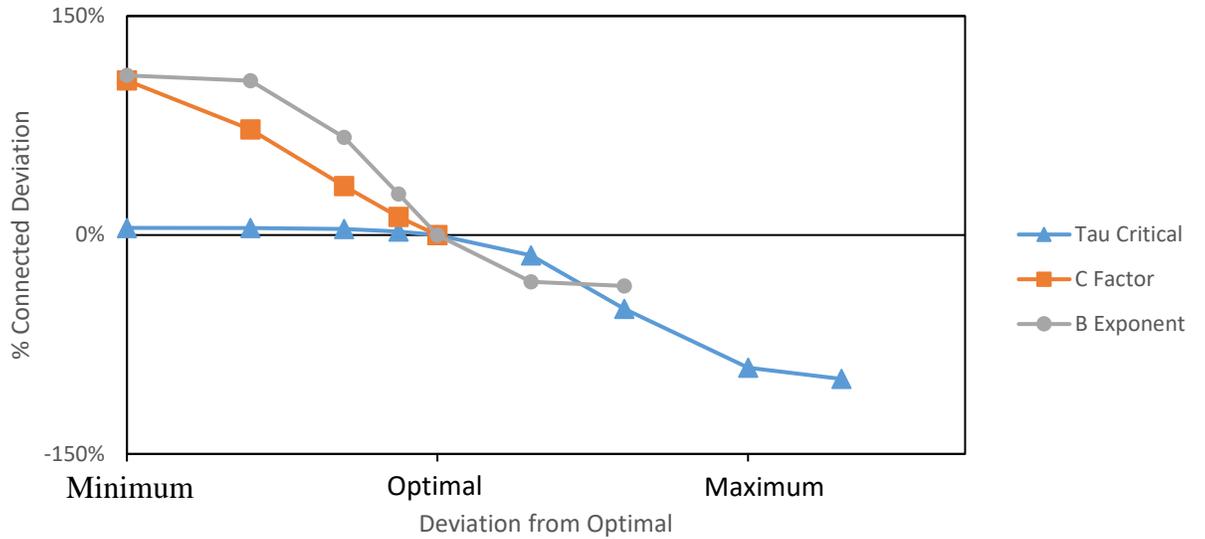
(b) Sensitivity of geospatial resolution
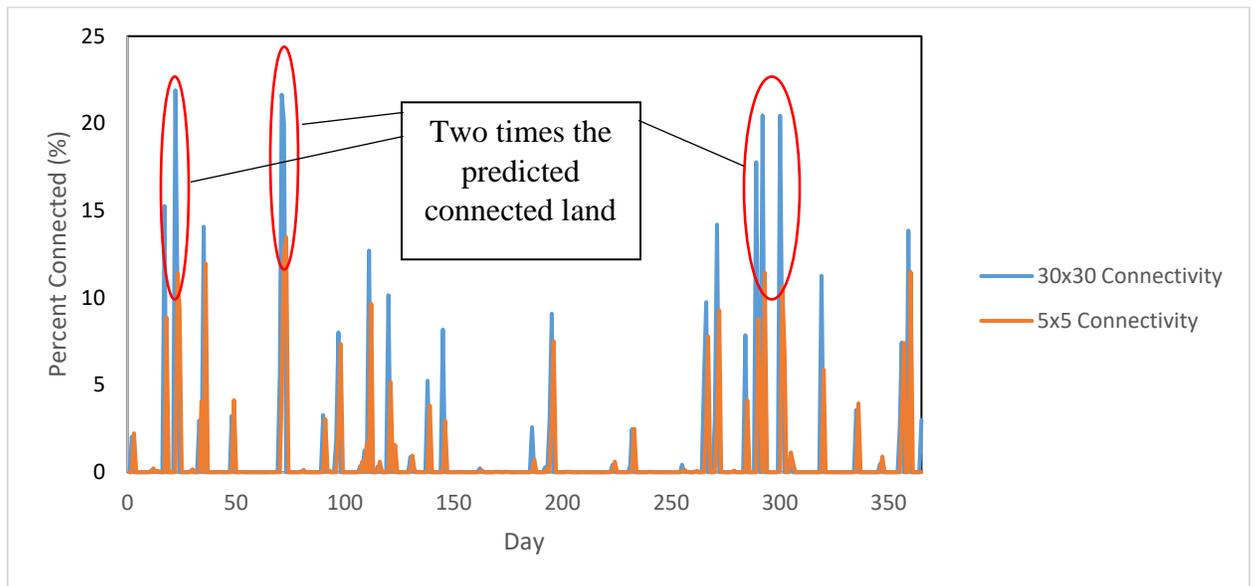
Figure 7.4 (continued) Sensitivity analysis for the probability of sediment connectivity including: (a) sensitivity of parameters, (b) sensitivity of geospatial resolution, (c) comparison of the 1.5 m by 1.5 m DEM and the 9 m by 9 m DEM, and (d) a comparison of the dissection of the 1.5 m by 1.5 m DEM and the 9 m by 9 m DEM.

(c) Comparison of the 1.5 m by 1.5 m DEM and the 9 m by 9 m DEM
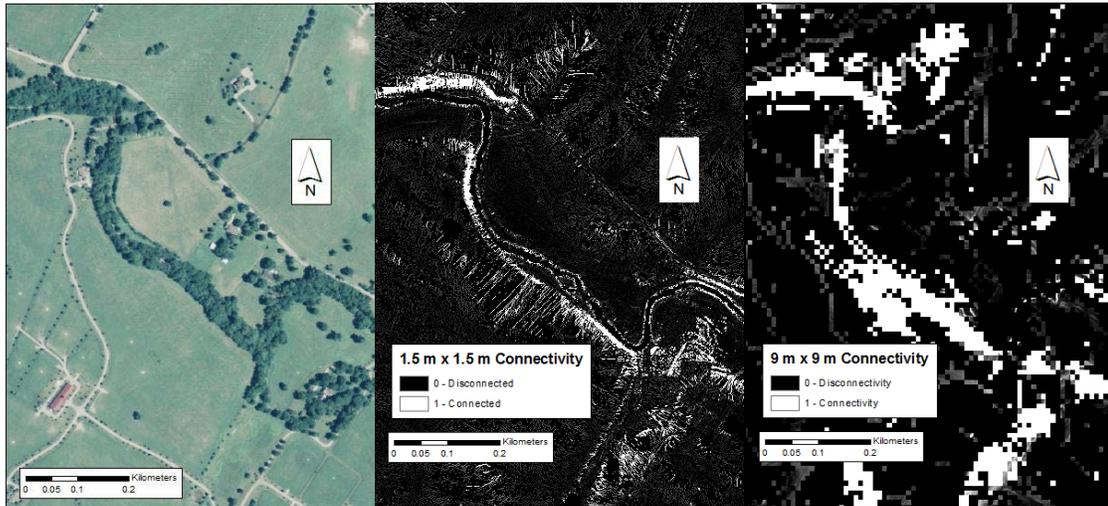
(d) Comparison of the dissection of the 1.5 m by 1.5 m DEM and the 9 m by 9 m DEM
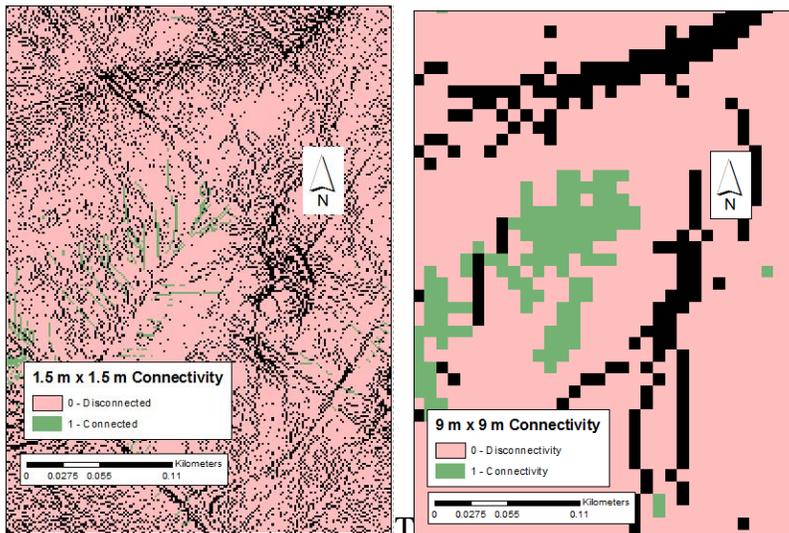
Figure 7.5: Probability of sediment connectivity results for the South Elkhorn Watershed including (a) results for one year, 2006 shown, and (b) spatial distribution on a day of high connectivity

(a) Probability of sediment connectivity results throughout one year

(b) Probability of sediment connectivity for March 12, 2006
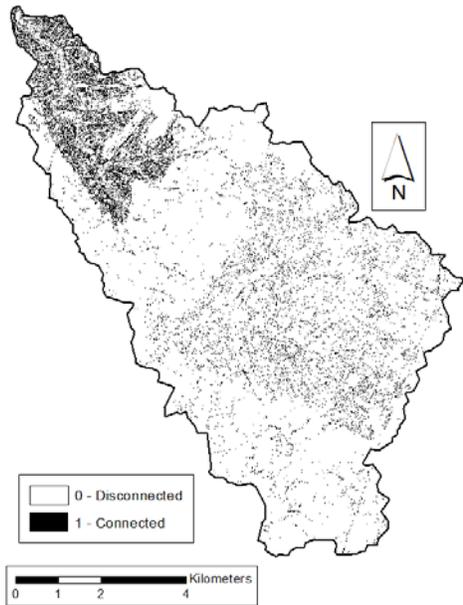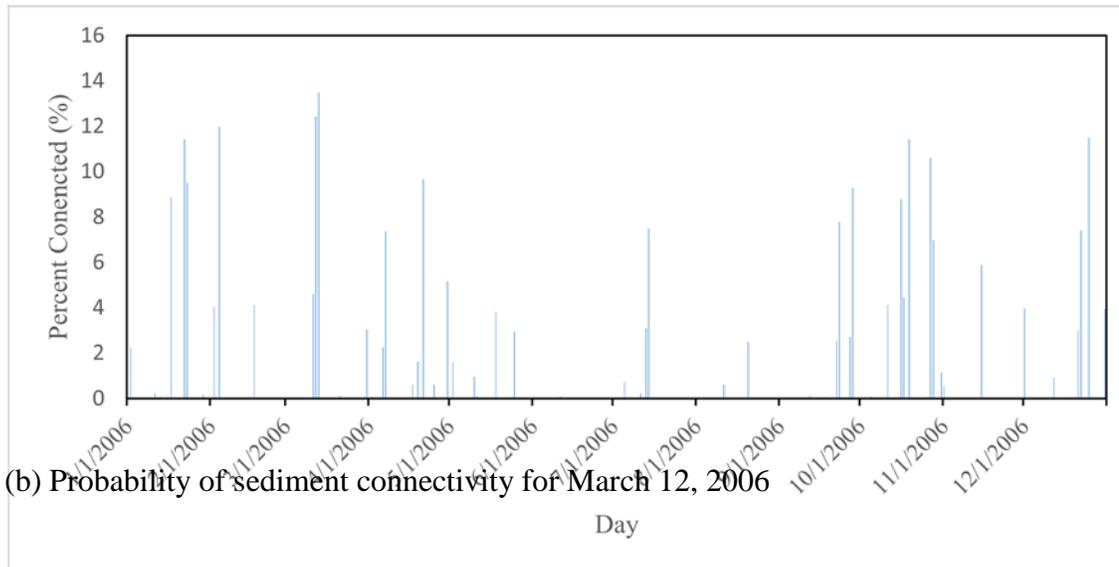
Figure 7.6: Spatial distribution of the probability of sediment connectivity for the South Elkhorn Watershed
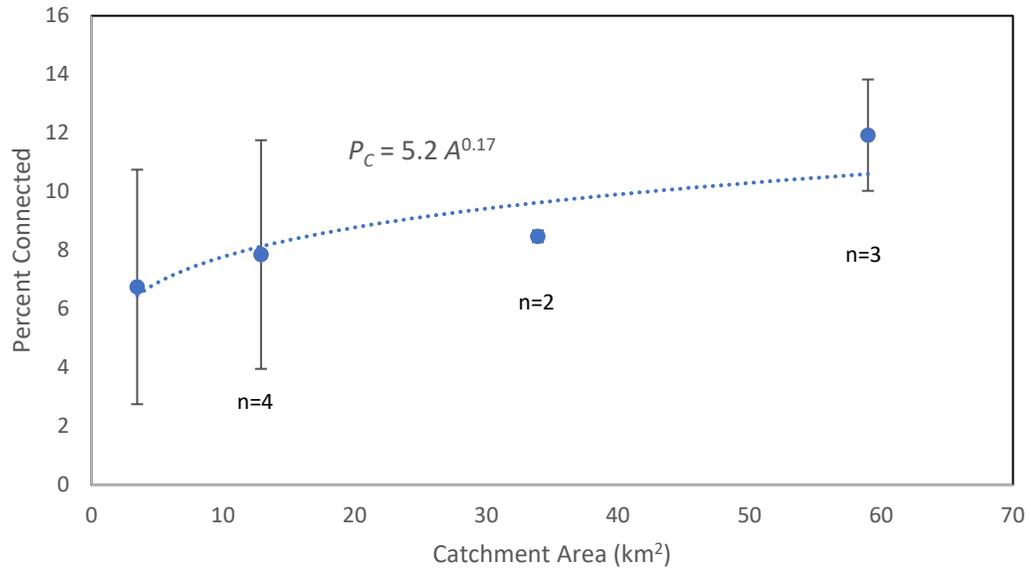
*Figure 7.7: Temporal distribution of the probability of sediment connectivity for the South Elkhorn Watershed*

(a) Frequency distribution for the probability of sediment connectivity (all days)
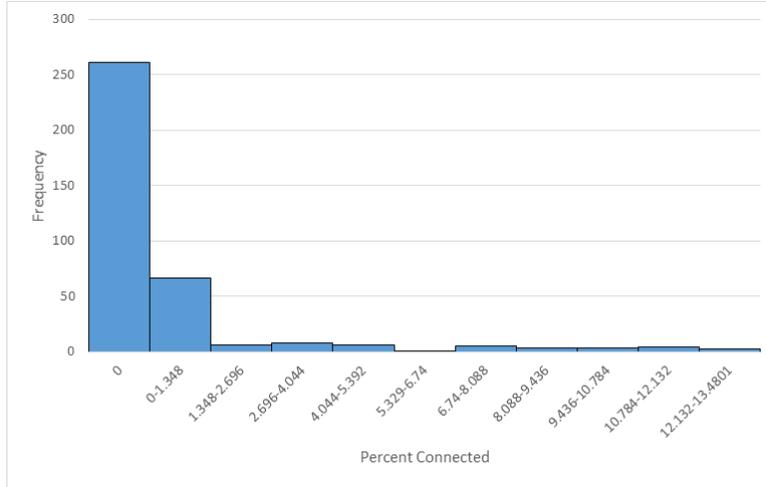
(b) Frequency distribution for the probability of sediment connectivity (connected days only)
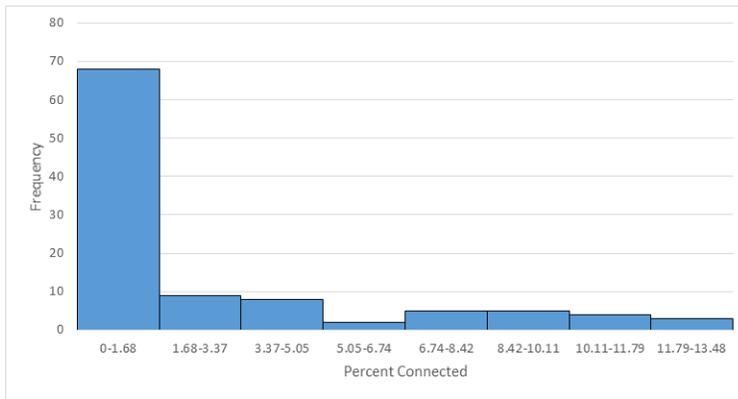
(c) Frequency distribution and model fit for the probability of sediment connectivity (connected greater than 1%)
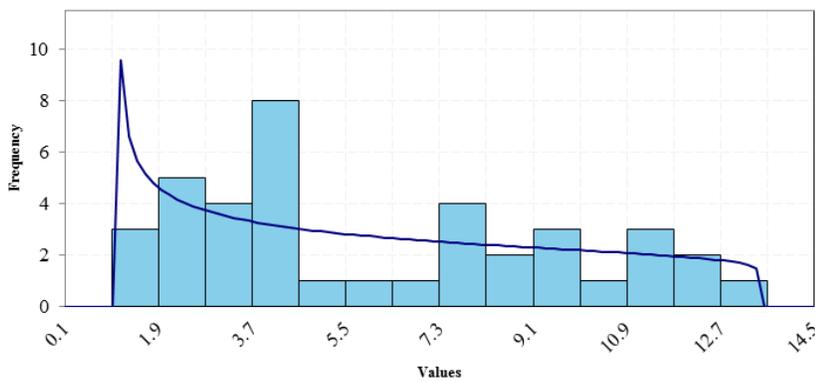
Figure 7.8: Evaluation of the watershed erosion model results

(a) Predicted and observed sediment flux for specified days of the study period
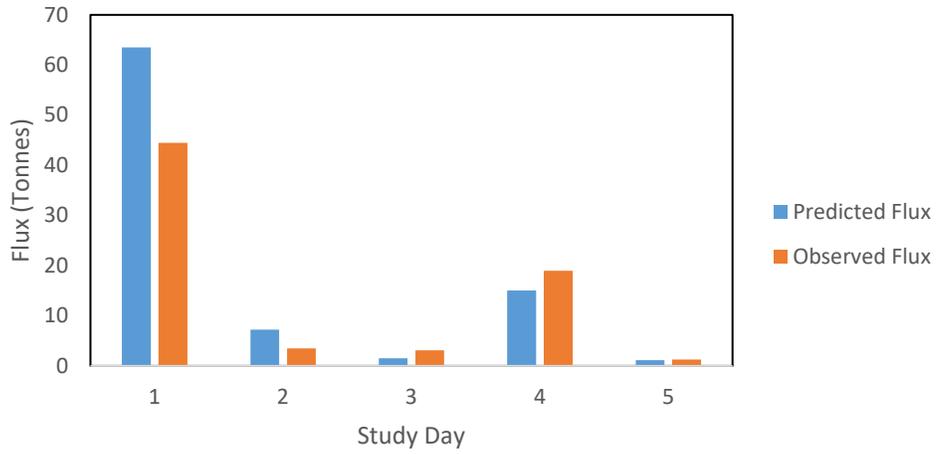
(b) Sediment flux estimated with non-assimilated and assimilated streamflow data
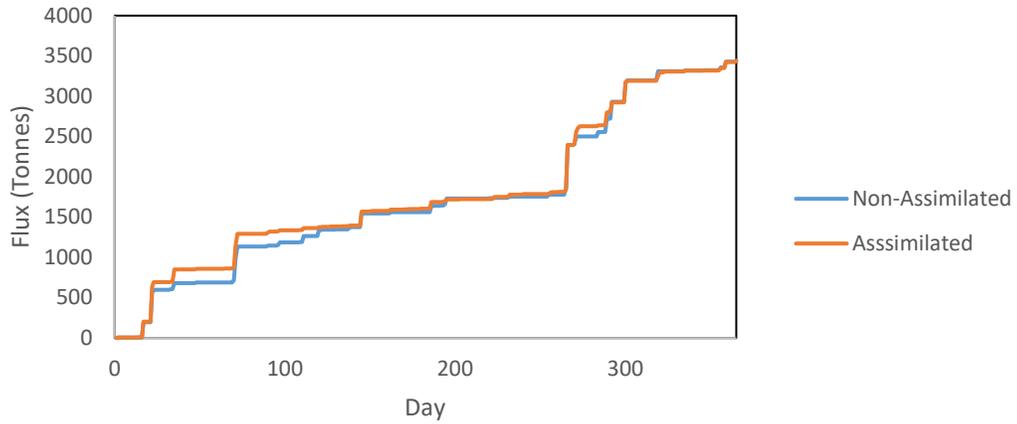
(c) Sensitivity analysis of parameters in the sediment transport model
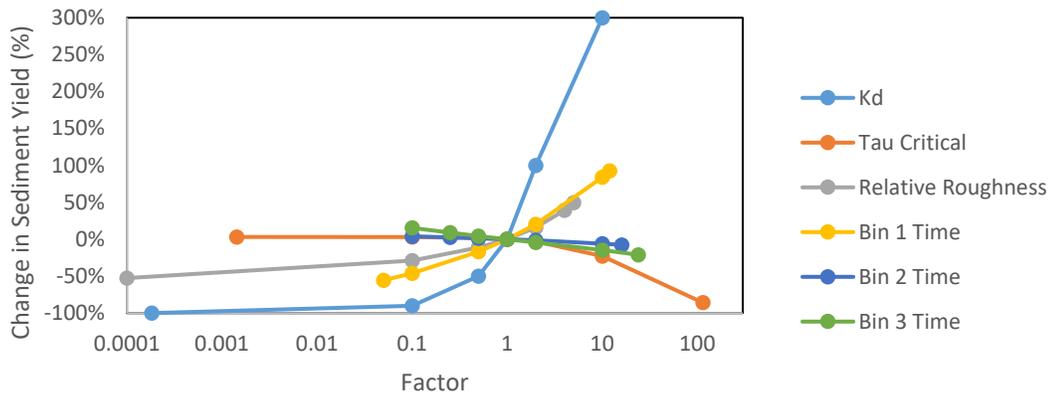
Table 7.2: Sediment flux by year for the watershed erosion model results

Year	Flux (tonnes/yr)
2006	3,440
2007	2,620
2008	3,630
Average	3,230

Figure 7.9: Results of percent connected and sediment flux for 2006
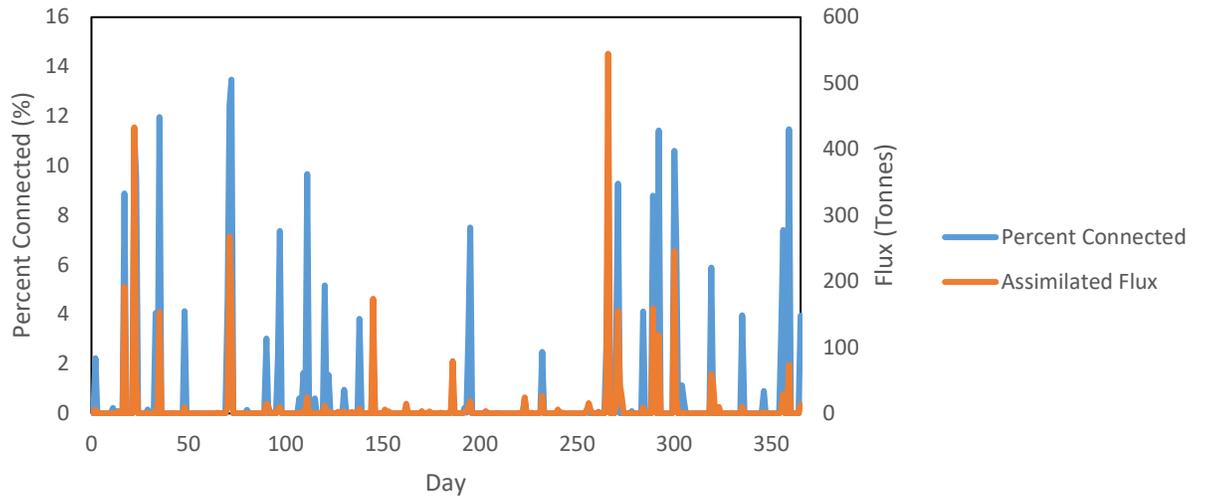
Figure 7.10: Connected areas and the erosion rates for connected cells for a road network on day 72 of 2006
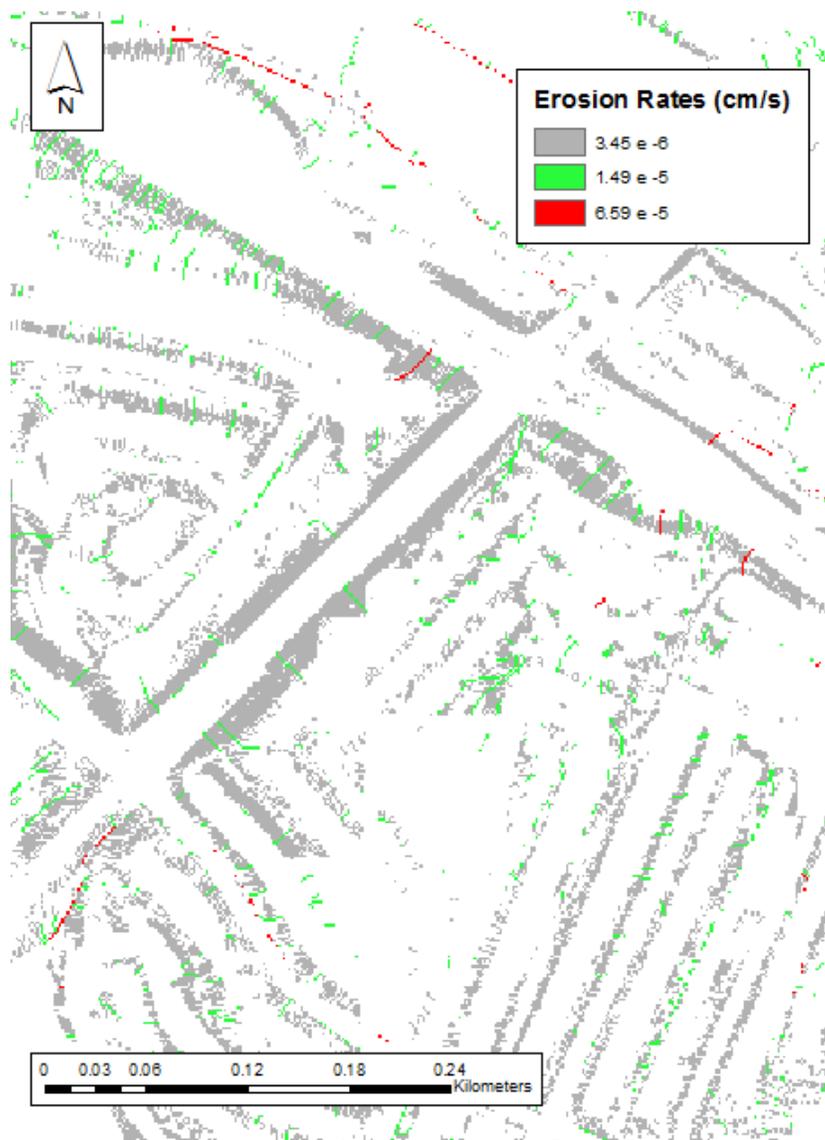
Chapter 8 Discussion

8.1 Watershed Erosion Modelling Advancement by Accounting for Sediment Connectivity

The present study shows the efficacy of coupling the sediment connectivity concept with watershed erosion modeling, perhaps for the first time, to our knowledge. The authors suggest the efficacy of the coupled sediment connectivity and watershed erosion model approach for a number of reasons.

First, it certainly appears that watershed erosion model platform accounts for spatial variability within the landscape by considering the probability of sediment connectivity using a 1.5 m by 1.5 m digital elevation model (DEM). Within the evaluation of the probability of sediment connectivity, the DEM resolution was shown to be the most sensitive component considered and the higher resolution was shown to better represent sediment transport processes across the landscape. The method offers the utility of resolving the spatial complexity of sediment transport across the landscape as DEM resolution continues to be improved and the high resolution DEMs become publically and freely available. It was particularly surprising to the authors how well the high resolution DEMs resolved sediment connectivity in and around roadside ditches. For this reason, the watershed erosion modelling approach adopted herein provides a methodology that allows inputs of the now highly resolved spatially explicit information available from the processing of satellite data.

Second, the watershed erosion model structure is suggested to aptly account for conservation criteria within the sediment transport model by reflecting concepts of supply, shear, and transport limitations. To this end, it is important to consider how models of

sediment connectivity are coupled with formulas for watershed erosion and sediment transport. Ideally, the research might perform a qualitative check by asking: have supply, shear, and transport conditions all been aptly considered in my coupled modeling analyses? In the present study, modelling of the probability of sediment connectivity considered sediment supply limitations in a spatially explicit manner across the watershed by calculating the probability of sediment supply using geospatial analyses. The transport limitation was also considered explicitly within the probability of sediment connectivity model when calculating the spatially and temporally explicit upstream and downstream probabilities of transport (see Fig 7.2). A further check of transport limitations and the sediment deposition that can accompany limited energy for sediment transport was considered via lateral discontinuities in the landscape as identified using field reconnaissance in the watershed and the spatially explicit calculation of the probability of sediment disconnectivity. The appropriateness of the probability of sediment connectivity model to reflect supply and transport limitations on a daily basis, placed emphasis upon the watershed erosion formula to more explicitly consider shear limitations. For this reason, the excessive shear method was adopted and the authors used a hydraulic approach so that fluid shear stress could be estimated when considering both runoff depth and the accumulation of fluid within concentrated flow pathways.

Third, site specific sediment transport features and processes that are associated with the watershed configuration and morphology were able to be represented by the watershed erosion model. Watershed features that were captured by the modelling included erosion-prone steep slopes in newly constructed, urban areas, accumulated flow pathways alongside roadways, and gully erosion from concentrated flow pathways in

agricultural areas. The erosion features represented within both the spatially explicit probability of sediment connectivity and sediment flux estimates were highly consistent with the authors' conversations with local watershed managers and conservationists as well as consistent with field information contained in the WAVES documentation. The agreement between the field and modelling results gave further confidence to the model efficacy.

Fourth, evaluation of watershed erosion model showed that the model performed well. The sediment flux estimates showed verification for both daily and annual time scales. In this manner, the modeling results compare well with sediment flux data collected in the watershed.

8.2 Lowland Watershed Configuration Identified with Sediment Connectivity

One attractive feature of a watershed erosion model that makes use of the sediment connectivity is that information regarding the watershed configuration might be derived from the model's results (Phillips, 2003; Fryirs, 2013). The results of the present study provide additional characterization of lowland watershed systems that has not been reported previously. In this context, the lowland watershed system can be regarded as a system contrary in many ways to that of high gradient watershed systems. Previous work has suggested the prominence of the biologically-active surficial fine grained laminae presence and the deposition of fine sediment within low-gradient watersheds that contrasts the high energy steeper watershed systems that transport fine sediments to the watershed outlet (Ford and Fox, 2014). Our morphologic understanding of the lowland system is further extended in this study as the author's find that the uplands of the system are most often de-coupled from the stream corridor. The lowland stream system studied here is only

coupled with about 10% of its uplands, even on the most hydrologically active day of a given year. The results show a stark contrast to steeper watershed systems, such as the steep catchment system studied in Fryirs et al. (2007) where a moderate-sized storm event induced pronounced sediment connectivity and activated approximately 50% of the upland catchment land area.

The configuration of the lowland watershed is worthy of discussion in terms of its connectivity, but even more so in terms of its disconnectivity. As previously mentioned, connectivity in the uplands, i.e., 10% of the watershed areas on the wettest days of the year, was a result of erosion-prone steep slopes in newly constructed urban areas, accumulated flow pathways alongside roadways, and gully erosion from concentrated flow pathways in agricultural areas. In general, urban and suburban regions were more highly connected than agricultural regions, when soil conditions were similar, given the presence of a higher concentration of impervious surfaces and the well-defined drainage network, i.e., ditches alongside roadways.

On the other hand, the lowland watershed was highly disconnected with many features contributing to this disconnectivity. 90% of the watershed area was disconnected on the wettest days of the year, attributed to the micro-topography across the landscape surface. The majority of disconnectivity within the watershed is attributed to undulating land surfaces of the lowland that included the presence of low gradient to flat slopes. This micro-topology of the land, or lack thereof, created locally flat surfaces causing micro-sources of disconnectivity such that runoff loses its energy and initiated sediment deposits. The authors' field visits during storm events qualitatively justified the geospatial results from the sediment connectivity modeling. The authors found that even during intensive

153

rainfall events when runoff and flow accumulation was pronounced within ditches and swales, there was little to no runoff or sediment transport across the pasture land surfaces and rather the authors found pooling within micro-topography as opposed to runoff. The micro-topography represented with the high resolution digital elevation model is worth mentioning given that the watershed itself was not flat (i.e., average watershed/hillslope gradient was 7%). Other less pronounced sources of disconnectivity within the watershed included supply limitations (20% of the disconnectivity) and floodplain buffers, which provided later disconnectivity (5% of the disconnectivity). Accounting for the mentioned disconnectivity has been reported as one of the most important considerations within modeling the sediment continuum (Fryirs, 2013), and it is expected that the new disconnectivity knowledge gained here for lowland watershed systems will assist with future research by others in similar agricultural and urban mild gradient systems.

Other features of the watershed configuration and its connectivity worth mentioning are that the spatial distribution of connectivity longitudinally in the system exhibited a power function relationship while the temporal distribution of the probability of sediment connectivity was best described with a beta distribution. These functions might be investigated and tested for other lowland systems in an effort towards describing a more universal description of sediment connectivity for watershed systems.

Another potentially attractive feature of the connectivity-based watershed erosion model is the ability to potentially reduce the cost of computational hydraulics. Yet the expense of the added subroutines for probability of sediment connectivity calculations might also be considered. In the present application, the watershed modeling included calculations for 3×10^{10} space-time combinations. The probability of sediment connectivity

154

subroutine added explicit formula to the watershed erosion model; and the calculations were performed in a geospatial modeling software that required several hours to run on a desktop PC. Considering all space-time combinations in the watershed modeling, only 0.7% of the combinations contained connectivity. Therefore, only 2×10^8 space-time combinations need to be considered within the hydraulic and sediment transport formula, and thus 2.98×10^{10} space-time combinations were removed from the watershed modeling. Hydraulic calculations are often computationally intensive requiring solution of implicit formula at each space-time step. Computational sediment transport is even more demanding as higher dimensional formula and advanced routing methods are implemented. For these reasons, the authors feel the inclusion of the connectivity-based watershed erosion model may have a net reduction in overall computational complexity. Further, the spatially explicit representation of sediment connectivity does not require strenuous data input requirements of some models (i.e., physically based models) thus further reducing the computational demands and complexity of the model domain. This sentiment is mirrored by Cavalli et al., (2013), whose only input to his iteration of Borselli et al.'s IC model (2008), was a DEM. At the same time, the connectivity-based watershed erosion model provides the flexibility to include advanced computational complexity, as needed. That is, simulation of the breach of a buffer, barrier, or blanket within the watershed configuration allows calling up sophisticated hydraulic and sediment subroutines that could simulate such spatiotemporal feedback and connectivity between sediment sources and sinks (Bracken et al., 2015).

8.3 Discussion of Connectivity in Existing Watershed Erosion Models

One potential criticism of this research might be the contention that many watershed erosion models already implicitly account for sediment connectivity. The authors provide some discussion of this idea to thwart such criticism but at the same time highlight where existing models do already account for connectivity.

Some spatially explicit watershed models may account for connectivity implicitly through the parameterization of watershed sedimentation processes such as deposition. This discussion assesses the ability of models to account for connectivity implicitly and compares this ability to the Probability of Connectivity model developed in this thesis. The watershed erosion and sedimentation models assessed here are widely popular in the soil science and engineering community (Merritt et al., 2006) and have been discussed by previous literature. The models assessed here are the Universal Soil Loss Equation (USLE) developed by Wischmeier and Smith (1978), and the Watershed Erosion Prediction Project (WEPP) developed in part by Laflen et al., (1991).

8.3.1 USLE

The Universal Soil Loss Equation (USLE) was developed by Wischmeier and Smith (1978) and is widely used in the United States. The USLE is an empirical model developed for small hillslopes. Derivatives of the USLE can predict erosion at the watershed scale on an annual basis. Annual rainfall, an estimate of soil erodibility, land cover, and topographic information determine annual soil loss. The USLE is given by the equation

$$A = RKLCSP \tag{Eq. 8.1}$$

where *A* is the annual soil loss per unit area, *R* is the rainfall erosivity factor, *K* is the soil erodibility factor, *L* is the slope-length factor, *S* is the slope-steepness factor, *c* is the cover and management factor, and *P* is the support practices factor. The USLE is generally popular because of its low input requirements and ease of use (Loch and Rosewell, 1992). However, USLE is not event based, does not account for gully erosion and mass movement, and it cannot model deposition. Ephemeral gullying is not accounted for because concentrated flow pathways are not taken into consideration. The use of the USLE is limited to the United States because empirical models are limited to data collected from the study site (Merritt et al., 2006).

The USLE seldom accounts for connectivity. Calculation of sediment yield on an annual basis does not account for the individual pathways of sediment transport and does not capture the dynamic nature of sediment connectivity. While the Probability of Connectivity model does not explicitly model deposition, deposition is implicitly parameterized via modelling of disconnectivitiy features, which are assumed to promote deposition.

8.3.2 WEPP

The Watershed Erosion Prediction Project (WEPP) model is a physically based model that uses the continuity equation to model rill and interrill detachment and/or deposition. The continuity equation is

$$\frac{dqs}{dx} = Dr + Di$$
(Eq. 8.2)

where *dqs/dx* is the sediment rate per unit width of the channel, *Dr* is the net rill detachment or deposition rate, and *Di* is the net interrill detachment or deposition rate. The model has

been widely applied to hillslopes in the United States (Laflen et al., 1991). WEPP does not consider sediment erosion, transport, or deposition in permanent channels, such as gullies and perennial streams. However, a version of WEPP has been developed that can model ephemeral gullies. WEPP predicts the spatial and temporal distributions of soil loss, sediment yield, and the soil-water balance; i.e. WEPP can predict the location and rates of deposition and erosion within the watershed. However, if rills do not form on hillslopes due to vegetative cover or limited hydraulic shearing, the WEPP model will not work properly. Foliage information and crop management practices are essential inputs to WEPP because they will largely affect soil erosion and hydrological processes at the site (Merritt et al., 2006). Hydraulic roughness predicts runoff and water loss. Flux at the watershed outlet is quantified using the three stages of erosion: detachment, transport, and deposition. Large data input requirements limit WEPP's usability.

(Dis)connectivity is best modeled implicitly through spatially explicit models because individual transport pathways of sediment are observable. Disconnectivity is implicitly accounted for in WEPP via deposition estimations. Disconnecting features, created via tillage operations and from plant/crop coverage, contribute to deposition and further disconnectivitiy. However, WEPP does not account for features that may completely cutoff entire regions of watersheds because of permanent disconnectivitiy. Since WEPP does not model instream transport or permanent gully erosion, longitudinal (dis)connectivity is not accounted for. The Probability of Connectivity model currently only accounts for lateral connectivity in catchment uplands, but soon will be coupled with a longitudinal, instream transport model, which accounts for barriers.

WEPP is computationally complex and requires numerous inputs in order to be calibrated. Coupling an erosion model with a predictive connectivity model may alleviate the complexity of simulating a spatially explicit, yet over-parameterized and computationally intensive, sediment transport model like WEPP.

Chapter 9 Conclusions

The authors were motivated to advance watershed erosion modelling tools through a better representation of spatially-explicit processes via including the probability of sediment connectivity concept within a modeling platform. The primary features included in the new watershed modeling platform, that extend current research within the peer-reviewed literature, include a new theoretical probability of sediment connectivity model that can incorporate the multiple processes impacting connectivity and (dis)connectivity; and a theoretical method to predict dynamic connectivity and couple it with a hydrology model. The authors applied the watershed erosion model within a geospatially explicit computational framework that includes sediment (dis)connectivity to the water supply problem in Kentucky USA.

Conclusions of this work suggest the efficacy of a watershed erosion modelling platform that includes inclusion of the probability of sediment connectivity concept. Efficacy of the methodology is supported by the fact that: (1) the watershed erosion model platform aptly accounts for spatial variability within the landscape when considering the probability of sediment connectivity using a 1.5 m by 1.5 m digital elevation model; (2) the watershed erosion model structure justifiably accounts for conservation criteria by reflecting concepts of supply, shear, and transport limitations; (3) site specific sediment transport features and processes that are associated with the watershed configuration and morphology were able to be represented by the watershed erosion model; and (4) evaluation of the watershed erosion model showed that the model performed well. Further, the authors highlight the potential of a connectivity-based watershed erosion model to reduce computational complexity and costs in future research. Limitations of the

modelling platform included its primary emphasis upon diffuse connectivity within the uplands and direct connectivity within gullies and swales, and it is expected that further emphasis upon direct connectivity within the stream corridor might enhance the model structure in future research. It is hopeful that the efficacy of the watershed erosion modeling platform be further validated by other researchers in other watershed systems in order that its limitations and advantages can be better understood.

Conclusions of this work also present a broader understanding of the sediment continuum within lowland watershed systems with agricultural and urban land uses—a class of watershed systems that have gained recent research interest due to their influence on water quality and water supply. The lowland system studied here is only coupled with about 10% of its uplands, even on the most hydrologically active day of a given year. The results show a stark contrast to steeper watershed systems, moderate events activate 50% of the upland catchment land area. Connectivity in the uplands, i.e., 10% of the watershed areas on the wettest days of the year, was a result of erosion-prone steep slopes in newly constructed urban areas, accumulated flow pathways alongside roadways, and gully erosion from concentrated flow pathways in agricultural areas. In general, urban and suburban regions were more highly connected than agricultural regions, when soil conditions were similar, given the presence of a higher concentration of impervious surfaces and the well-defined drainage network, i.e., ditches alongside roadways. The lowland watershed was highly disconnected with many features contributing to this disconnectivity. 90% of the watershed area was disconnected on the wettest days of the year, attributed to the micro-topography across the landscape surface. The majority of disconnectivity within the watershed is attributed to undulating land surfaces causing

161

micro-sources of disconnectivity such that runoff loses its energy and initiated sediment deposits. The micro-topography represented with the high resolution digital elevation model is worth mentioning given that the watershed itself was not flat (i.e., average watershed/hillslope gradient was 7%). Other less pronounced sources of disconnectivity within the watershed included supply limitations (20% of the disconnectivity) and floodplain buffers, which provided later disconnectivity (5% of the disconnectivity). It is hopeful that the watershed configuration results found in this study be further investigated in other lowland systems, in order that a greater morphologic understanding of watersheds be gained.

References

Adams, E., and Elliott, S. (2006). Physically based modelling of sediment generation and transport under a large rainfall simulator. *Hydrological Processes,* Vol. 20, pp. 2253-2270.

Aksoy, H., & Kavvas, M. L. (2005). A review of hillslope and watershed scale erosion and sediment transport models. *Catena*, *64*(2), 247-271.

Alberts, E., Nearing, M., Weltz, M., Risse, L., Pierson, F., Zhang, X., Laflen, J., and Simanton, J. (1995). WEPP Chapter 7 Soil Component. United States Department of Agricultural.

Ambroise, B. (2004). Variable 'active'versus 'contributing'areas or periods: a necessary distinction. *Hydrological Processes*, *18*(6), 1149-1155.

Andrews Jr., William Morton. (2004). Geologic controls on Plio-Pleistocene drainage evolution of the Kentucky River in central Kentucky. *University of Kentucky Doctoral Dissertations*. 366. http://uknowledge.uky.edu/gradschool_diss/366

Annandale, G.W. (1987). Reservoir Sedimentation. Developments in Water Science. Elsevier Science Publishing Company, Inc.

Arnold, J. G., Kiniry, J. R., Srinivasan, R., Williams, J. R., Haney, E. B., & Neitsch, S. L. (2011). Soil and Water Assessment Tool input/output file documentation: Version 2009. *Texas Water resources institute technical report*, *365*.

Auzet, V., Boiffin, J., Papy, F., Ludwig, B. and Maucorps, J., 1993. Rill erosion as a function of the characteristics of cultivated catchments in the North of France. Catena, 20: 41-62.

Baade, J., Barsch, D., M~iusbacher, R. and Schukraft, G., 1993. Sediment yield and sediment retention in a small loess-covered catchment in SW-Germany. Z. Geomorph. Suppl., 92: 201- 216.

Backlund, P. et al. (2008). The Effects of Climate Change on Agriculture, Land Resources, Water Resources, and Biodiversity in the United States. U.S. Environmental Protection Agency, Washington, DC.

Bailey, G. W., & Waddell, T. E. (1979). Best management practices for agriculture and silviculture: An integrated overview.

Banks, P. (2014). Kentucky River Keeper. Kentucky River Facts. http://kyriverkeeper.org/kentucky-river-facts/. Accessed on 11/10/2015.

Banks, P. Personal Communication. October 20, 2015.

Benda, L., & Dunne, T. (1997). Stochastic forcing of sediment supply to channel networks from landsliding and debris flow. *Water Resources Research*, *33*(12), 2849-2863.

163

Bjorkland, R., Pringle, C. M., & Newton, B. (2001). A stream visual assessment protocol (SVAP) for riparian landowners. *Environmental Monitoring and Assessment*, *68*(2), 99-125.

Blanco-Canqui, H., Gantzer, C. J., Anderson, S. H., Alberts, E. E., & Thompson, A. L. (2004). Grass barrier and vegetative filter strip effectiveness in reducing runoff, sediment, nitrogen, and phosphorus loss. *Soil Science Society of America Journal*, *68*(5), 1670-1678.

Blanford, S. Personal Communication. February 27, 2017.

Borselli, L., Cassi, P., & Torri, D. (2008). Prolegomena to sediment and flow connectivity in the landscape: a GIS and field numerical assessment. *Catena*, *75*(3), 268-277.

Bracken, L. J., & Croke, J. (2007). The concept of hydrological connectivity and its contribution to understanding runoff-dominated geomorphic systems. Hydrological Processes, 21(13), 1749-1763.

Bracken, L. J., Turnbull, L., Wainwright, J., & Bogaart, P. (2015). Sediment connectivity: a framework for understanding sediment transfer at multiple scales. *Earth Surface Processes and Landforms*, *40*(2), 177-188.

Brooks, B. W., Lazorchak, J. M., Howard, M. D., Johnson, M. V. V., Morton, S. L., Perkins, D. A., ... & Steevens, J. A. (2016). Are   harmful algal blooms becoming the greatest inland water quality threat to public health and aquatic ecosystems?. *Environmental Toxicology and Chemistry*, *35*(1), 6-13.

Brown, K. (2000). Urban stream restoration practices: an initial assessment.*The Center for Watershed Protection. Ellicott City,   Maryland, USA.*

Burt, T. P., Matchett, L. S., Goulding, K. W. T., Webster, C. P., & Haycock, N. E. (1999). Denitrification in riparian buffer zones: the role of floodplain hydrology. *Hydrological processes*, *13*(10), 1451-1463.

Campbell, M.R., 1996, Description of the Richmond Quadrangle, Kentucky: U.S. Geological
Survey Geological Atlas Folio No. 46, 4 p.

Castro, J., & Reckendorf, F. F. (1995). *Effects of sediment on the aquatic environment: potential NRCS actions to improve aquatic   habitat* (No. 6). US Department of Agriculture, Soil Conservation Service.

Cavalli, M., Trevisani, S., Comiti, F., & Marchi, L. (2013). Geomorphometric assessment of spatial sediment connectivity in small Alpine catchments. Geomorphology, 188, 31-41.

Colebrook, C. F., & White, C. M. (1937). Experiments with fluid friction in roughened pipes. *Proceedings of the royal society of london. series a, mathematical and Physical sciences*, 367-381.

Currens, J. C., & Paylor, R. L. (2009). Karst groundwater basins in Kentucky; Kentucky Geological Survey, unpublished map, scale 1:500,000.

Currens, J. C., Paylor, R. L., Beck, E. G., & Davidson, B. (2012). A method to determine cover–collapse frequency in the Western Pennyroyal karst of Kentucky. *J Cave Karst Stud*, *74*(3), 292-299.

Davis, C. M. (2008). "Sediment fingerprinting using organic matter tracers to study streambank erosion and streambed sediment storage processes in the South Elkhorn Watershed." M.S. Dissertation, University of Kentucky, Lexington, Kentucky.

De Vente, J., Poesen, J., & Verstraeten, G. (2005). The application of semi-quantitative methods and reservoir sedimentation rates for the prediction of basin sediment yield in Spain. Journal of Hydrology, 305(1), 63-86.

D'Haen, K., Dusar, B., Verstraeten, G., Degryse, P., & De Brue, H. (2013). A sediment fingerprinting approach to understand the geomorphic coupling in an eastern Mediterranean mountainous river catchment. Geomorphology, 197, 64-75.

Effler, S. W., Matthews, D. A., Kaser, J. W., Prestigiacomo, A. R., & Smith, D. G. (2006). Runoff event impacts on a water supply reservoir: suspended sediment loading, turbid plume behavior, and sediment deposition.

Einstein, H. A. (1950). *The Bed Load Function for Sediment Transportation in Open Channels*. Technical Bulletin 1026, US Department of Agricultural.

ESRI. (2013). ArcHydro: GIS for Water Resources. Accessed 5/4/2017. https://www.esri.com/library/fliers/pdfs/archydro.pdf

Evans, S. Personal Communication. March 20, 2017.

Federal Interagency Stream Restoration Working Group (FISRWG). 1998. *Stream Corridor Restoration: Principles, Processes, and Practices*. Federal Interagency Stream Restoration Working Group (FISRWG). GPO Item No. 0120-A; SuDocs No. A 57.6/2:EN 3/PT.653. ISBN-0-93421359-3

Ferguson, R.I., 1981. Channel forms and channel changes. In: Lewin, J. (Ed.), British Rivers. Allen and Unwin, London, pp. 90–125.

Ford, William I. III. (2014). Control of the surficial fine-grained laminae upon stream carbon and nitrogen cycles. *Theses and Dissertations--Civil Engineering*. 21. http://uknowledge.uky.edu/ce_etds/21

Ford, William Isaac III. (2011). Particulate organic carbon fate and transport in a lowland, temperate watershed. *University of Kentucky Master's Theses*. 647. http://uknowledge.uky.edu/gradschool_theses/647

Ford, W. I., & Fox, J. F. (2014). Model of particulate organic carbon transport in an agriculturally impacted stream. Hydrological Processes, 28(3), 662-675.

Foster, I. D. (1995). Lake and reservoir bottom sediments as a source of soil erosion and sediment transport data in the UK. *Sediment and water quality in river catchments*, 265-283.

Huston, D. L., & Fox, J. F. (2015). Clogging of fine sediment within gravel substrates: Dimensional analysis and macroanalysis of experiments in hydraulic flumes. Journal of Hydraulic Engineering, 141(8), 04015015.

Fryirs, K. (2013). (Dis) Connectivity in catchment sediment cascades: a fresh look at the sediment delivery problem. *Earth Surface Processes and Landforms*, *38*(1), 30-46.

Fryirs, K. A., Brierley, G. J., Preston, N. J., & Kasai, M. (2007). Buffers, barriers and blankets: the (dis) connectivity of catchment-scale sediment cascades. *Catena*, *70*(1), 49-67.

Fryirs, K. A., Brierley, G. J., Preston, N. J., & Spencer, J. (2007). Catchment-scale (dis) connectivity in sediment flux in the upper Hunter catchment, New South Wales, Australia. *Geomorphology*, *84*(3), 297-316.

Furnans, J., & Austin, B. (2008). Hydrographic survey methods for determining reservoir volume. Environmental Modelling & Software, 23(2), 139-146.

Gumbert, A. Personal Communication. February 21, 2017.

Hanson, G. J., & Simon, A. (2001). Erodibility of cohesive streambeds in the loess area of the midwestern USA. *Hydrological processes*, *15*(1), 23-38.

Haregeweyn, N. et al. (2012). Reservoir Sedimentation and its Mitigating Strategies: a Case Study of Angereb Reservoir (NW Ethiopia). Journal of Soils and Sediments.

Haregeweyn, N., Melesse, B., Tsunekawa, A., Tsubo, M., Meshesha, D., & Balana, B. B. (2012). Reservoir sedimentation and its mitigating strategies: a case study of Angereb reservoir (NW Ethiopia). *Journal of Soils and Sediments*, *12*(2), 291-305.

Harvey, A. M. (2002). Effective timescales of coupling within fluvial systems. Geomorphology, 44(3), 175-201.

Hayhoe, K., et al. (2014). National Climate Assessment. U.S. Global Change Research Program. http://nca2014.globalchange.gov/report. Accessed on 11/10/2015.

Heckmann, T., & Schwanghart, W. (2013). Geomorphic coupling and sediment connectivity in an alpine catchment—Exploring sediment cascades using graph theory. *Geomorphology*, *182*, 89-103.

Jain, S.K. (2001) Development of Integrated Sediments Rating Curves Using ANNs. *J. of Hydraulic Engineering*, 127, 1, 30.

Jain, V., & Tandon, S. K. (2010). Conceptual assessment of (dis) connectivity and its application to the Ganga River dispersal system. *Geomorphology*, *118*(3), 349-358.

Jencso, K. G., McGlynn, B. L., Gooseff, M. N., Wondzell, S. M., Bencala, K. E., & Marshall, L. A. (2009). Hydrologic connectivity between landscapes and streams: Transferring reach-and plot-scale understanding to the catchment scale. Water Resources Research, 45(4).

Jillson, W.R., 1963, Delineation of the Mesozoic course of the Kentucky River across the inner Bluegrass Region of the State: Frankfort, Kentucky, Roberts Printing Co.,

Jin, C.X., Romkens, M.J.M., 2001. Experimental studies of factors in determining sediment trapping in vegetative filter strips. Trans. ASAE 44, 277-288.

Jin, C.X., Dabney, S.M., Romkens, M.J.M., 2002. Trapped mulch increases sediment removal by vegetative filter strips: A flume study. Trans. ASAE 45, 929-939.

Johnson, L.R. and Parrish, C.E. (1999). Engineering the Kentucky River: The Commonwealth's Waterway. U.S. Army Corps of Engineers, Louisville District.

Juracek, K. E. (2013). *Suspended-sediment loads and reservoir sediment trap efficiency for Clinton Lake, Kansas, 2010-12* (No.   2013-5153). US Geological Survey.

Kansas State University. (2008). Sedimentation in Our Reservoirs: Causes and Solutions. Contribution no. 08-250-S from the   Kansas Agricultural Experiment Station.

KDOW. (2013). 2012 Integrated Report to Congress on the Condition of Water Resources in Kentucky. Volume II. 303(d) List of Surface Waters.

Kent, K.M. (1964). Chapter 15 documentation. U.S. Dept. of Agriculture, Soil Conservation Service, Washington, DC.

Kentucky Department of Fish and Wildlife Resources. (2013). Kentucky's Comprehensive Wildlife Conservation Strategy, #1 Sportsman's Lane, Frankfort, Kentucky 40601. http://fw.ky.gov/WAP/Pages/Default.aspx (Date updated 2/5/2013)

Kentucky Division of Water. (2012). 2012 Integrated 305b/303d Report. Accessed 2/12/2016. http://water.ky.gov/waterquality/Pages/IntegratedReport.aspx

Kentucky Geologic Survey. (2012). Geologic Map of Kentucky. Accessed 5/13/2017. http://www.uky.edu/KGS/geoky/geologymap.htm

Kentucky River Authority. (2016). Kentucky River Locks and Dams. Accessed: 5/4/2017 http://finance.ky.gov/offices/kra/Documents/2016/Locking%20Instructions%202020 16.pdf

Kirkby, M., Bracken, L., & Reaney, S. (2002). The influence of land use, soils and topography on the delivery of hillslope runoff to channels in SE Spain. Earth Surface Processes and Landforms, 27(13), 1459-1473.

Kirpich, Z. P. 1940. Time of concentration of small agricultural watersheds. Civ. Eng. (N.Y.), 106, 362.

Kundzewicz, Z.W. et al. (2007) Freshwater Resources and their Management. Climate Change 2007: Impacts, Adaptation, and Vulnerability. Cambridge University Press, Cambridge, United Kingdom.

KYAPED. 2014. Kentucky Aerial Photography and Elevation Data Program. http://kygeonet.ky.gov/kyfromabove/ Accessed: 01/30/13.

Laflen, J. M., Lane, L. J., & Foster, G. R. (1991). WEPP: A new generation of erosion prediction technology. *Journal of Soil and Water Conservation*, *46*(1), 34-38.

Lal, R. (1999). Soil management and restoration for C sequestration to mitigate the accelerated greenhouse effect. *Progress in Environmental Science*, 1(4), 307-326.

Latocha, A. (2014). Geomorphic connectivity within abandoned small catchments (Stołowe Mts, SW Poland). Geomorphology, 212, 4-15.

Le Bissonnais, Y., Lecomte, V., Cerdan, O., 2004. Grass strip effects on runoff and soil loss. Agronomie 24, 129-136.

Letcher, R.A., Jakeman, A.J., Calfas, M., Linforth, S., Baginska, B., and Lawrence, I. (2002). *A comparison of catchment water quality models and direct estimation techniques.* Environmental Modeling & Software, Vol. 17, pp. 77-85.

Leverett, F., 1902, Glacial formations and drainage features of the Erie and Ohio basins: U.S. Geological Survey Monograph, 802 p.

Lexartza-Artza, I., & Wainwright, J. (2009). Hydrological connectivity: Linking concepts with practical implications. Catena, 79(2), 146-152.

Liu, X.M., Mang, X.Y., Zhang, M.H., 2008. Major factors influencing the efficacy of vegetated buffers on sediment trapping: A review and analysis. J. Environ. Qual. 37, 1667-1674.

Long, J.L.A., House, W.A., Parker, A., and Rae, J.E. (1998). *Micro-organic compounds associated with sediments in the Humber rivers.* The Science of the Total Environment, Vol. 210-211, pp. 229-253.

López-Vicente, M., Poesen, J., Navas, A., & Gaspar, L. (2013). Predicting runoff and sediment connectivity and soil erosion by water for different land use scenarios in the Spanish Pre-Pyrenees. Catena, 102, 62-73.

McCully, P. (1996). *Silenced rivers: The ecology and politics of large dams*. Zed Books.

McDowell, R. C. (1986). *The geology of Kentucky; a text to accompany the Geologic Map of Kentucky* (No. 1151-H). USGPO,.

McDowell-Boyer, L. M., Hunt, J. R., & Sitar, N. (1986). Particle transport through porous media. *Water Resources Research*, *22*(13), 1901-1921.

McFarlan, A. C. (1943). *Geology of Kentucky*. University of Kentucky.

McGrain, P. (1983). *The geologic story of Kentucky* (Vol. 8). Kentucky Geological Survey, University of Kentucky.

McGriff, E.C. (1972). The Effects of Urbanization on Water Quality. Journal of Environmental Quality, Vol. 1, No. 1.

Medeiros, P. H., Güntner, A., Francke, T., Mamede, G. L., & Carlos de Araújo, J. (2010). Modelling spatio-temporal patterns of sediment yield and connectivity in a semi-arid catchment with the WASA-SED model. Hydrological Sciences Journal–Journal des Sciences Hydrologiques, 55(4), 636-648.

Merritt, W. S., Letcher, R. A., & Jakeman, A. J. (2003). A review of erosion and sediment transport models. *Environmental Modelling & Software*, *18*(8), 761-799.

Messenzehl, K., Hoffmann, T., & Dikau, R. (2014). Sediment connectivity in the high-alpine valley of Val Müschauns, Swiss National Park—linking geomorphic field mapping with geomorphometric modelling. *Geomorphology*, *221*, 215-229.

Michaelides, K., & Wainwright, J. (2002). Modelling the effects of hillslope–channel coupling on catchment hydrological response. Earth Surface Processes and Landforms, 27(13), 1441-1457.

Mockus, V. 1973. Estimation of direct runoff from storm rainfall. National Engineering Handbook, Ch. 10, Soil Conservation Service, USDA, 21 pp.

Montgomery, D.R. and Dietrich, W.E., 1994. Landscape dissection and drainage area-slope thresholds. In: M.J. Kirkby (Editor), Process Models and Theoretical Geomorphology. Wiley, Chichester, pp. 221-246.

Morris, G. L., & Fan, J. (1998). Reservoir sedimentation handbook: design and management of dams, reservoirs, and watersheds for sustainable use. McGraw Hill Professional.

Morris, G.L. and Fan, J. (2009). Reservoir Sedimentation Handbook. Design and Management of Dams, Reservoirs, and Watersheds for Sustainable Use. McGraw-Hill.

Murray, S.P. (1970). Settling Velocities and Vertical Diffusion of Particles in Turbulent Water. Journal of Geophysical Research. Vol. 75, No. 9.

Nachtergaele, J., Poesen, J., Sidorchuk, A., & Torri, D. (2002). Prediction of concentrated flow width in ephemeral gully channels. *Hydrological Processes*, *16*(10), 1935-1953.

Natural Resource Conservation Service NRCS. 1972. "Hydrology." National engineering handbook, Sec. 4, U.S. Department of Agriculture, Washington, D.C.

Natural Resource Conservation Service NRCS. 1986. "Urban hydrology for small watersheds." Technical Release 55, Washington, D.C.

Natural Resource Conservation Service NRCS. (2009). Web soil survey. *URL http://www. websoilsurvey. ncsc. usda. gov/app/[verified October 29, 2009]*.

Natural Resource Conservation Service NRCS. (2010). Time of Concentration. Part 630 Hydrology National Engineering Handbook. Accessed 5/4/2017.

https://directives.sc.egov.usda.gov/OpenNonWebContent.aspx?content=27002.w
ba

Natural Resources and Environmental Protection Cabinet. Section 303(d) List of
Waterbodies for Kentucky. Accessed 2/12/2016.
http://water.ky.gov/waterquality/303d%20Lists/303d90.pdf

Neitsch, S. L., Arnold, J. G., Kiniry, J. R., & Williams, J. R. (2011). Soil and water
assessment tool theoretical documentation version 2009. Texas Water Resources
Institute.

Nicoll, T., & Brierley, G. (2016). Within-catchment variability in landscape connectivity
measures in the Garang Catchment, Upper Yellow River. Geomorphology.

NOAA. 1981-2010 Climate Normals. Lexington, Kentucky. Accessed 2/12/2016.
http://www.ncdc.noaa.gov/cdo-web/datatools/normals

Nyssen, J. et al. (2007). On-site Evaluation of Stone Bunds to Control Soil Erosion on
Cropland in Northern Ethiopia. Soil Till Res 94:151–163

Odell, L. (2013). The Impact of Water Treatment Plant Processes on Algae and Algal
Toxins. *Oregon Health Authority*.
https://public.health.oregon.gov/HealthyEnvironments/DrinkingWater/Operations
/Treatment/Documents/algae/Odell-WaterOnline.pdf

Owens, P.N., Walling, D.E., Carton, J., Meharg, A.A., Wright, J., and Leeks, G.J.L.
(2001). *Downstream changes in the transport and storage of sediment-associated
contaminates (P, Cr and PCBs) in agricultural and industrialized drainage
basins.* The Science of the Total Environment, Vol. 266, pp. 177-186.

Owens, P.N., Duzant, J.H., Deeks, L.K., Wood, G.A., Morgan, R.P.C., Collins, A.J.
(2007). Evaluation of contrasting buffer features within an agricultural landscape
for reducing sediment and sediment-associated phosphorus delivery to surface
waters. Soil Use and Management 23, 165-175.

Partheniades, E. (1965). Erosion and deposition of cohesive soils. Journal of the
Hydraulics Division, 91(1), 105-139.

Phillips, J. D. (2003). Sources of nonlinearity and complexity in geomorphic
systems. *Progress in Physical Geography*, *27*(1), 1-23.

Pringle, C. (2003). What is hydrologic connectivity and why is it ecologically
important?. *Hydrological Processes*, *17*(13), 2685-2689.

Pringle, C. (2003). What is hydrologic connectivity and why is it ecologically important?.
Hydrological Processes, 17(13), 2685-2689.

Rabení, C. F., Doisy, K. E., & Zweig, L. D. (2005). Stream invertebrate community
functional responses to deposited sediment. *Aquatic Sciences-Research Across
Boundaries*, *67*(4), 395-402.

Randle, T.J. and Collins, K.L. (July 2012). Avoiding the Inevitable? Capacity Loss from Reservoir Sedimentation. Eos. John Wiley & Sons.

Ray, J. A., Currens, J. C., & Hounshell, T. (1998). *Mapped karst ground-water basins in the Beaver Dam 30 x 60 Minute Quadrangle*. Kentucky Geological Survey, University of Kentucky.

Reid, L.M. and Dunne, T. (1996). Rapid Evaluation of Sediment Budgets. USDA Forest Service, Pacific Southwest Research Station, Arcata, California, USA.

Renard, F., Ortoleva, P., & Gratier, J. P. (1997). Pressure solution in sandstones: influence of clays and dependence on temperature and stress. *Tectonophysics*, *280*(3), 257-266.

Richardson, J., I.G. Jowett. (2002). *Effects of sediment on fish communities in East Cape streams, North Island, New England*. New Zealand Journal of Marine and Freshwater Research. Vol 36. 431-442.

Rosgen, D. L. (2001, March). A practical method of computing streambank erosion rate. In *Proceedings of the Seventh Federal Interagency Sedimentation Conference* (Vol. 1).

Russo, J., Fox, J. (2012). The Role of the Surface Fine-Grained Laminae in Low-Gradient Streams: A Model Appraoch. Geomorphology. Vol 171-172.

Russo, Joseph Paul. (2009). Investigation of surface fine grained laminae, streambed, and streambank processes using a watershed scale hydrologic and sediment transport model. *University of Kentucky Doctoral Dissertations*. 750.

Singh, K. P., & Durgunoğlu, A. (1989). A new method for estimating future reservoir storage capacities.

Smallwood, R. Personal Communication. February 16, 2017

Smart, P. L., & Hobbs, S. L. (1986, October). Characterization of carbonate aquifers: A conceptual base. In *Proceedings of the Environmental Problems in Karst Terranes and Their Solutions Conference, Bowling Green, KY* (pp. 1-14).

Smith, D. R., King, K. W., Johnson, L., Francesconi, W., Richards, P., Baker, D., & Sharpley, A. N. (2015). Surface runoff and tile drainage transport of phosphorus in the midwestern United States. *Journal of environmental quality*, *44*(2), 495-502.

Souza, J. O., Correa, A. C., & Brierley, G. J. (2016). An approach to assess the impact of landscape connectivity and effective catchment area upon bedload sediment flux in Saco Creek Watershed, Semiarid Brazil. Catena, 138, 13-29.

Sumi T. and Hirose T. (2005). Accumulation of Sediment in Reservoirs. Encyclopedia of Life Support Systems (EOLSS). Kyoto, Japan.

Sumi, T. (2004). Reservoir Sedimentation Management with Bypass Tunnels in Japan. Proceedings of the Ninth International Symposium on River Sedimentation. Yichang, China.

Sumi, T., & Hirose, T. (2009). Accumulation of sediment in reservoirs. *Water storage, transport and distribution. UNESCO-IHE and EOLSS Publishers Co. Ltd., Paris, France*, 224-252.

Third Rock Consulting. LFUCG Stormwater Stakeholder Advisory Committee. Accessed 2/18/2016. http://www.lexingtonky.gov/Modules/ShowDocument.aspx?documentid=27603

Tight, W.G., 1903, Drainage modifications in southeastern Ohio and adjacent parts of West

Tisdall, J. M., & Oades, J. (1982). Organic matter and water-stable aggregates in soils. *Journal of soil science*, *33*(2), 141-163.

Torri, D., & Borselli, L. (2003). Equation for high-rate gully erosion. *Catena*, *50*(2), 449-467.

Torri, D., & Poesen, J. (2014). A review of topographic threshold conditions for gully head development in different environments. *Earth-Science Reviews*, *130*, 73-85.

Toy, T.J., et al. (2002). Soil Erosion: Processes, Prediction, Measurement, and Control. John Wiley & Sons, Inc.

Trimble, S.W. (1997). Contribution of Stream Channel Erosion to Sediment Yield from an Urbanizing Watershed. Vol. 278: 1442-1444

Ulack, R., Raitz, K., Pauer, G., 1998, Atlas of Kentucky: Lexington, University Press of Kentucky, 316 p.

U.S. Environmental Protection Agency (1999). *Protocol for Developing Sediment TMDLs*. EPA 841-B-99-004. Office of Water (4503F), United States Environmental Protection Agency, Washington D.C. 132 pp.

U.S. Environmental Protection Agency. 2009. Current and previously registered section 3 PIP registrations. (http://www.epa.gov/pesticides/biopesticides/pips/pip_list.htm).

USDA. Bluegrass Series Soil Data. Accessed 2/21/2016. https://soilseries.sc.egov.usda.gov/OSD_Docs/B/BLUEGRASS.html

USEPA (Environmental Protection Agency). (2009). National water quality inventory: Report to congress. EPA 841-R-08-001. Washington, DC: US Environmental Protection Agency, Office of Water.

USEPA (United States Environmental Protection Agency), Office of Science and Technology. (2004). The Incidence and Severity   of Sediment Contamination in Surface Waters of the United States, EPA 823-R-04-007. http://www.epa.gov/waterscience/cs/report/2004/nsqs2ed-complete.pdf.

USGS. (2015). The Effects of Urbanization of Water Quality. U.S. Department of
    Interior. U.S. Geological Survey. http://water.usgs.gov/edu/urbanquality.html.
    Accessed on 10/27/2015.

USGS. (2016). Lakes and Reservoirs. U.S. Department of Interior. U.S. Geological
Survey.   http://waterdata.usgs.gov/wa/nwis/current/?type=lakes.

USGS. National Water Information Systems. South Elkhorn Creek at Fort Spring, KY.
    Accessed 2/12/2016.
    http://waterdata.usgs.gov/nwis/dv?cb_00060=on&format=rdb&site_no=0328900
    0&referred_module=sw&period=&begin_date=1980-01-01&end_date=2015-01-
    01

Van Oost, K., Govers, G., Quine, T. A., & Heckrath, G. (2004). Comment on "Managing
    soil carbon"(I). *Science*, *305*(5690), 1567-1567.

Van Rijn, L. C. (1993). *Principles of sediment transport in rivers, estuaries and coastal
    seas* (Vol. 1006).   Amsterdam: Aqua publications.

Vandaele, K. and Poesen, J., 1995. Spatial and temporal patterns of soil erosion rates in
    an agricultural catchment, central Belgium. Catena, 25: 213-226.
Vandaele, K., 1993. Assessment of factors affecting ephemeral gully erosion in cultivated
    catchments of the Belgian Loam Belt. In: S. Wicherek (Editor), Farm Land
    Erosion in Temperate
Vandaele, K., Poesen, J., Govers, G., vanWesemael, B., 1996. Geomorphic threshold
    conditions for ephemeral gully incision. Geomorphology 16, 161–173.

Verachtert, E., Van Den Eeckhaut, M., Poesen, J., & Deckers, J. (2010). Factors
    controlling the spatial distribution of soil piping erosion on loess-derived soils: A
    case study from central Belgium. *Geomorphology*, *118*(3), 339-348.

Vigiak, O., Borselli, L., Newham, L. T. H., McInnes, J., & Roberts, A. M. (2012).
    Comparison of conceptual landscape metrics to define hillslope-scale sediment
    delivery ratio. *Geomorphology*, *138*(1), 74-88.

Walling, D. E. (1983). The sediment delivery problem. *Journal of hydrology*, *65*(1-3),
    209-237.

Wanielista, M., Kersten, R., & Eaglin, R. (1997). *Hydrology: Water quantity and quality
    control*. John Wiley and Sons.

Ward, J. V., Tockner, K., & Schiemer, F. (1999). Biodiversity of floodplain river
    ecosystems: ecotones and connectivity. *Regulated Rivers: Research &
    Management*, *15*(1), 125-139.

Wischmeier, W. H., & Smith, D. D. (1978). Predicting rainfall erosion losses-a guide to
    conservation planning. *Predicting rainfall erosion losses-a guide to conservation
    planning.*

Wood, P. J., & Armitage, P. D. (1997). Biological effects of fine sediment in the lotic environment. *Environmental management*, *21*(2), 203-217.

Zappou, C. (2001). *Review of urban storm water models.* Environmental Modeling & Software, Vol. 16, pp. 195-231.

David Tyler Mahoney, B.S. CE

Frankfort, Kentucky

Education

M. S. Civil Engineering, University of Kentucky (currently enrolled). 4.0 GPA.
   Advisor: James F. Fox.

B. S. Civil Engineering, University of Kentucky, 2015. 3.9 GPA

   Emphasis: Water Resources Engineering

Employment History

Research Associate, University of Kentucky (2016-Present)

Undergraduate Researcher, University of Kentucky (2014-2016)

Intern, Stantec Inc. (2015)

Intern, HMB Professional Engineers (2012)

Awards and Recognition

1. Nominated for the UK College of Engineering Dean's Award for Outstanding Master's Student (2017)
2. Nominated for Chi Epsilon Outstanding Graduate Student Award (2017)
3. Nominated for Chi Epsilon Outstanding University Scholar Award (2016)
4. Recipient of the Chi Epsilon Outstanding University Scholar Award (2016)
5. Lauderdale Fellowship Recipient (2016, 2017)
6. Phi Gamma Delta Outstanding Senior Award (2015)
7. Kentucky Society of Professional Engineers George M. Binder Scholarship (2015)
8. University of Kentucky University Scholar (2015)
9. Phi Gamma Delta Highest GPA Scholarship (2015, 2016)
10. University of Kentucky Presidential Scholarship (2011)
11. HMB Professional Engineers Scholarship (2011)
12. University of Kentucky Dean's List (2011-2016)
13. Kentucky Governor's Scholars Program (2010)

Journal Publications

1. Mahoney, D.T., Fox, J.F., Al-Aamery, N. Upland Erosion and Sediment Transport Modelling using Probabilistic Sediment (Dis)Connectivity Prediction at the Catchment Scale, *in preparation.*
2. Mahoney, D.T., Fox, J.F., Al-Aamery, N. Longitudinal Sediment Transport Modelling using the Probability of Sediment (Dis)Connectivity in a Bedrock Controlled Catchment, *in preparation.*

Conference Presentations: Peer-Reviewed Abstract

1. Mahoney D.T., Fox J.F. and Al Aamery N. 2017. Sediment Transport Modelling using Dynamic (Dis)Connectivity Prediction for a Bedrock Controlled Catchment, 2017 World Environmental & Water Resources Congress, EWRI, ASCE, May 21-25, 2017, Sacramento, CA, USA.
2. Mahoney D.T., Fox J.F., Clare E., Kendig R., Cambron A. 2017. WAVES: A comprehensive visual assessment of watershed sedimentation processes, Kentucky Water Resources Annual Symposium, Lexington, KY, March 20, 2017.
3. Mahoney D.T., Fox J.F., and Al Aamery N. 2017. Sediment transport modeling using dynamic (dis)connectivity to assess sediment impacts on water supply, Kentucky Water Resources Annual Symposium, Lexington, KY, March 20, 2017.

Extension Publications

1. Mahoney D.T., Agouridis C.T., Warner R.C. 2016. Hydrologic Modeling. University of Kentucky Cooperative Extension Service: AEN-127